Investigating intrathecal adeno-associated virus vectors for the study of analgesic interactions at the spinal level

A DISSERTATION
SUBMITTED TO THE FACULTY OF
UNIVERSITY OF MINNESOTA
BY

Daniel J. Schuster

IN PARTIAL FULFILLMENT OF THE REQUIREMENTS
FOR THE DEGREE OF
DOCTOR OF PHILOSOPHY

Advisors: George L. Wilcox, Ph.D., Carolyn A. Fairbanks, Ph.D.

July 2013

Acknowledgements

A very special thanks to all of the people that helped me through this process…

Lucy Vulchanova for being my unofficial third advisor and an endless scientific resource.
Kelley Kitto for all the intrathecal injections…couldn't have done it without him.
Maureen Riedl for numerous thoughtful discussions and much technical help.
Galina Kalyuzhnaya for extensive technical support.
Steve Schnell for help with methods.
Matthew Metcalf for thoughtful discussions on opioid ligands.
Carrie Wade for all the help in the beginning, and valuable perspective on many things.
Chuck Coste for being my primary support outside of the lab.
My committee members, Bill Elmquist and Scott McIvor, for their input and support
And my advisors, Carolyn Fairbanks and George Wilcox,
for scientific support and career guidance

Dedication

This thesis is dedicated to my loving parents, Thomas and Joyce Schuster

Abstract

Pain signals from the periphery enter the central nervous system (CNS) via axons of primary afferent sensory neurons residing in dorsal root ganglia (DRG). Inhibition of pain signals directly at the spinal level provides an opportunity to reduce pain at the most basic level. Several G protein-coupled receptors, including opioid and adrenergic receptors, are known to be potent regulators of pain signaling at the spinal level. Co-activation of different subtypes of these receptors can lead to synergistic inhibition of pain signaling. Understanding how these receptors interact at the cellular level may provide insight into how to exploit such mechanisms for improved pain management strategies. This thesis has taken two approaches to advance the study of interactions involving opioid and adrenergic receptors at the spinal level: develop the use of adeno-associated virus (AAV) vectors for gene-transfer to sensory neurons where the expression of involved proteins can be modulated, and to further characterize these interactions by understanding of the cellular processes underlying their outcomes. The first part of this thesis describes the transduction pattern in DRG and CNS resulting from intrathecal delivery of AAV serotypes 5, 8, and 9. The results obtained demonstrate differential tropism of AAV vectors for subpopulations of primary afferent neurons and some brain areas. The second part of this thesis characterizes interactions between spinally delivered combinations of an opioid and an adrenergic agonist, or two opioid agonists, based on the requirement of protein kinase C-epsilon (PKC-epsilon) for analgesic synergy. The results obtained suggest that PKC-epsilon is not involved in analgesic activity of agonists delivered singly, but is necessary for synergistic interactions resulting from specific

agonist combinations. The last part of this thesis integrates the primary results from the first two parts, and suggests ways that differences in tropism of AAV vectors can be exploited to study various aspects of signaling interactions between G protein-coupled receptors at the spinal level.

Table of Contents

List of Tables

List of Figures

Chapter 1

Introduction

Treatment of pain is an ongoing worldwide health issue. Though opioid analgesics remain a mainstay for treatment of both acute and chronic pain conditions, in many cases they are lacking in efficacy for various reasons. In cases of chronic pain where opioids are effective, their use can be limited by tolerance to analgesic effects along with relative lack of tolerance to unwanted side effects such as constipation. In cases of acute pain, opioid use can be limited by side effects such as sedation and respiratory depression. As it is clear that current therapies could be improved upon, it remains important to further understand ways to modulate or inhibit pain signaling. One approach is to better understand how opioids and other analgesics work at a very basic level in hopes of gaining insight into ways to maximize and expand their utility for pain control.

A more specific strategy is to investigate modulation of pain signals at the spinal level, where information from the periphery crosses the first synapse to enter the central nervous system in the dorsal horn of the spinal cord. Analgesics can work through several receptors at the spinal level, including opioid and adrenergic receptors. All three opioid receptor subtypes, mu, delta, and kappa, as well as alpha-2A and alpha-2C adrenergic receptors have been found to be involved in analgesia at the spinal level (Li et al., 2010; Chakrabarti et al., 2010; Fairbanks et al., 2002; Stone et al., 1997). These receptors are G protein-coupled receptors and can be located on primary afferent terminals entering from the periphery, as well as on neurons intrinsic to the spinal cord (Wang et al., 2010; Riedl et al., 2009; Olave and Maxwell, 2003; Olave and Maxwell, 2002; Aicher et al., 2000; Stone et al., 1998). Additionally, co-delivery of two opioid

receptor and adrenergic receptor agonists at the spinal level will often produce synergistic, or greater-than-additive, inhibition of nociception (Hylden and Wilcox, 1983; Sullivan et al., 1987; Wilcox et al., 1987; Stone et al., 1997; Overland et al., 2009). The mechanisms underlying these interactions are not well defined, but it seems that better understanding of these interactions at the spinal level could inform future strategies for pain management.

It is possible to study G protein-coupled receptors, their interactions, and signaling pathways using techniques to manipulate gene expression. Adeno-associated virus (AAV) vectors have recently emerged as tools for gene transfer that not only have good potential for basic research, but also for translation to human therapies due to minimal safety concerns (Milligan et al., 2005; Xu et al., 2003; Luebke et al., 2001; Kaemmerer et al., 2000; Kaplitt et al., 1994). There are several reasons that these vectors are attractive for gene transfer studies. They have an expression cassette capacity of approximately 4.3 kb (Beutler and Reinhardt, 2009), which is large enough to accommodate many genes including some enzymes and G protein-coupled receptors. They can allow for over expression of proteins of interest as well as knockdown of endogenous proteins when combined with other approaches such as the use of siRNA (Samad et al., 2013; Askou et al., 2012; Hirai et al., 2012; Wang et al., 2006). They allow for long-term expression, on the order of months, or possibly years, after a single dose (Mason et al., 2010; Storek et al., 2008). There are several serotypes of AAV available, which differ by the specific protein structure of the capsid. Evidence suggests tropism for various cell or tissue types varies with the serotype used (Jacques et al., 2012;

Xu et al., 2012; Mason et al., 2010; Vulchanova et al., 2010; Towne et al., 2009; Royo et al., 2008). This appears to be due to differential binding of the virus capsid to certain cell surface molecules that allow for binding and subsequent internalization (Weller et al., 2010; Zhong et al., 2007; Seiler et al., 2006; Wu et al., 2006; Walters et al., 2001; Kaludov et al., 1998; Summerford and Samulski, 1998). Differences in expression of cell-surface receptors for AAV particles allow significant potential for preferential transduction of certain cells or areas based on the chosen serotype. Recent studies suggest that differences in tropism are evident in the nervous system (Jacques et al., 2012; Xu et al., 2012; Mason et al., 2010; Vulchanova et al., 2010; Towne et al., 2009; Royo et al., 2008). With regard to pain signaling at the spinal level, the use of AAV vectors to transduce primary afferent neurons has been demonstrated using several different methods with varying degrees of success.

Adeno-associated virus vectors for gene delivery to primary sensory neurons of the dorsal root ganglia

The methods resulting in the most robust transduction of dorsal root ganglion neurons have primarily been those using injection directly into either the ganglia itself or associated peripheral nerve fibers (Xu et al., 2003; Lee et al., 2007; Mason et al., 2010). As injections directly into nervous tissue can cause significant damage, less invasive methods are preferable. Peripheral administration methods, such as intravenous or intramuscular delivery, have had varied success in transduction of dorsal root ganglion neurons, and can result in significant off-target transduction of peripheral tissues (Gray et

al., 2011; Towne et al., 2009; Gu et al., 2005). Intrathecal administration, especially as acute lumbar puncture, allows delivery to be concentrated at the spinal level while minimizing off-target exposure and risk for tissue damage associated with parenchymal injections.

The use of intrathecal administration methods for delivery of AAV vectors has been explored with mixed results that appear to depend on the specific delivery method and serotype used. Studies of intrathecal delivery of AAV vectors have primarily used various catheterization approaches (Milligan et al., 2005; Storek et al., 2006; Storek et al., 2008; Towne et al., 2009). Some early studies using catheterization from either the lumbar approach to deliver AAV2 (Milligan et al., 2005) or the atlanto-occipital approach using AAV1 (Storek et al., 2006) yielded little-to-no transduction of primary sensory neurons. Other reports in the following years indicated substantial transduction of DRG neurons after delivery of different serotypes via the atlanto-occipital catheterization approach (Storek et al., 2008; Towne et al., 2009). Storek et al. (2008) used an AAV8 vector and reported transduction of several subtypes of DRG neurons including those displaying classical markers of nociceptors; however, quantification was not completed in this study to determine the overall level of transduction in DRG relative to the level in nociceptive subpopulations. Towne et al. (2009) used a different serotype, AAV6, also delivered via atlanto-occipital catheter, along with thorough quantification methods to demonstrate transduction of 1/3-1/2 of lumbar DRG neurons, with the majority of these being of the small-diameter, presumably nociceptive type.

Though it has been demonstrated that significant numbers of primary sensory neurons can be transduced after delivery of AAV vectors by intrathecal catheter, few studies have investigated non-catheter based acute intrathecal delivery. Those that have delivered to the intrathecal space without the use of a catheter have either injected under anesthesia into the cisterna magna (Iwamoto et al., 2009), or have injected at the lumbar level without investigating transduction of DRG (Watson et al., 2006). Considering that placement of an intrathecal catheter requires surgical anesthesia and may itself cause irreparable damage to the spinal cord, along with the ability of a single dose of AAV vector to produce stable, long-term gene-expression, it is clear that a non-catheter based lumbar delivery approach would be preferable for delivery to DRG.

We know that delivery of vector can be concentrated at the spinal level via intrathecal injection, but the overall distribution of AAV vectors delivered by acute lumbar puncture remains poorly characterized. Furthermore, the tropism of different AAV serotypes for sensory neurons of interest relative to off-target regions in the central nervous system and various peripheral tissues after intrathecal delivery has not been thoroughly described. Thus, further investigation into the transduction efficiency and tropism of AAV vectors acutely administered at the lumbar level for gene delivery to primary sensory neurons is an important next step before moving on to study proteins of interest.

In this case we are interested in the proteins involved in analgesic interactions between spinally delivered opioid and adrenergic agonists. The initial goal of this thesis project was to use AAV vectors to overexpress delta opioid and/or alpha2A adrenergic

receptors in DRG neurons, and subsequently study the effects of overexpression on analgesia and drug interactions involving these receptors. As there was much work to do in characterizing trans-gene expression after intrathecal AAV vectors, and the constructs we wished to use were difficult to obtain, a parallel line of investigation was initiated in order to expand our potential pool of genes of interest to manipulate via AAV vectors.

Mechanisms of spinal analgesic synergy between opioid and adrenergic agonists delivered at the spinal level

Spinal analgesic synergy involving opioid and adrenergic agonists is well documented, but the mechanisms underlying these interactions remain poorly understood. To better understand these interactions it is important to determine specifically which receptors are involved, their normal signaling pathways, and their locations relative to the basic sensory neuroanatomy of the spinal cord and to each of the other receptors involved in a given interaction. There are four receptor subtypes that have been primarily implicated in spinal analgesic interactions involving opioid and adrenergic agonists: mu opioid receptors, delta opioid receptors, alpha-2A adrenergic receptors, and alpha-2C adrenergic receptors (Riedl et al., 2009; Overland et al., 2009; Fairbanks et al., 2002; Stone et al., 1997). All four of these receptors are classically thought to couple to inhibitory G proteins, and their relative anatomical locations in the spinal cord have already been generally characterized.

Alpha-2A adrenergic receptors and delta opioid receptors are found primarily to co-localize on incoming primary afferent fibers in the superficial dorsal horn of the spinal

cord, specifically peptidergic afferents expressing the markers substance P (SP) and/or calcitonin gene-related peptide (CGRP) (Riedl et al., 2009; Bao et al., 2003 Stone et al., 1998; Zhang et al., 1998). However, there is some evidence to indicate that a small portion of these receptors reside on cells intrinsic to the spinal cord, especially in the case of the delta opioid receptor (Cahill et al., 2001; Cheng et al., 1997). Mu opioid receptors are known to be located both in primary afferent neurons (also typically of the peptidergic type) as well as in neurons in the spinal cord receiving input from primary afferents (Beaudry et al., 2011; He et al., 2011; Gupta et al., 2010; Wang et al., 2010; Aicher et al., 2000). Alpha-2C adrenergic receptors have been established to be primarily located on interneurons of the spinal cord, and to a much lesser degree on incoming primary afferents (Olave and Maxwell, 2004; Olave and Maxwell, 2003; Olave and Maxwell, 2002; Stone et al., 1998). Considering the relative locations of the receptors participating in spinal analgesic synergy between opioid and adrenergic agonists, it appears that the mechanisms underlying the interactions between these receptors may vary with the receptors involved.

It has been shown through immunohistochemical methods that alpha-2A adrenergic receptors and delta opioid receptors are located on the same population of primary afferent neurons (Riedl et al., 2009), but only recently has there been direct functional evidence that these receptors interact within a single cell (Overland et al., 2009; Riedl et al., 2009). Overland et al. (2009) showed that protein kinase C is required for synergistic inhibition of CGRP release from spinal cord slices by clonidine (an alpha-2A agonist) and deltorphin II (a delta opioid agonist), as well as for analgesic synergy

between spinally co-delivered clonidine and deltorphin II. These results were further expanded by Riedl et al. (2009) to show that clonidine and deltorphin II also synergistically inhibit CGRP release from isolated spinal synaptosomes, indicating that the interaction between receptors is occurring at the level of single pre-synaptic terminals in the spinal cord.

Knowing that protein kinase C (PKC) is required for spinal analgesic synergy between delta opioid receptors and alpha-2A adrenergic receptors yields a starting point from which to further investigate the signaling pathways involved in this specific interaction. Several isoforms of PKC can be found in dorsal root ganglion neurons including, but not limited to, alpha, beta, gamma, delta and epsilon (Cesare et al., 1999). Protein kinase C signaling is very complex, and different isoforms do not always become activated by the same stimuli or signal to the same downstream effectors (Newton and Messing, 2010), making it difficult to know how PKC, or which PKC, is involved in synergy between delta opioid and alpha-2A adrenergic agonists. Preliminary data from the thesis of Aaron C. Overland evaluated activation of various PKC isoforms, as indicated by translocation to the plasma membrane, in primary cultures of DRG. These experiments indicated that it is specifically the epsilon isoform of PKC that is required for the interaction between delta opioid and alpha-2A adrenergic agonists; however, these data were not entirely conclusive. Therefore, further investigation is needed to confirm this preliminary result, and subsequently determine what other molecules might be involved. No matter which isoform is responsible, the fact that PKC appears to mediate synergy between delta opioid and alpha-2A adrenergic receptors at the level of a single

cell indicates that it may be involved in interactions between other receptor pairs that are co-localized in the same cell type.

It is likely that the mechanisms responsible for synergistic analgesic interactions between G protein-coupled receptors not located within the same cells may be different than those underlying interactions between receptors that are found in the same cells. Drugs acting on receptors located in two different cells will presumably act independently regarding the intracellular pathway activated upon receptor binding. In this case, the synergistic interaction would theoretically be due not to a change in the intracellular signaling pathway activated by the drugs, but rather to coincident inhibition of two neurons signaling in series in the same anatomical pathway. Gaining a basic understanding of the receptors and mechanisms involved in various drug interactions, as well as the cellular localization of these receptors provides a foundation for designing experiments to study such interactions using AAV vectors that have been characterized with regard to the relevant cell types.

Objectives

The studies described in the body of this thesis address some of the unknowns raised so far in the introduction. The first part of this series of experiments includes evaluation of transduction by adeno-associated virus vectors delivered to the intrathecal space via direct lumbar puncture. Specifically, we evaluated the extent to which these vectors result in trans-gene expression in dorsal root ganglia neurons generally, as well as in specific subtypes of DRG neurons that are involved in pain signaling. In addition, the

overall distribution and level of expression in areas of the central nervous system has been considered relative to the level of expression in the sensory neurons of interest. The results of the aforementioned studies will be used to guide choices of vector serotype and delivery method for future experiments using AAV vectors to study analgesic interactions involving opioid and adrenergic agonists in primary sensory neurons.

The second part of this thesis expands on the results of Overland et al. (2009) in exploration of the signaling pathway underlying intracellular synergy involving opioid and adrenergic agonists. Specifically, preliminary results implicating the epsilon isoform of protein kinase C in the interaction between clonidine and deltorphin II have been confirmed. Subsequently, agonist pairs other than clonidine and deltorphin II have been evaluated for dependence on PKC-epsilon to determine if other receptor pairs may synergize through the same mechanism as delta opioid and alpha-2A adrenergic receptors. Additionally, an inquiry has been made into what other molecules might be involved in the signaling pathway underlying these interactions.

Finally, the results from the first and second parts will be synthesized through review and discussion to propose future experiments. Specifically, AAV vectors and delivery methods will be indicated based on where trans-gene expression is required. Manipulation of expression levels of proteins selected based on the results enumerated within this thesis can be used in an effort to help determine involvement of those proteins in intracellular analgesic synergy at the spinal level.

Summary of objectives

1. Evaluate biodistribution of various AAV vectors after acute lumbar intrathecal delivery.
    a. Determine efficiency of transduction of primary sensory neurons by AAV serotypes 5, 8, and 9 with and without mannitol treatment
    b. Determine tropism of AAV serotypes 5, 8, and 9 for subpopulations of primary afferent neurons
    c. Determine overall distribution of transgene expression in the central nervous system and peripheral tissues after delivery of AAV serotypes 5, 8, and 9

2. Expand data on mechanisms of spinal intracellular synergy specifically involving PKC-epsilon.
    a. Determine what receptor or agonist pairs require PKC-epsilon for spinal analgesic synergy
    b. Find other targets within the signaling pathway to manipulate via AAV-based methods

Chapter 2

Gene expression in spinal cord and dorsal root ganglia after delivery of AAV5, AAV8, or AAV9 by direct lumbar puncture

Portions of the work described in this chapter have been published (data and some images from figures 1-5) in the article listed below. This chapter was written by Daniel J. Schuster based on data from the published article and additional unpublished data. All figures within were produced by Daniel J. Schuster

Vulchanova L, **Schuster DJ**, Belur LR, Riedl MS, Podetz-Pedersen KM, Kitto KF, Wilcox GL, McIvor RS, Fairbanks CA (2010) Differential adeno-associated virus mediated gene transfer to sensory neurons following intrathecal delivery by direct lumbar puncture. Mol Pain 6:31.

Author contributions from the publication:
LV contributed to the experimental design and drafting of the manuscript. In addition, she participated in all perfusions, dissections, histochemical analyses, and imaging as well as in interpretation of results and generation of figures.
DJS assisted in perfusions and dissections and performed immunohistochemistry, cell quantification and imaging. He assisted in the preparation of the figures, contributed to the analysis and interpretation of the data, and edited the manuscript.
LRB initiated the studies, contributed to experimental design and edited the manuscript.
MSR performed all perfusions and dissections and participated in histochemical analyses and interpretation of results.
KPP performed the intravenous injections.
KFK conducted all intrathecal injections.
GLW participated in the experimental design and edited the manuscript.
RSM initiated the study with GLW and CAF as collaborators and edited the manuscript.
CAF organized the team, contributed to the experimental design, drafted and edited the manuscript and supported the studies.

We evaluated immunoreactivity for green fluorescent protein (GFP-ir) in spinal cord and dorsal root ganglia (DRG) six weeks after intrathecal administration of adeno-associated virus serotypes 5, 8, or 9 (AAV5, AAV8, or AAV9) with an intravenous mannitol pretreatment. Mannitol pretreatment was found to significantly increase the number of DRG neurons transduced by AAV5. The pattern of expression after AAV5 or AAV8 was nearly identical in spinal cord, and very similar in DRG. Both AAV5 and AAV8 transduced more medium to large DRG neurons than small DRG neurons, and did not efficiently transduce isolectin-B4 (IB4) -binding neurons. AAV5 transduced more small CGRP-positive neurons than AAV8. AAV9 appeared to efficiently transduce the majority of DRG neurons at all spinal levels, including the IB4-binding subpopulation. In spinal cord, expression was primarily limited to sensory fibers of the dorsal horn after AAV5 or AAV8, but was also found in many spinal neurons after AAV9. Expression at thoracic spinal levels was very low relative to lumbar and cervical levels after AAV5 or AAV8, but was comparable to expression at the lumbar and cervical levels after AAV9. Here we have demonstrated efficient gene transfer to DRG neurons after intrathecal delivery of AAV vectors and have identified differences in tropism between AAV5, AAV8, and AAV9.

INTRODUCTION

Primary sensory neurons residing in dorsal root ganglia (DRG) transmit pain signals from the periphery to the central nervous system. Delivery of therapeutic genes to primary sensory neurons has the potential to provide long-term pain relief by reducing pain signaling at the first step of pain transmission. Adeno-associated virus (AAV) vectors have emerged as a useful tool for gene transfer studies that provide a high degree of versatility due to the availability of several different serotypes which show differential tropism for various tissues (Mason et al., 2010; Howard et al., 2008; Royo et al., 2008; Schultz and Chamberlain, 2008). The differences observed in tropism of various AAV vectors is thought to be the result in variations in binding of virus particles to various cell-surface molecules that act as receptors and allow for internalization (Weller et al., 2010; Zhong et al., 2007; Seiler et al., 2006; Wu et al., 2006; Walters et al., 2001; Kaludov et al., 1998; Summerford and Samulski, 1997). Considering that DRG neurons are a heterogeneous population characterized by differences in cell size and expression of neuropeptides, among other things, it is feasible that some AAV serotypes may display tropism for specific subpopulations of primary afferent neurons.

Studies that have achieved the greatest transduction rates in DRG neurons have typically delivered the vectors either by direct tissue injection or to the intrathecal space via a catheter implanted by the atlanto-occipital approach (Mason et al., 2010; Towne et al., 2009, Storek et al., 2008; Xu et al., 2003). Both of these methods require surgery and have significant potential for associated tissue damage and inflammation. Direct lumbar puncture delivery of AAV vectors provides an alternative that does not require

anesthesia, and has minimal risk of tissue damage. It has been reported that pretreatment with mannitol delivered intravenously may enhance distribution of AAV-mediated expression after intracisternal or intraneural delivery (Fu et al., 2003; Carty et al., 2010). Mannitol causes osmotic stress in cells by drawing water into the extracellular fluid and bloodstream (Cloyd et al., 1986). It is thought that this increase in extracellular fluid volume, along with the associated decrease in intracellular fluid volume, enlarges the space between cells allowing the enhanced distribution of virus particles observed in the aforementioned studies. We hypothesized that mannitol pretreatment would similarly enhance transduction of primary afferent neurons after direct lumbar puncture intrathecal delivery of AAV vectors.

Several AAV serotypes, including 5, 6, 8 and 9 (AAV5, AAV6, AAV8, and AAV9), have shown promise for effective transduction of DRG neurons (Gray et al., 2013; Samaranch et al., 2013; Mason et al., 2010; Towne et al., 2009; Storek et al., 2008). At the time the studies detailed in this chapter were completed we chose to start with AAV5 and AAV8, as those vectors were readily available to us. We set out to compare transduction in subpopulations of primary sensory neurons after intrathecal delivery of AAV5 and AAV8. Specifically we characterized subpopulations relative to cell soma size, expression of calcitonin gene-related peptide (CGRP), and binding of isolectin-B4 (IB4). Additionally, we have recently acquired AAV9 vector and have begun to compare results using AAV9 to the initial data using AAV5 and AAV8.

METHODS

AAV Vector and Packaging

AAV vector TRUF11, containing a CAGS-regulated GFP sequence, has been previously described (Kaemmerer et al., 2000). Packaging using AAV5 or AAV8 serotype capsid was carried out at the University of Florida Vector Core as previously described (Kaemmerer et al., 2000). AAV9 vector was purchased from the vector core at University of Pennsylvania (AV-9-PV1963).

Animals

Experimental subjects were 20 to 25g adult male C57BL/6 mice (Harlan, Madison, WI). All experiments were approved by the University of Minnesota Institutional Animal Care and Use Committee.

Injections

Adult male mice were injected via the tail vein with 25% mannitol solution (200 µL), or saline, twenty minutes prior to intrathecal injection of the viral constructs. AAV constructs were delivered intrathecally by direct lumbar puncture in awake mice (Hylden and Wilcox, 1980) by an experimenter (KFK) with 20 years experience in this method of drug delivery. A minor modification of the protocol was required to conserve AAV vector. The needle (a 30-gauge, 0.5-inch) was connected to a length of PE10 tubing, which was then connected to a second needle that was attached to a 50-µl Luer-hub Hamilton syringe. For all vectors, AAV5-GFP, AAV8-GFP, and AAV9-GFP, 10 µL of the construct containing ~10^{11} virus particles were injected intrathecally. The injection was administered by gripping gently the iliac crest of the rodent and inserting the needle

(bevel side up) at about a 45 ° angle centered between the hipbones. A reflexive flick of the tail indicated puncture of the dura. Following the injection, the animals were returned to the vivarium where they remained for six weeks, until the time of transcardial perfusion, fixation, and extraction of fixed spinal cord and DRG for immunohistochemical analysis.

Immunohistochemistry

All animals were killed by perfusion fixation as previously described (Vulchanova et al., 1998). Briefly, animals were isoflurane anaesthetized via nosecone inhalation and perfused with a solution of calcium-free tyrodes solution (in mM:NaCl 116, KCl 5.4, $MgCl_2 \cdot 6H_20$ 1.6, $MgSO_4 \cdot 7H_2O$ 0.4, NaH_2PO_4 1.4, glucose 5.6, and $NaHCO_3$ 26) followed by fixative (4% paraformaldehyde and 0.2% picric acid in 0.1M phosphate buffer, pH 6.9) followed by 10% sucrose in PBS. Spinal cord and DRG were removed and incubated in 10% sucrose overnight at 4˚C. Sections were cut at 14 μm thickness and thaw mounted onto gel-coated slides. Tissue sections were incubated for 1 hour at room temperature in diluent (PBS containing 0.3% Triton, 1% BSA, 1% normal donkey serum) and then incubated overnight at 4°C in primary antisera diluted in the same diluent. In some instances, GFP fluorescence was enhanced by immunostaining with antisera to GFP. Primary antibodies used were: rabbit anti-GFP, 1:500 (Invitrogen; Eugene, OR), rabbit anti-CGRP, 1:500 (Immunostar; Hudson, WI), mouse anti-NeuN. 1:500 (Chemicon; Temecula, CA), mouse anti-GFAP, 1:400 (Sigma; St. Louis, MO)), and/or biotinylated isolectin-B4, 10 mg/ml (Sigma; St. Louis, MO). After rinsing with PBS, sections were incubated one hour at room temperature with appropriate combinations of

Cy2-, Cy3-, Cy5- (1:300), and AMCA- (1:400) conjugated secondary antisera (Jackson ImmunoResearch, West Grove, CA). Sections were rinsed again in PBS and coverslipped using glycerol and PBS containing 0.1% p-phenylenediamine (Sigma). Some DRG sections were also incubated for 20 minutes at room temperature with NeuroTrace® Red (Invitrogen; Eugene, OR). Images were collected using confocal microscopy (Biorad MRC1024, or Olympus Fluoview1000), analyzed using Image J (NIH), and processed in Adobe Photoshop. For figure 6, images were collected using an Olympus BX60 fluorescence microscope with a Spot Insight camera and Spot image acquisition software, and processed in Adobe Photoshop.

Cell Counting

Initial data from AAV8 treated animals were collected from nine non-overlapping images taken across five DRG sections spaced at least 70μm apart. Comparison of the full data set to a subset taken from seven images across three sections showed no difference between the full set and the subset, indicating that seven images from three sections provides an adequate sample size to be representative of the larger population. Subsequently, full analyses were performed on each DRG by using at least seven images taken across three sections at least 70 μm apart. These sections were labeled with anti-CGRP, biotinylated-IB4, and NeuroTrace® Red for analysis of co-localization and cell size. Seven non-overlapping images were taken across these three sections and analyzed using ImageJ to measure cell body size and fluorescence intensity. Neurons were identified and outlined based on their Nissl-like NeuroTrace® labeling. Only cells with a visible nucleus were counted. The cutoff of 22μm for categorization of neurons by size

was chosen based on the width of the largest peak in size histograms of DRG neurons. For CGRP fluorescence intensity, a method adapted from that of Fang and colleagues was used (Fang et al., 2006). The average intensity of the brightest 10% and the dimmest 10% of neurons in each image was measured and relative fluorescence intensity for each cell was defined as 100[(intensity of selected cell - average of dimmest 10%) / (average of brightest 10% - average of dimmest 10%)]. Cells with a relative fluorescence intensity of 28% or greater were considered positive, and this number consistently coincided with cells identified as positive by visual inspection. Because the number of GFP expressing cells in each section was low, an alternative method was used to determine background fluorescence of GFP. The average fluorescence of three GFP-negative cells in each image was calculated, and GFP-positive cells were defined as cells with average intensity greater than that of the 3 negative cells plus 3 standard deviations. IB4 positive cells were defined using the same method as that for GFP positive cells.

RESULTS

Immunoreactivity for green fluorescent protein (GFP-ir) was evaluated six weeks after intrathecal administration of AAV vectors. Intravenous administration of mannitol 20 minutes prior to intrathecal administration of AAV5 significantly enhanced expression in lumbar DRG neurons (Figure 1; Mann-Whitney $U_{.05(1),3,3} = 9$, $p = 0.05$), as well as in corresponding primary afferent fibers in spinal cord dorsal horn. Spinal cord images from an animal that received AAV5 with a mannitol pretreatment are shown in Figure 2. GFP-ir was observed at all spinal levels after both AAV5 (Figure 2) and AAV8 (data not

shown), but was distinctly less pronounced at thoracic levels (Figure 2B). Expression across all spinal levels appeared to be primarily located in incoming afferent fibers, but was minimal in substantia gelatinosa relative to the rest of the dorsal horn. GFP-positive neurons and astrocytes intrinsic to the spinal cord were also consistently observed after AAV5 or AAV8 (Figure 3), but were few in number and primarily located at the lumbar and sacral levels.

In DRG, expression was found in many neurons after both AAV5 and AAV8 (Figure 4); however, after AAV8 expression was also observed in some non-neuronal cells that did not co-label with markers of glial cells (data not shown). To determine the relative distribution of expression across neuronal subpopulations in DRG, quantitative image analysis was performed on sections co-labeled for GFP, CGRP, IB4, and counterstained with NeuroTrace (as seen in Figure 4). The proportions of CGRP-positive and IB4-positive neurons determined in these experiments (AAV5: CGRP, 37.0 +/- 1.6 %, IB4, 23.4 +/- 1.7 %; AAV8: CGRP, 28.6 +/- 0.5 %; IB4, 24.4 +/- 2.2 %; mean +/- SEM) were consistent with previous reports (Baiou et al., 2007; Price and Flores, 2007; Zwick et al., 2002). This analysis revealed that both AAV5 and AAV8 transduced a higher number of neurons with diameter above 22μm than neurons with diameter less than or equal to 22μm (Figure 5A). More CGRP-positive neurons less than or equal to 22μm in diameter were found to express GFP after AAV5 compared to AAV8 (t-test, $t_{0.05,2,4} = 3.42$, $p<0.05$; Figure 5B). The number of IB4-binding neurons expressing GFP was very low after either AAV5 or AAV8 (Figures 4H, 4P, and 5B).

AAV9 has recently emerged as a serotype with very high potential for transduction of nervous tissue after various routes of delivery (Samaranch et al., 2012; Foust et al., 2009). To determine the relative transduction efficiency and pattern of AAV9 compared to AAV5 and AAV8, we injected AAV9 vector using our delivery protocol. Expression of GFP after intrathecal AAV9 was very robust in both DRG and spinal cord (Figure 6). The majority of DRG neurons appeared to be transduced at all spinal levels (Figure 6B, D and F), compared to an average of around 10% with AAV5 or AAV8 at the lumbar level (as seen in Figure 5). GFP expression was also detected in some non-neuronal cells in DRG. In spinal cord, the expression pattern after AAV9 was notably different than that observed with AAV5 or AAV8. Expression was observed in many primary afferent fibers entering the dorsal horn, including those in the substantia gelatinosa (Figure 6A, C and E), which showed little expression after AAV5 or AAV8. Expression was also found in several spinal neurons, primarily in the ventral horn, but also in the dorsal horn. Some GFP-expressing astrocytes were observed as well (data not shown). Unlike AAV5 and AAV8, AAV9 resulted in substantial GFP-ir in thoracic spinal cord (Figure 6C).

DISCUSSION

Here we report successful transduction of DRG neurons by the minimally invasive method of acute lumbar puncture administration of AAV5, AAV8, and AAV9. We found that mannitol pretreatment significantly enhanced transduction of DRG neurons with AAV5, and had a similar effect on AAV8. Conversely, pretreatment with

mannitol did not have an appreciable effect on transduction of DRG neurons by AAV9 (data not shown). This suggests that AAV9 particles, compared to those of AAV5 and AAV8, have a greater ability to penetrate into nervous system parenchyma where they can access cell surface molecules necessary for transduction. This result is not entirely surprising considering that others have previously reported a similar lack of effect of mannitol on transduction by AAV9 (Gray et al., 2011). The transduction pattern in DRG and across all spinal levels after AAV5 and AAV8 was generally similar, with one difference in transduction of small CGRP-positive neurons. However, AAV9 resulted in a markedly different pattern that appeared to be the result of increased transduction efficiency in several subpopulations of neurons in both DRG and spinal cord. These results demonstrate differences in tropism of AAV serotypes for subpopulations of primary afferent and spinal neurons.

In spinal cord, the pattern of GFP expression following AAV5 was generally indistinguishable from the pattern after AAV8. Immunoreactivity for GFP was most prominent in primary afferent sensory fibers in the dorsal horn. Expression was observed in the dorsal columns and across most dorsal laminae with the exception of lamina II. This is consistent with the observations that both AAV5 and AAV8 transduced more medium and large diameter DRG neurons than those of small diameter, and very few IB4-binding neurons. Recently, a study by Towne et al. (2009) using intrathecal delivery of AAV6 via an implanted catheter reported preferential transduction of small diameter DRG neurons including the IB4-binding population. Thus, AAV6 may be more useful than AAV5 and AAV8 for transfer of therapeutic genes to nociceptors.

In the ventral spinal cord of AAV5 and AAV8 treated mice, expression was relatively low, although a few nicely labeled neurons and astrocytes were consistently observed at the sacral and lumbar levels. Labeling was also minimal at the thoracic level, where GFP-ir was mainly confined to the dorsal columns and Clarke's columns. This lack of expression in thoracic spinal cord was also reported with intrathecal administration of AAV6 (Towne et al., 2009), suggesting that the limiting factor in access of virus particles to thoracic spinal cord and DRG is common to many AAV serotypes. One possible explanation for this observation is variation in fenestrations of the pia mater. It has been reported that pial fenestrations are differentially distributed across spinal levels, and are lacking at thoracic levels (Reina et al., 2004). Thus, it seems feasible that the pia mater is a barrier to most AAV serotypes that prevents access to the parenchyma of various parts of the nervous system. The exception in this case is AAV9, which yields efficient transduction at thoracic levels, as well as in spinal neurons of both the dorsal and ventral horns. AAV9 has been reported to readily cross the blood-brain barrier (Samaranch et al., 2012; Gray et al., 2011; Foust et al., 2009). The ability to cross cellular barriers appears to be a special feature of AAV9, which allows it to transduce nervous system tissues more robustly than some other serotypes.

Considering that AAV6 (Towne et al., 2009) and AAV9 seem to efficiently transduce IB4-binding neurons, whereas AAV5 and AAV8 do not, it appears that differential tropism of AAV serotypes can be exploited for preferential transduction of subpopulations of DRG neurons. The differences observed are likely due primarily to lack of cell-surface receptors necessary for binding and entry of AAV5 and AAV8 on

IB4-binding neurons. Conversely, it appears from Towne et al. (2009) that large diameter DRG neurons are lacking in the receptor or complex necessary for binding and entry of AAV6 particles. Our preliminary data indicates that AAV9 has access to several, if not all, subpopulations of primary afferent neurons, as it appears to transduce the majority of DRG neurons overall. However, further characterization is necessary to determine if there are any subtle differences in tropism of AAV9 for various DRG neurons.

The observation of substantial expression at cervical spinal levels indicates that a significant amount of virus particles travel rostral from the injection site through the cerebrospinal fluid, which likely results in transduction of some brain regions. Thus, before studying functional genes of interest, it is important to characterize expression across the brain to more completely understand where trans-genes will be expressed after intrathecal administration of AAV vectors. Chapter 3 will cover this topic in detail.

FIGURES

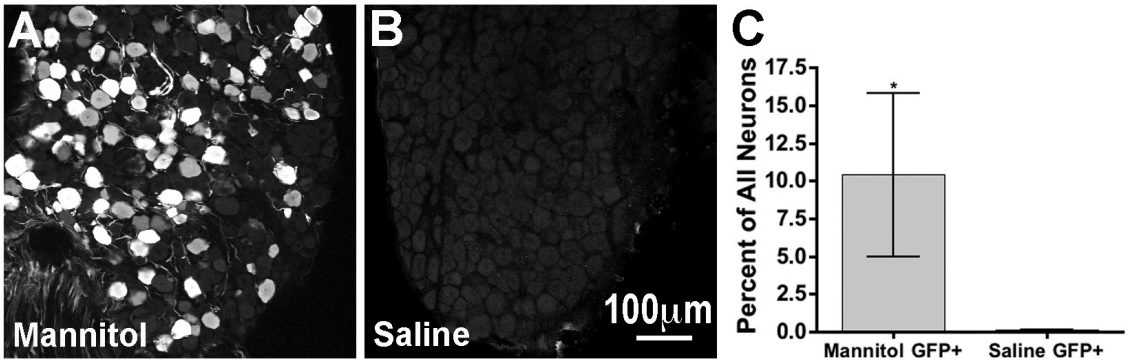

Figure 1. Intravenous mannitol pretreatment significantly enhances the number of lumbar dorsal root ganglion (DRG) neurons transduced by intrathecal AAV5. **A)** Image of a mouse DRG after intrathecal AAV5 with a mannitol pretreatment. **B)** Image of a mouse DRG after intrathecal AAV5 with a pretreatment of intravenous saline. **C)** Graph illustrating that mannitol pretreatment significantly enhanced transduction of DRG neurons by intrathecal AAV5 (Mann-Whitney $U_{.05(1),3,3} = 9$, $p = 0.05$).

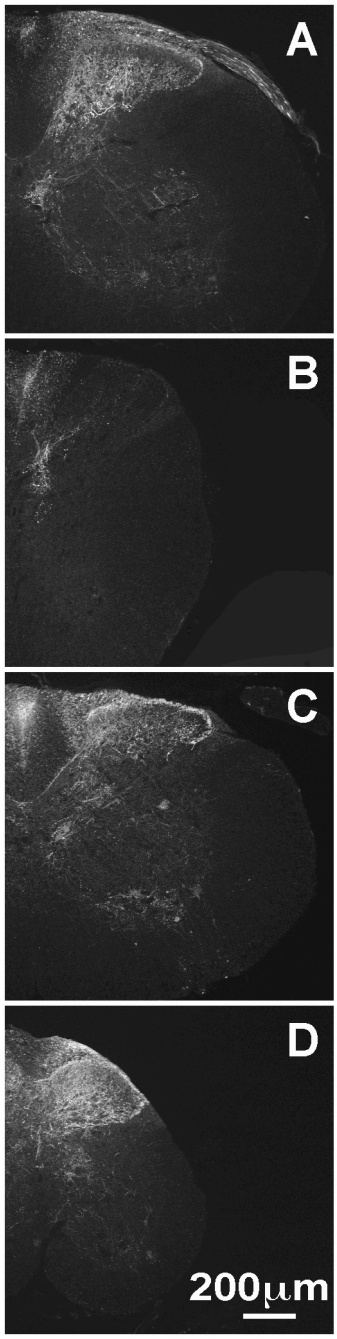

Figure 2. Expression of GFP across spinal levels after intrathecal AAV5 with an intravenous mannitol pretreatment. **A)** Cervical, **B)** thoracic, **C)** lumbar, and **D)** sacral mouse spinal cord stained for GFP.

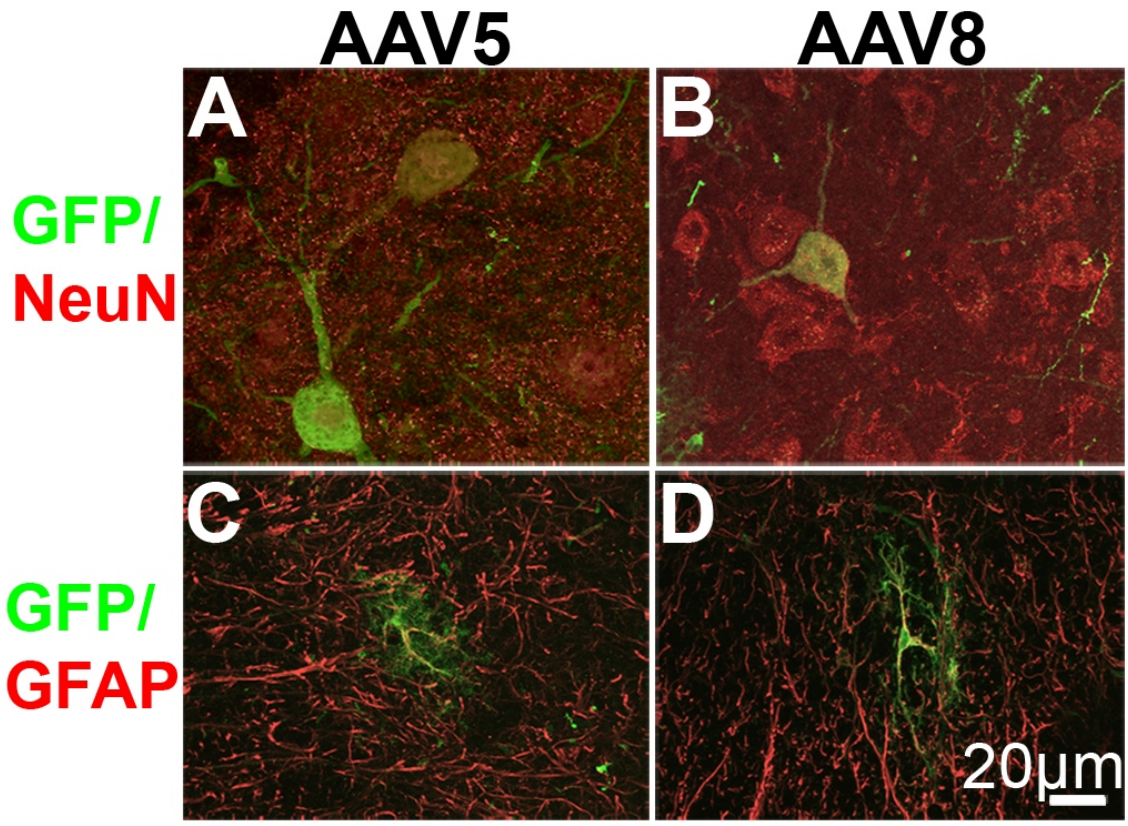

Figure 3. GFP expression in neurons and astrocytes in ventral horn of mouse spinal cord after intrathecal AAV5 or AAV8. **A and B)** Co-localization of GFP-ir with ir for NeuN after AAV5 (A) or AAV8 (B) illustrating expression in neurons. **C and D)** Co-localization of GFP-ir with ir for GFAP after AAV5 (C) or AAV8 (D) illustrating expression in astrocytes.

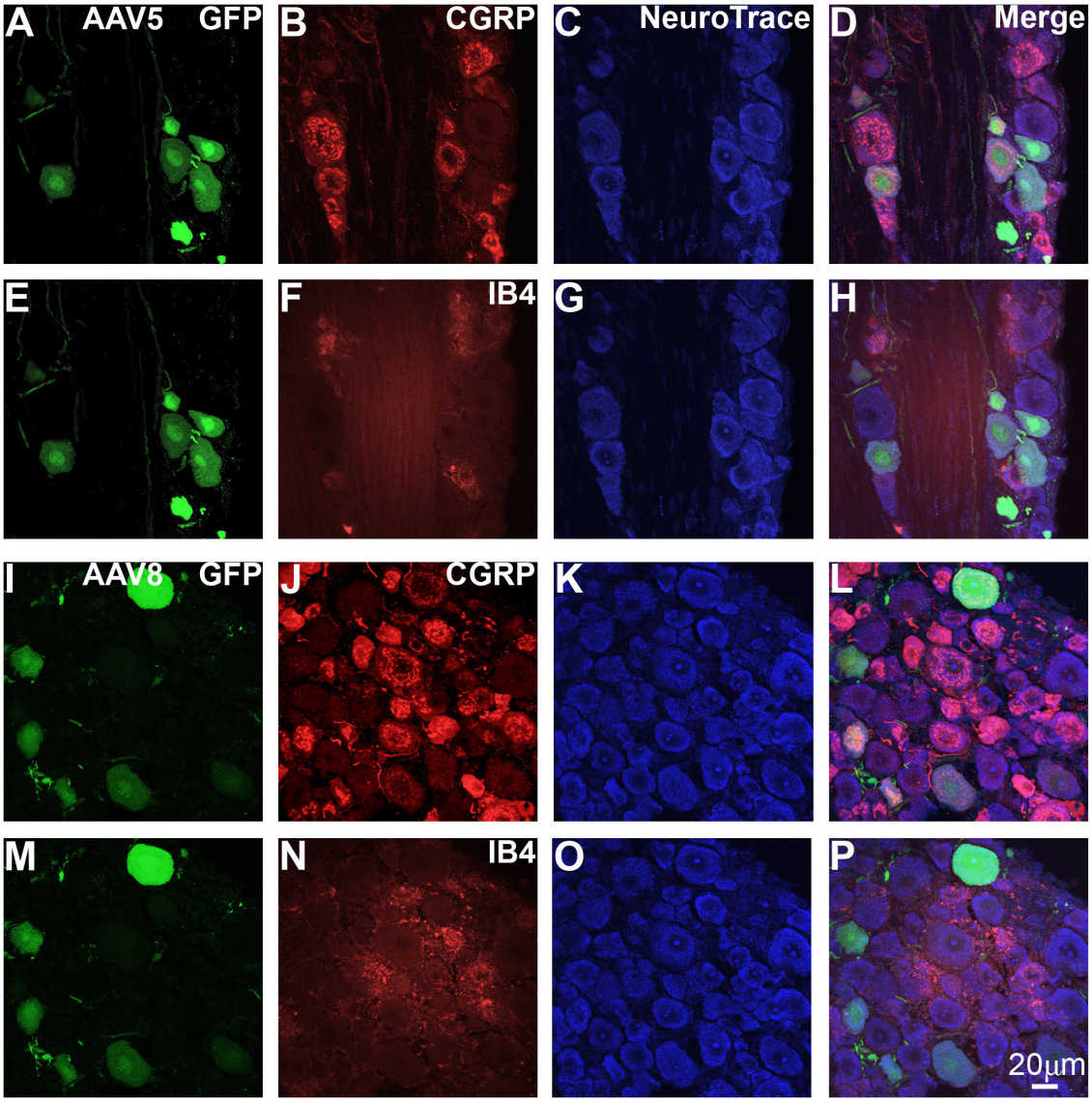

Figure 4. GFP expression after intravenous mannitol pretreatment and intrathecal injection of either AAV5 (**A-H)**, or AAV8 (**I-P**) in L5 DRG in mouse. GFP expression (green) is found in cells expressing CGRP-ir (red) (**A-D and I-L)** but not in cells that bind IB4 (red) (**E-H and M-P)**.

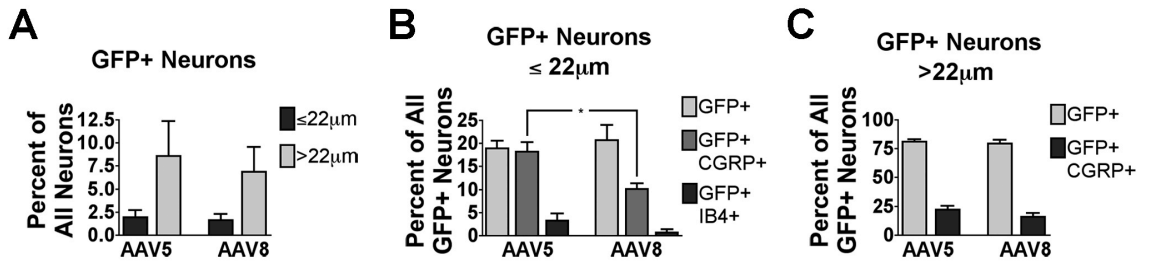

Figure 5. Quantitative image analysis of DRG neurons from mice that received intravenous mannitol pretreatment followed by intrathecal AAV5 or AAV8. **A)** A similar number of neurons smaller than 22μm (≤22μm), or larger than 22μm (>22μm) expressed GFP after both AAV5 and AAV8 injection. Both vectors preferentially targeted large neurons. **B)** Injection of AAV5 resulted in more GFP expression in CGRP-positive neurons smaller than 22μm than was seen with injection of AAV8 (t-test, $t_{.05,2,4}$=3.421, p=0.0268). Injection of either vector did not result in GFP expression in a substantial portion of the IB4-binding population. **C)** Approximately 80% of the DRG neurons expressing GFP were larger than 22μm, regardless of whether AAV5 or AAV8 was injected. Approximately 20% of these GFP-expressing neurons were also CGRP positive.

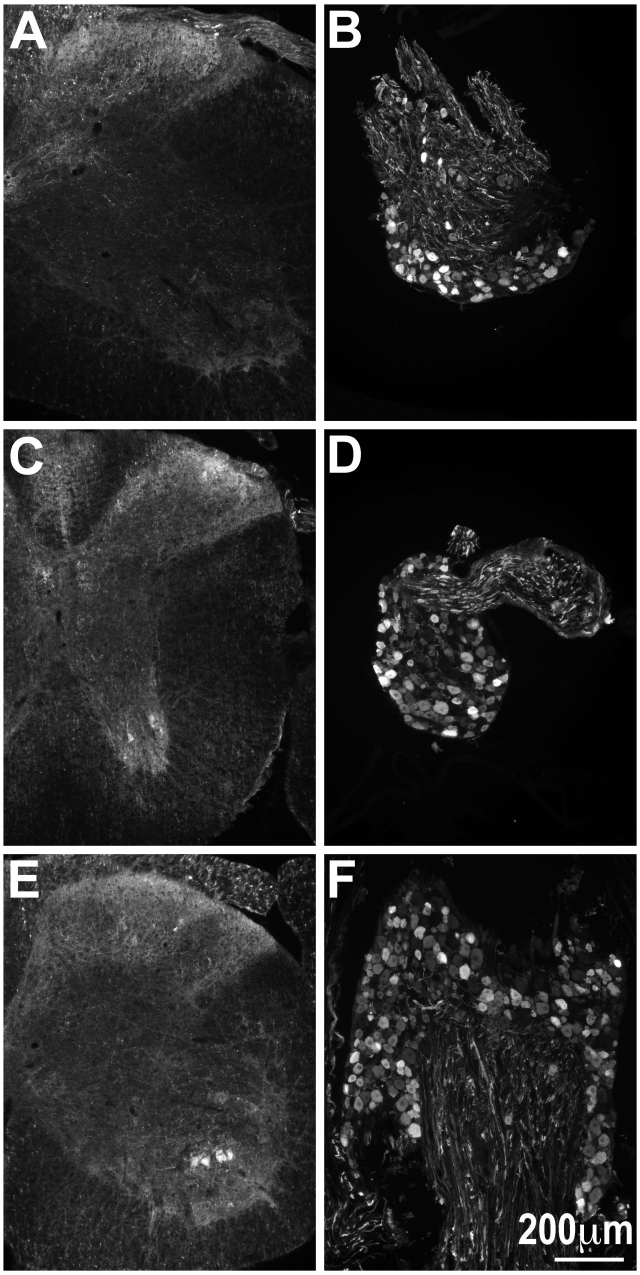

Figure 6. Expression across spinal levels after intrathecal delivery of AAV9 with a pretreatment of mannitol delivered intravenously. **A and B)** Lumbar spinal cord (A) and DRG (B). **C and D)** Thoracic spinal cord (C) and DRG (D). **E and F)** Cervical spinal cord (E) and DRG (F).

Chapter 3

Gene expression in the central nervous system after intrathecal delivery of AAV5 or AAV9

The results detailed in this chapter are a continuation of the work described in chapter 2, and as such, are the product of varied contributions from the same group of authors.

Author contributions:
DJS wrote the chapter, prepared the figures, performed immunohistochemistry, cell quantification, imaging and data analysis, some of the intravenous injections, dissections, and assisted in perfusions.
LRB initiated the studies and contributed to the experimental design.
MSR performed all perfusions, dissections, and participated in interpretation of results.
KPP performed some of the intravenous injections.
KFK conducted all intrathecal injections.
GLW participated in the experimental design and edited the chapter.
RSM initiated the study with GLW and CAF as collaborators.
CAF organized the team, contributed to the experimental design, edited the chapter and supported the studies.
LV contributed to the experimental design, participated in all perfusions, dissections, histochemical analyses, interpretation of results, and edited the chapter.

We report the pattern of transgene expression in brain after intrathecal delivery of adeno-associated virus serotype 5 (AAV5). In addition to detailed AAV5 results, we summarize a general comparison to animals given AAV9. Six weeks after injection of AAV5, labeling was found primarily in neurons, but also in some astrocytes. In hindbrain GFP-ir was detected in sensory nuclei of medulla, pontine nuclei, and cerebellar cortex. GFP-ir in midbrain was limited to dorsolateral margins and cerebral peduncle astrocytes. GFP-ir in thalamus was strongest in medial geniculate nucleus, and otherwise primarily limited to the lateral geniculate and posterior nuclei. Diffuse GFP-ir was found in caudal cortex. Labeling was also observed in hippocampal formation and amygdaloid complex. In hippocampal formation GFP-ir was found in cell bodies of the rostral-ventral portion, but restricted to fiber-like staining in the molecular layer and stratum lacunosum of the rostral-dorsal region. A caudal-to-rostral gradient of decreasing GFP-ir was present in choroid plexus and Purkinje cells. Areas where expression was significantly higher than surrounding regions, such as hippocampal formation and olfactory bulb, are likely resulting of factors including variations in cell-surface receptors and inter-parenchymal space. These findings suggest that AAV5-mediated gene transfer via intrathecal delivery results in a distinct pattern of gene expression that highlights certain anatomical features of the brain. Expression after AAV9 followed the same general pattern as AAV5, but was much more robust throughout and included regions not transduced by AAV5. All brain regions showed some degree of expression after AAV9, but relative intensity across several areas was consistent with that of AAV5.

INTRODUCTION

In recent years a growing body of evidence has indicated that adeno-associated virus (AAV) may be a useful vector for delivery of therapeutic genes to the central nervous system (CNS). Direct injection of AAV vectors into a specific CNS nucleus can result in a high level of gene expression in that nucleus, as well as physically adjacent and functionally connected areas (Ciesielska et al., 2010; White et al., 2010; Fu et al., 2002). However, this method carries the drawback of tissue damage that is potentially both detrimental and irreparable. Therefore, alternative approaches for CNS delivery of AAV vectors, such as delivery to the cerebrospinal fluid (CSF), are necessary for translational development of AAV-mediated gene therapy.

Delivery to the CSF can be achieved in a variety of ways including injection into the cerebral ventricles, the posterior cistern, and the spinal intrathecal space. Acute injection of AAV vectors into the posterior cistern, without the use of any method to enhance distribution, has resulted in a relatively limited pattern of gene expression that appears analogous to that seen with ventricular injection (Fu et al., 2003). On the other hand, methods to improve vector distribution upon cisternal administration, such as pretreatment with mannitol delivered intravenously or removal of some CSF followed by a large injection volume, have shown the potential for an enhanced pattern of gene expression spanning several CNS regions (Fu et al., 2003; Iwamoto et al., 2009).

Surgical access to the posterior cistern has also been used for intrathecal catheter placement with the goal of delivery of AAV6 or AAV8 directed at the lumbar spinal level (Towne et al., 2009; Storek et al., 2008). Substantial transduction of lumbar dorsal

root ganglion (DRG) neurons was achieved in both of these studies. Additionally, Towne et al (2009) observed transduction in cervical DRG and several areas of the brain. An alternative method for delivery to the lumbar intrathecal space is direct lumbar puncture, which is minimally invasive, does not require anesthesia, presents negligible risk for tissue damage, and has long been used both experimentally and clinically.

In chapter 2 we demonstrated transduction of DRG neurons following delivery of AAV5, AAV8 and AAV9 by direct lumbar puncture with an intravenous mannitol pretreatment. The initial goal of the current study was to determine the extent of expression in the CNS after lumbar puncture delivery of AAV5 with intravenous mannitol pretreatment. The goal has since expanded to compare the results obtained with AAV5 to those from animals given AAV9. Using immunohistochemical (IHC) techniques, we have characterized the distribution of transgene expression in mouse brain after intrathecal AAV5 or AAV9.

METHODS

AAV Vector and Packaging

AAV vector TRUF11, containing a CAGS-regulated GFP sequence, has been previously described (Kaemmerer et al., 2000). Packaging using AAV5 serotype capsid was carried out at the University of Florida Vector Core Lab of the Gene Therapy Center (Gainesville, Florida) as previously described (Kaemmerer et al., 2000). AAV9 vector was purchased from the vector core at University of Pennsylvania (AV-9-PV1963).

Animals

Experimental subjects were 20 to 25g adult male C57BL/6 mice (Harlan, Madison, WI). All experiments were reviewed and approved by the Institutional Animal Care and Use Committee (IACUC) of the University of Minnesota.

Injections

Subjects were injected via the tail vein with 25% mannitol solution (200 μL), or saline, twenty minutes prior to intrathecal injection of the viral construct. The AAV construct was delivered intrathecally by direct lumbar puncture in awake mice by an experimenter (KFK) with extensive experience in this method of drug delivery (Hylden and Wilcox, 1980). A minor modification of the protocol was required to conserve AAV vector. The needle (30-gauge, 0.5-inch) was connected to a length of PE10 tubing, which was then connected to a second needle that was attached to a 50-μl Luer-hub Hamilton syringe. Ten microliters of the construct containing ~10^{11} viral vector genomes was injected intrathecally. The injection was administered by gripping gently the iliac crest of the rodent and inserting the needle (bevel side up) at about a 45° angle centered between the hipbones. A reflexive flick of the tail indicated puncture of the dura. Following the injection, the animals were returned to the vivarium where they remained for six weeks, until the time of transcardial perfusion, fixation, and extraction of fixed brain tissue for immunohistochemical analysis.

Immunohistochemistry

All animals were sacrificed by perfusion fixation as previously described (Vulchanova et al., 1998). Briefly, animals were isoflurane anaesthetized via nosecone inhalation and perfused with a solution of calcium-free tyrodes solution (in mM:NaCl 116, KCl 5.4,

$MgCl_2 \cdot 6H_20$ 1.6, $MgSO_4 \cdot 7H_2O$ 0.4, NaH_2PO_4 1.4, glucose 5.6, and $NaHCO_3$ 26) followed by fixative (4% paraformaldehyde and 0.2% picric acid in 0.1M phosphate buffer, pH 6.9) followed by 10% sucrose in PBS. Brain was removed and incubated in 10% sucrose overnight at 4˚C. Sections were cut at 14 μm thickness and thaw mounted onto gel-coated slides. Tissue sections were incubated for 1 hour at room temperature in diluent (PBS containing 0.3% Triton, 1% BSA, 1% normal donkey serum) and then incubated overnight at 4°C in primary antisera diluted in the same diluent. Primary antibodies used were: rabbit anti-GFP, 1:500 (Invitrogen; Eugene, OR), mouse anti-NeuN, 1:500 (Chemicon; Temecula, CA), mouse anti-GFAP, 1:400 (Sigma; St. Louis, MO), and mouse anti-calbindin, 1:1000 (Sigma; St. Louis, MO). After rinsing with PBS, sections were incubated one hour at room temperature with appropriate combinations of Cy2-, Cy3-, and Cy5- (1:300) conjugated secondary antisera (Jackson ImmunoResearch, West Grove, CA). Sections were rinsed again, and in some cases, were also incubated with DAPI nucleic acid stain for 3-5 minutes, 300nM (Invitrogen; Eugene, OR). Following the final rinses, sections were cover-slipped using glycerol and PBS containing 0.1% p-phenylenediamine (Sigma).

Microscopy

Anatomical analysis was based on the 'The Mouse Brain In Stereotaxic Coordinates', Second Edition (Paxinos and Franklin, 2001). Images for figures 3, 4, and 10 were collected at a resolution of 1600 by 1200 pixels on an Olympus BX60 fluorescence microscope with a Spot Insight camera and Spot image acquisition software. All other images were collected on an Olympus Fluoview 1000 confocal microscope with

associated software at a resolution of 512 by 512 pixels. Images were processed for fluorescence measurements using ImageJ, and for contrast, brightness and color in Adobe Photoshop.

Quantification

For quantification of number of fourth ventricle choroid plexus cells transduced, 3 sections per ventricle, spaced at least 100μm apart were counted for each of 4 animals. The total number of choroid plexus cells in each section was determined by counting nuclei within each ventricle identified by DAPI stain. Choroid plexus cells immuno-positive for GFP were identified by overlaying images of DAPI fluorescence and GFP-ir, and counting nuclei that were surrounded by GFP-ir. Two independent observers performed counts yielding results that consistently varied by less than six percent per section.

For quantification of transduced Purkinje cells, at least 6 sections, spaced at least 70μm apart, were counted for each of the 4 animals. Only Purkinje cell bodies that showed GFP-ir were counted, and were identified by co-labeling with calbindin-ir.

For visual scoring of expression intensity across brain regions, a single observer scored the selected regions from 1-6, with 6 being most intense. Scores were compiled across several slides and the highest score for each animal from each region was used for analysis. Difference scores were obtained by totaling the scores from all animals for each region from each treatment (N = 6 per group), then subtracting the saline treated-score from the mannitol-treated score. Statistics performed on the raw scoring data include

Mann-Whitney rank test and chi-squared analysis of number of scores above, and not above the median.

For quantification of fourth ventricle choroid plexus fluorescence intensity, at least 8 images were taken from at least 3 tissue sections spaced at least 100μm apart for each animal. Choroid plexus was outlined in each image based on background cy3 immunofluorescence, and measurements of GFP fluorescence intensity taken using ImageJ. All intensity measurements for a single animal were averaged, then values for each animal were used to compute group mean and error (N = 6 per group) for statistical analysis.

RESULTS

AAV5-mediated gene expression across brain regions after intrathecal delivery

Six weeks after intrathecal administration of AAV5-GFP with an intravenous mannitol pretreatment, GFP expression was observed in several areas of the central nervous system (CNS) as detailed in Figures 1-8. At the level of the medulla, GFP-immunoreactivity (-ir) was found in neuronal fibers in the gracile and cuneate nuclei (Figure 1), as well as in the external cuneate nucleus and the spinal trigeminal tract (Figure 2B and C). In the gracile, cuneate, and external cuneate nuclei these fibers are likely to have originated from primary sensory neurons in dorsal root ganglia (DRG), as supported by our previously published observations of GFP-ir in nerve fibers within the dorsal columns of spinal cord (Vulchanova et al., 2010). In line with this observation, fibers in the spinal trigeminal tract are likely to have originated from neurons in the

trigeminal ganglion. Expression was also observed in the vestibular, cochlear, and facial nuclei, and the area postrema (data not shown). In the solitary nuclear complex, GFP-ir was found in neuronal cell bodies as well as fibers (Figure 2D). The level of GFP expression in the nucleus of the solitary tract was low, but consistently observed.

In the fourth ventricle there was substantial GFP-ir in the choroid plexus (Figure 3), the structure that produces and secretes cerebrospinal fluid (CSF). Quantification of transduced choroid plexus cells throughout the ventricular system revealed that expression in the fourth ventricle was significantly higher than in the third or lateral ventricles (Figure 3D). This finding indicates that rostral flow through CSF from the injection site may be an important factor in vector distribution.

In cerebellum, GFP-ir was observed in Purkinje cells (Figure 4), as well as cell bodies and fibers of the granular cell layer (data not shown). Quantification of GFP-ir Purkinje cells co-labeled for calbindin showed a trend toward decreasing transduction of Purkinje cells in caudal-to-rostral fashion (Figure 4D). Although this trend did not reach significance, it supports the hypothesis that vector is distributed partially via diffusion through CSF.

Expression of GFP found in pons, midbrain and thalamus was primarily limited to neurons, with the exception of astrocytes in the cerebral peduncles. Co-localization of GFP-ir with NeuN-ir is shown in pontine nuclei (Figure 6F and G). Expression of GFP in midbrain nuclei was minimal, and was observed only in the dorsolateral margins (Figure 5B, lower right). In thalamus, GFP- ir was found in neurons of the medial geniculate

nucleus (Figure 6D and E), and to a lesser degree of the lateral geniculate, and posterior nuclei (Figure 7E).

GFP expression was observed in several caudal cortical areas. In primary visual cortex GFP-ir was seen in both neurons (Figure 5B) and astrocytes (Figure 5C) as evidenced by co-localization of GFP-ir with NeuN-ir or GFAP-ir respectively. GFP expression was also found in the pre-subiculum (Figure 5B), para-subiculum (Figure 5D), subiculum (Figure 5E) and lateral entorhinal cortex (Figure 5F). Astrocytes displaying GFP-ir were consistently observed in close proximity to GFP-ir neurons in cortical areas. Evaluation of more rostral brain regions revealed GFP expression in granule cells of the dentate gyrus (Figure 6B), as well as pyramidal cells of the CA3 region of hippocampus (Figure 6C). As shown in the left portion of Figure 6D, some GFP expression was also observed in the molecular layer of the dentate gyrus.

In regions further rostral, more substantial GFP expression was observed in granule cells of the ventral dentate gyrus and pyramidal neurons of the ventral hippocampus (Figure 7B). GFP-ir was found nearby in astrocytes in the cerebral peduncles (Figure 7B and C). Some GFP-expressing neurons were also observed in areas of the amygdala (Figure 7C and D). In addition, Figure 7D (upper right) illustrates GFP-ir in the choroid plexus of the lateral ventricles. Interestingly, in the same slice, but in the dorsal hippocampal formation, GFP expression was observed only in fibers of the molecular layer of the dentate gyrus and the stratum lacunosum-moleculare of the hippocampus (Figure 7E). At this level of the brain, scattered expression of GFP could still be found throughout the cortices, but was less than that observed in more caudal

regions (data not shown). Furthermore, expression was generally absent from striatum and surrounding neocortex, with the exception of a few neurons in the cingulate gyrus (data not shown). In the ventral forebrain, sparse GFP-ir was also found in the islands of Calleja and the olfactory tubercle (data not shown). In the olfactory bulbs expression of GFP was considerable, and appeared mostly restricted to neurons and astroglia in the medial portions of the glomerular, external plexiform, and mitral cell layers (Figure 8).

To determine if intravenous mannitol pretreatment had an effect on overall transduction by intrathecal AAV5, we visually scored several brain regions that displayed GFP-ir for relative intensity of expression in animals given a pretreatment of either intravenous mannitol or intravenous saline (Figure 9A). Scores were generated as described in methods, and are displayed in the figure as difference scores between the group sums of mannitol and saline pretreatments (mannitol group score - saline group score) to illustrate the trend. A positive score indicates greater observed expression in mannitol-pretreated animals. Though there was no significant difference between groups (Mann-Whitney $U_{0.05(2),6,6} = 27$, $p = 0.23$), all but two areas, cerebellum and the vestibulocochlear nuclear complex, were scored higher in mannitol-pretreated animals. We also quantified overall fluorescence of GFP-ir in choroid plexus of the fourth ventricle in the same animals (Figure 9B; $t_{0.05(2),10} = 1.272$, $p = 0.23$). Though statistical analysis revealed no significant difference between mannitol and saline pretreatments, there was an overall trend towards enhanced transduction by AAV5 with an intravenous mannitol pretreatment.

Overview of intrathecal AAV9-mediated gene expression in CNS

Six weeks after intrathecal administration of AAV9-GFP with a pretreatment of mannitol delivered intravenously, immunoreactivity for GFP was found throughout the brain (Figure 10). The overall pattern of relative expression intensity was comparable between AAV5 and AAV9 in that all areas highlighted by AAV5 were also highlighted by AAV9, as well as some additional areas. For example, areas that showed the highest expression after AAV5 also showed some of the highest expression after AAV9 (e.g. gracile and cuneate nuclei; Figures 1 and 10A), many areas that showed minimal to moderate expression after AAV5 showed more robust transduction after AAV9 (e.g. marginal regions of midbrain nuclei; Figure 10B), and in areas where GFP was not detected after AAV5 at least some low level of neuropil-like staining was observed after AAV9 (e.g. striatum; Figure 10G).

Images shown in Figure 10 were chosen for regional comparisons to AAV5 data and include the following: brainstem (10A bottom), cerebellum (10A top), midbrain (10B right), caudal cortex (10B left), rostral-dorsal hippocampal formation (10C and 10D), third ventricle with choroid plexus (10C center), rostral cortex (10C top, 10E left, 10F), and striatum (10E bottom right and 10G). After intrathecal AAV9, expression in limbic cortex appeared to be primarily neuronal (10B right), and expression in neocortex appeared to be primarily astrocytic (10E left, 10F), though both GFP-positive neurons and astrocytes were found throughout all cortex. Notably, expression in cortex after AAV9 was very patchy and appeared to be concentrated around blood vessels (10B and 10F), whereas cortical expression after AAV5 was more diffuse.

DISCUSSION

In this report we have demonstrated AAV-mediated gene delivery to CNS regions following direct lumbar puncture intrathecal injection of viral vector in combination with an intravenous mannitol pretreatment. These observations raise the possibility for development of CNS gene therapy approaches using this minimally invasive route of administration. Rostral distribution of viral particles has also been reported for rAAV6-GFP delivered to the lumbar intrathecal space via an indwelling catheter, although in this case the distribution of expression within specific brain regions was not evaluated (Towne et al., 2009). The process by which AAV vectors are distributed to rostral CNS regions after lumbar intrathecal delivery is not entirely clear. Here we discuss the potential contribution of diffusion through CSF and distribution through the vascular system as routes for the spread of virus particles as well as the influence of additional factors such as parenchymal accessibility and the presence of cell surface virus receptors.

We observed a caudal-to-rostral gradient of GFP expression within certain brain structures. For example, we found that a significantly larger portion of fourth ventricle choroid plexus cells express GFP relative to the third and lateral ventricles after AAV5. Considering the closer proximity of the fourth ventricle to the injection site, these results suggest that virus particles become less concentrated as they move through CSF rostral to the spinal column. Consistent with this observation, in cerebellum there appears to be a caudal to rostral trend from higher to lower number of GFP-expressing Purkinje cells. A similar trend was also observed with neurons and astrocytes of neocortex.

The expression of vector genes or protein products in peripheral tissues suggests that intrathecally delivered viral vectors may also be distributed through the vascular system. Expression was observed in the liver in our experiments (not shown), and the patchy appearance of expression around deep blood vessels in cortex after AAV9 suggests that some virus may be redistributed through the vasculature after intrathecal delivery of AAV vectors. The highly increased cortical transduction and distribution around blood vessels with AAV9 may be due in part to the ability of this serotype to readily bypass the blood-brain barrier (Samaranch et al., 2012, Gray et al., 2011; Foust et al., 2009).

The appearance of concentrated transduction around blood vessels in cortex has been reported previously with intracisternal delivery AAV9 (Samaranch et al., 2013; Samaranch et al., 2012); however, intravenous delivery of AAV9 results in a more uniform, evenly distributed pattern of transduction (Samaranch et al., 2012; Gray et al., 2011; Foust et al., 2009). This suggests that if vascular redistribution of virus particles is occurring after intrathecal delivery, it is distributed differently than when virus is delivered directly to the blood stream. This could potentially be explained by uneven local redistribution through CNS vasculature while concentration of virus remains high. To address this hypothesis, we injected the same total dose of virus that was given intrathecally, but delivered it intravenously after a mannitol pretreatment. After delivery of AAV5 by this method we saw no appreciable expression in the CNS (data not shown); however, after delivery of AAV9, expression was observed in a small number of astrocytes near blood vessels of neocortex. After intravenous AAV9, labeled astrocytes

were more disperse, rather than in clusters as observed after intrathecal delivery. This suggests that concentration of expression in close proximity to vasculature after intrathecal delivery of AAV9 is not due to recirculation throughout the entire blood stream. Instead it may be locally redistributed by vasculature within the CNS, either by entering the vessels or by some method of perivascular transport. Further experiments are needed to determine the method and extent of vascular distribution after intrathecal delivery of AAV9. All things considered, it appears likely that spread of AAV particles in general after intrathecal injection is dependent primarily on diffusion through the CSF, though some local vascular redistribution may occur.

A remarkable finding that does not fit with a simple caudal-to-rostral distribution of virus particles through the CSF is the relatively high level of GFP expression in the medial portion of the olfactory bulb that was observed with both serotypes tested. Although the mechanism by which this level of expression is achieved is unknown, other groups have reported similar findings after injection of other AAV serotypes (AAV1 and AAV2) into either the posterior cistern or the lumbar intrathecal space (Iwamoto et al., 2009; Watson et al., 2006; Fu et al., 2003). Considering the position of the olfactory bulb in a small recess at the rostral end of the skull, it is possible that in this pocketed structure CSF flow may be restricted in a way that increases the retention of virus particles. In fact, it is known that CSF is able to drain along the olfactory nerve through the cribriform plate, and that this drainage constitutes a major pathway for CSF absorption in multiple species (Mollanji et al., 2001; Kiwic et al., 1998; Williams et al., 1990; Erlich et al.,

1986). Significant CSF flow toward the olfactory nerve may cause virus particles following this current to get bottlenecked in the space near the olfactory bulb.

Another brain region where expression was notably high relative to surrounding regions and non-uniform within the structure is the hippocampal formation. GFP-positive cell bodies (primarily neuronal) were found in the hippocampal formation, and were most prevalent in the rostral-ventral and more caudal regions. Although GFP-ir was also present in the rostral-dorsal hippocampal formation, it was rarely found in neuronal cell bodies (Figures 7E, 10C and 10D) suggesting that the fiber-like staining originates from cell bodies in another location, and making this an interesting anatomical feature of intrathecal AAV-mediated transduction. Considering that we observed cell bodies in other portions of the hippocampal formation and the hippocampal-cortical loop (entorhinal cortex and subiculum), it is likely that the GFP-ir in rostral-dorsal hippocampus originates from one or more of these regions.

The distinct pattern of AAV transduction reported here might be the result of differences in expression of cell-surface receptors necessary for entry of virus particles. Specific cell surface molecules are required for binding and entry of particular AAV serotypes. In some cases co-expression of two different receptor molecules may be necessary for transduction (Qing et al., 1999). For AAV5, there are two known receptors: α2,3 N-linked sialic acid and platelet-derived growth factor receptor (PDGFR) types alpha and beta (Di Pasquale et al., 2003; Walters et al., 2001). There is currently no literature directly describing the pattern of expression of α2,3 N-linked sialic acid in the mouse brain. Preliminary data gathered in our lab using lectin-histochemistry to

investigate α2,3 N-linked sialic acid in DRG showed diffuse staining with no apparent relationship between labeling intensity and expression of vector-delivered GFP (unpublished). For both PDGFR alpha and beta, high expression levels have been reported in CNS regions where AAV5 transduction was limited or absent in our experiments, suggesting that PDGFR is not the limiting factor for transduction by AAV5 in the CNS (Ishii et al., 2006; Fruttiger et al., 1999). Further investigation into expression of AAV receptors in the CNS may lead to a greater degree of predictability for transduction patterns of various serotypes.

In summary, the pattern of transduction in the CNS following intrathecal administration of an AAV vector with an intravenous mannitol pretreatment appears to be the result of several factors discussed above, including: rostral movement through CSF, overall CSF flow, parenchymal permeability, and expression of cell surface receptors for virus particles. The current study has revealed that under appropriate delivery conditions, specific brain areas appear highly susceptible to transduction by AAV5 and AAV9, resulting in a pattern that highlights certain anatomical features of the CNS.

TRANSITION

These data indicate the potential for future studies of genetic manipulation in various brain regions via intrathecal AAV vectors; however, the overall goal of this thesis is to develop the use of AAV vectors for gene-transfer to primary sensory neurons for the study of analgesic interactions and modulation of pain transmission at the spinal level. The results in chapter 2 demonstrated differential transduction of DRG neurons by AAV vectors delivered intrathecally. The data in chapter 3 has illustrated that intrathecal

administration of AAV vectors also results in significant transduction of several brain regions.

With AAV5, expression in brain was relatively low compared to that observed in lumbar and cervical DRG indicating that off-target effects of trans-genes delivered by AAV5 are unlikely to play a significant role in the results obtained in study of pain modulation at the spinal level. Transduction of DRG neurons, as well as across the CNS, was much more robust with AAV9 than with AAV5. The very high level of expression across brain regions after AAV9 indicates that this vector must be used cautiously when trying to evaluate effects of trans-genes in specific regions, and that it would be highly suitable for cases where widespread CNS expression is the goal. Very strong generic promoters, such as CMV and Cags, are typically used with AAV vectors, as tissue specific promoters have resulted in much lower expression levels. In the case of AAV9, where transduction and expression levels are so high, tissue specific promoters could be the best option for studies of expression in specific areas of the nervous system. For example relative to the current goals, intrathecal deliver of AAV9 with a promoter that is specific to DRG neurons would provide a high degree of specificity, while possibly retaining a substantial level of expression. Further studies using tissue specific promoters with AAV9 are needed to better evaluate how expression levels will be affected. In chapter 4, the focus shifts to spinal opioid adrenergic analgesic interactions, and associated protein targets for genetic manipulation by the AAV vectors that have been covered in chapters 2 and 3.

FIGURES

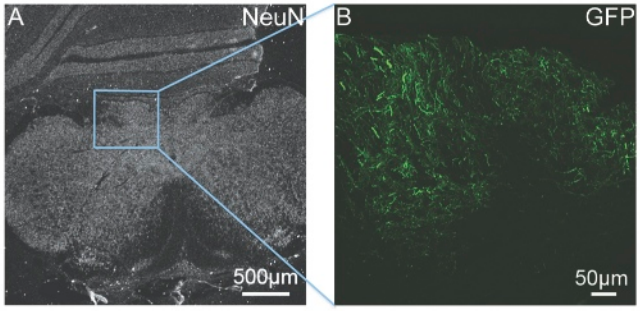

Figure 1. GFP-ir fibers in somatosensory nuclei of the medulla. **A)** Low-magnification image showing the pattern of NeuN-ir in this tissue section. **B)** GFP-ir in the gracile (right) and cuneate (left) nuclei.

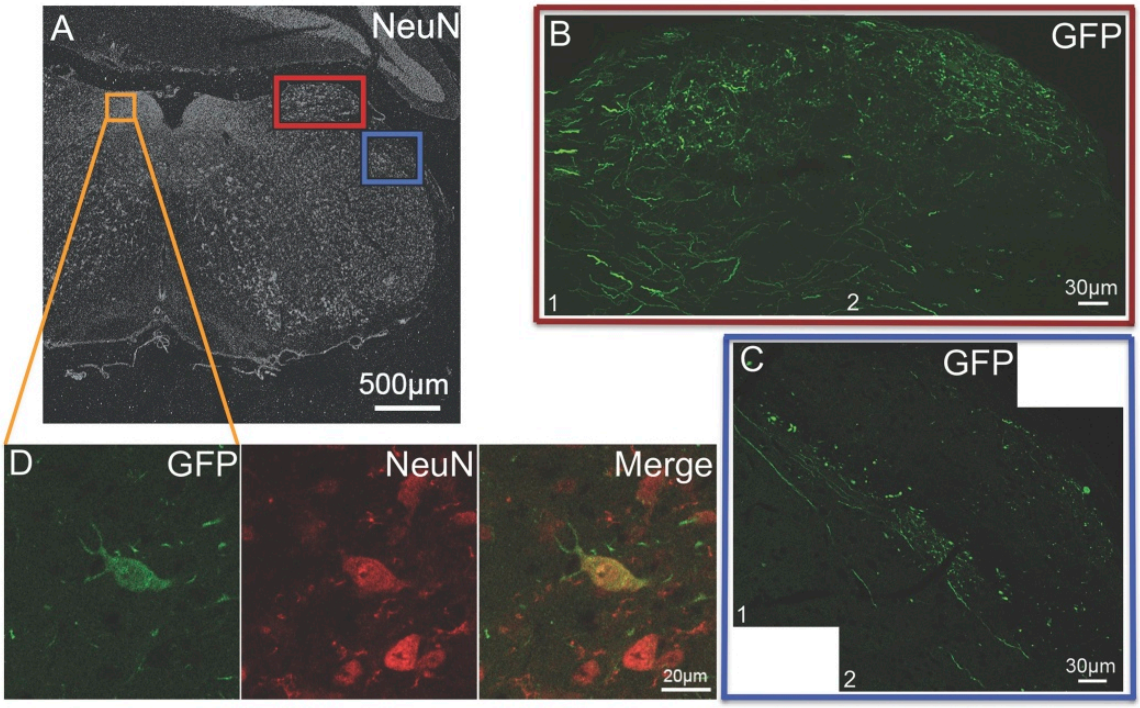

Figure 2. GFP-ir in other sensory nuclei of the medulla. **A)** Low-magnification image showing the pattern of NeuN-ir in this tissue section. Colored inset boxes show the locations of the images from B-D. **B)** GFP-ir in the external cuneate nucleus. Images were collected sequentially (as indicated by numbering) with identical settings. **C)** GFP-ir in the spinal trigeminal tract (center) and inferior cerebellar peduncle (right). Images were collected sequentially (as indicated by numbering) with identical settings, and were processed identically. **D)** A GFP-positive neuron in the nucleus of the solitary tract.

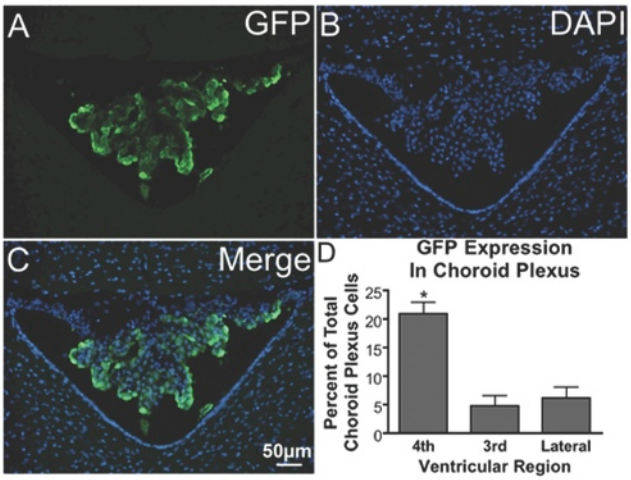

Figure 3: GFP expression in the choroid plexus. **A)** GFP-ir in choroid plexus of the 4th ventricle. **B)** DAPI staining in the same section showing cellular nuclei in the choroid plexus (center), cerebellum (top), and medulla (bottom left and right). **C)** Overlay of images in A and B showing a substantial portion of the choroid plexus cells to be transduced. **D)** Graph illustrating that transduction of choroid plexus cells is significantly higher in the 4th ventricle compared to the third and lateral ventricles ANOVA; $p<0.01$ (n=4).

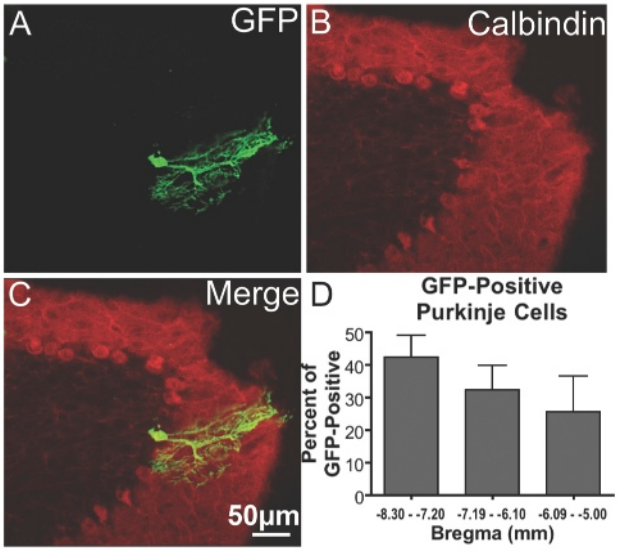

Figure 4. GFP-ir in Purkinje cells of the cerebellum. **A)** GFP-ir, showing one labeled-cell. **B)** Calbindin-ir illustrating the difference in morphology between the molecular, Purkinje, and granule cell layers of the cerebellum. **C)** Overlay of images in A and B illustrating that this GFP-positive neuron is a Purkinje cell. **D)** A graph showing the fraction of GFP-positive Purkinje cells found at different distances from Bregma, which indicates a trend towards decreasing transduction of Purkinje cells in more rostral portions of cerebellum (n=4).

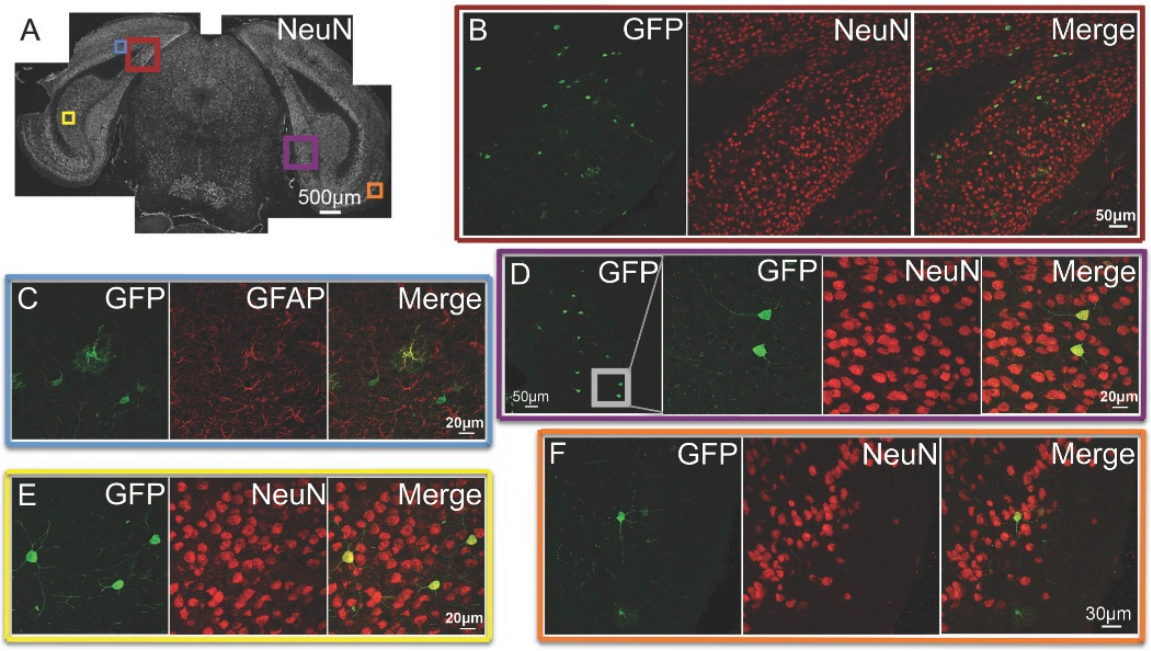

Figure 5. Co-localization of GFP with neuronal and astroglial markers in caudal cortex. **A)** Low magnification image of NeuN-ir. Colored inset boxes show the locations of images from B-F. **B)** GFP-ir neurons of primary visual cortex (top) and presubiculum (bottom). Cells with astrocytic morphology are also observed in these areas. **C)** Co-localization of GFP-ir with GFAP-ir illustrates that astrocytes are also transduced, and can be distinguished by their morphology. **D)** GFP-ir in neurons of the subiculum. **E)** GFP-ir is also observed in neurons of the parasubiculum. **F)** GFP-ir in neurons and an astrocyte in lateral entorhinal cortex.

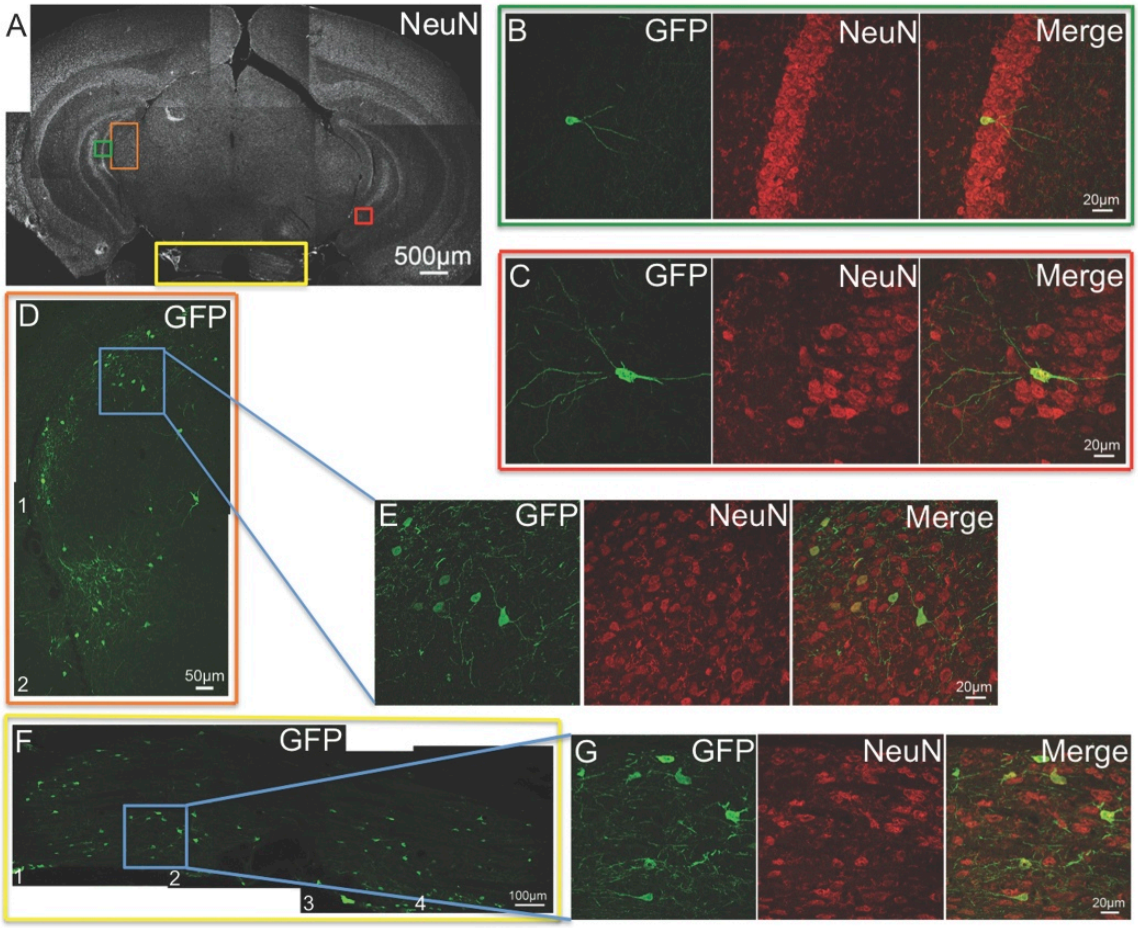

Figure 6. GFP expression in the caudal thalamus, hippocampal formation, and pons. **A)** Low magnification image of NeuN-ir illustrating the relative anatomy of the tissue section. Colored inset boxes show the locations of images in B-G. B-G) Green shows GFP-ir, red shows NeuN-ir, and merged images illustrate co-localization in yellow. D and F) Images for each layout were collected sequentially (as indicated by numbering) with identical settings, and were processed identically. **B)** A GFP-positive neuron in the granular layer of the dentate gyrus. **C)** A GFP-positive neuron in the pyramidal layer of hippocampus area CA3. **D)** GFP-ir in the medial geniculate nucleus (MGN) of the thalamus. **E)** High magnification image of the area outlined by the blue box in D,

illustrating that expression in the MGN is neuronal. **F)** GFP expression in pontine nuclei. **G)** High magnification image of the area outlined by the blue box in F, illustrating co-localization with NeuN-ir.

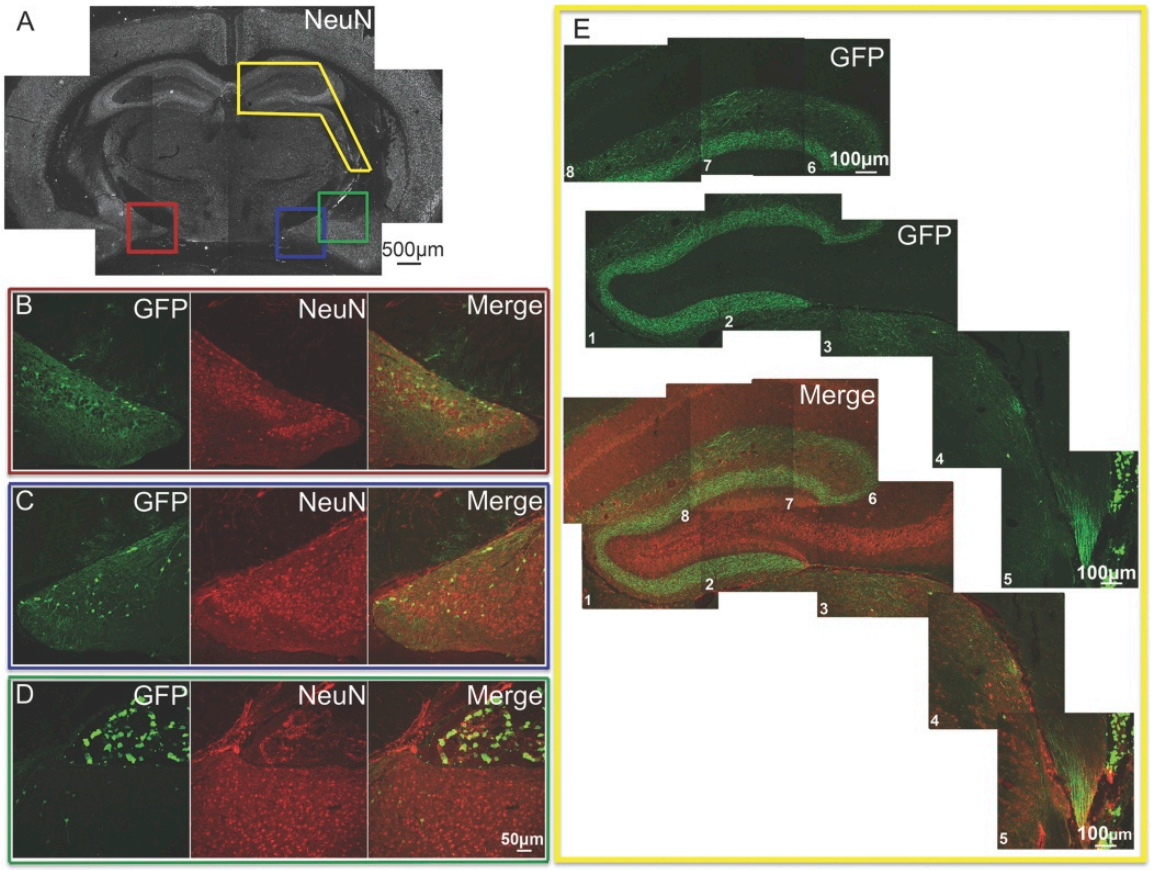

Figure 7. GFP expression in the hippocampal formation, amygdala, and thalamus. **A)** Low magnification image of NeuN-ir to show the relative anatomy of this section. Colored inset boxes show the locations of images in B-E. B-E) Green shows GFP-ir, red shows NeuN-ir, and merged images show co-localization in yellow. **B)** Substantial GFP expression in cells of the ventral dentate gyrus, ventral hippocampus, and superior to those, astrocytes in the cerebral peduncle. **C)** GFP-ir in ventral dentate gyrus and amygdala on the opposite side of the slice, and superior to those, astrocytes in the cerebral peduncle. **D)** GFP expression in the amygdala, and superior to that, in choroid plexus. **E)** Layout showing GFP-expression in the dorsal hippocampal formation (image numbers 1-3 and 6-8), and inferior and lateral to that, in thalamus including portions of

the lateral geniculate, and posterior nuclei (image numbers 3-5). Note that GFP-ir in the dorsal hippocampal formation appears restricted to fibers in the molecular layer of the dentate gyrus and the stratum lacunosum of the hippocampus. Images 1-5 were collected sequentially with identical settings, and were processed identically. Images 6-8 were collected sequentially with identical settings at a later date than images 1-5, processed identically, and were rotated slightly and cropped for the combined merge layout.

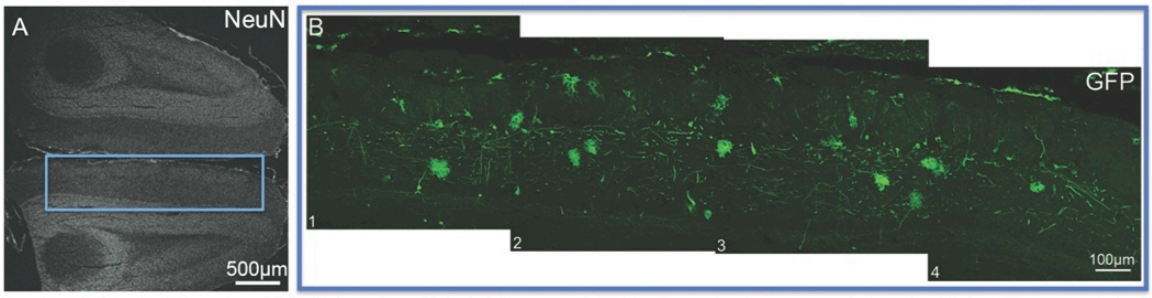

Figure 8. GFP expression in the olfactory bulb. **A)** Low magnification image showing NeuN-ir in the olfactory bulb. **B)** GFP-ir in what appear to be both neurons and astrocytes in the glomerular, external plexiform, and mitral cell layers of the medial olfactory bulb. Images were collected sequentially (as indicated by numbering) with identical settings, and were processed identically.

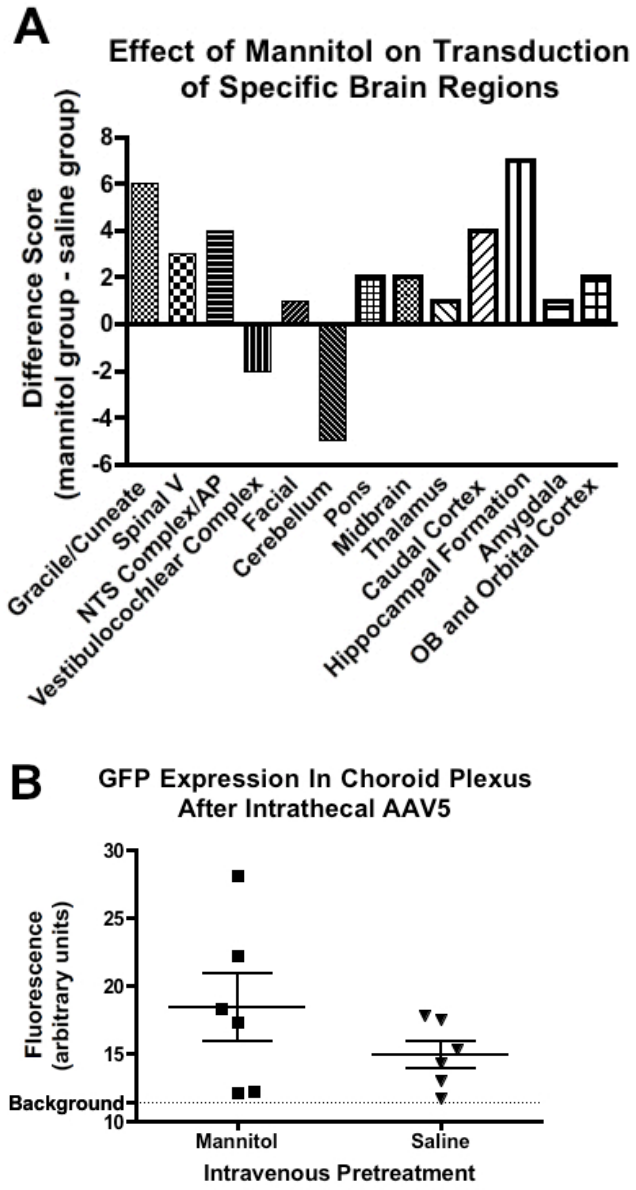

Figure 9. Quantification of GFP expression in brain and fourth ventricle choroid plexus after intrathecal AAV5 with or without an intravenous mannitol pretreatment. **A)** Several brain regions expressing GFP were scored for relative intensity, and individual scores were summed to make group scores. The difference score is equal to mannitol group score minus the saline group score. **B)** Quantification of GFP fluorescence intensity in fourth ventricle choroid plexus ($t_{0.05(2),10} = 1.272$, $p = 0.23$).

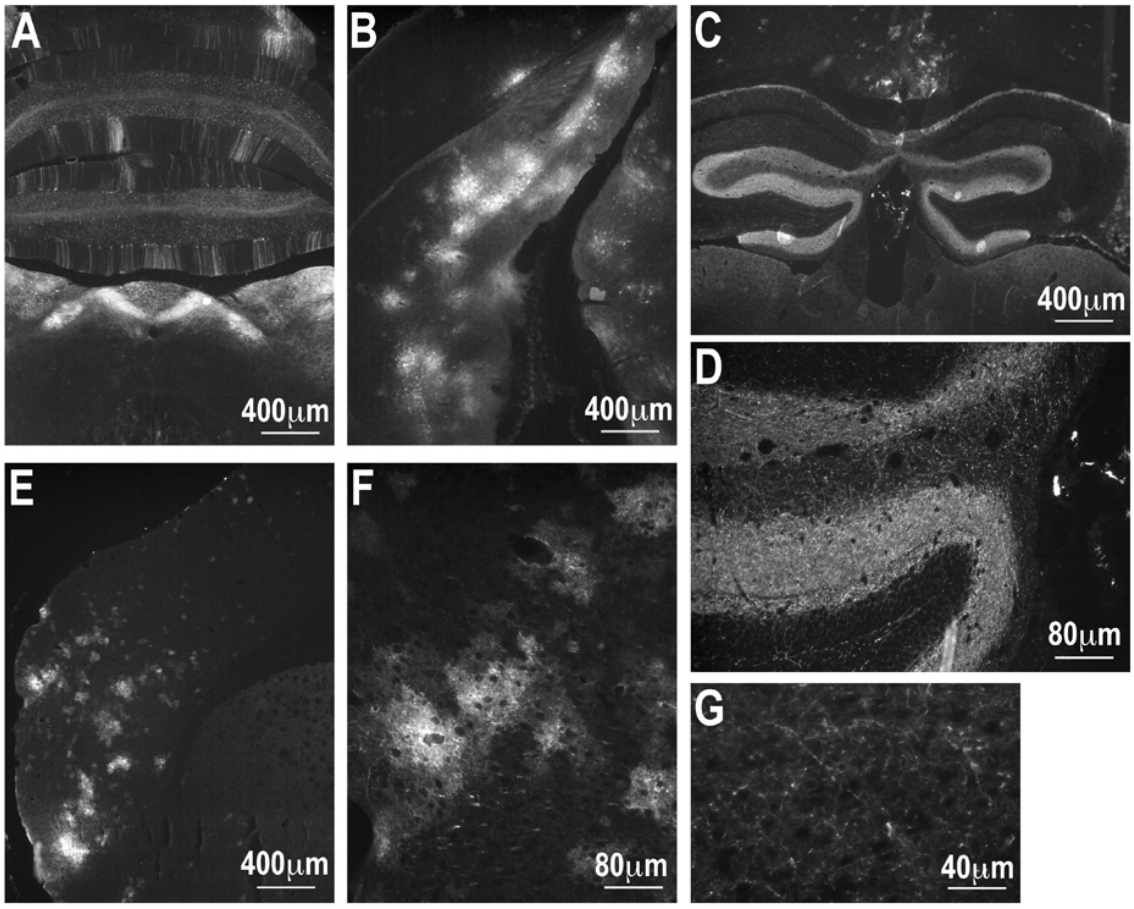

Figure 10. Overview of GFP expression across brain regions after intrathecal AAV9 with an intravenous mannitol pretreatment. **A)** Brainstem (bottom) and cerebellum (top). **B)** Midbrain (right) and caudal cortex (left). **C)** Rostral-dorsal hippocampal formation (center), third ventricle with choroid plexus (center), rostral cortex (top), and thalamus (bottom). **D)** Higher magnification of left side of hippocampal formation shown in C. **E)** Rostral cortex (left) and striatum (bottom right). **F)** Higher magnification of rostral cortex shown in E. **G)** High magnification image of striatum shown in E, showing low-level expression in an area that looks blank at low magnification.

Chapter 4

Protein kinase C-epsilon is required for spinal analgesic synergy between delta opioid and alpha-2A adrenergic receptor agonist pairs

The work presented in this chapter has been published in the article listed below.

Schuster DJ, Kitto KF, Overland AC, Messing RO, Stone LS, Fairbanks CA, Wilcox GL. Protein kinase Cε is required for spinal analgesic synergy between delta opioid and alpha-2A adrenergic receptor agonist pairs. *The Journal of Neuroscience* 2013, 33(33).

Author contributions from the publication:
DJS designed research, performed research, analyzed data and drafted the manuscript
KFK performed research
ACO designed research and edited the manuscript
ROM contributed published and unpublished reagents
LSS designed research and edited the manuscript
CAF designed research and edited the manuscript
GLW designed research and edited the manuscript

Synergistic analgesic interactions at the spinal level between delta opioid receptors (delta-ORs) and alpha$_{2A}$ adrenergic receptors (alpha$_{2A}$-ARs) have recently been shown to require protein kinase C (PKC). To identify which PKC isoforms contribute to analgesic synergy, we evaluated the effects of various PKC isoform-specific peptide inhibitors on synergy between delta-ORs and alpha$_{2A}$-ARs using the tail flick assay of thermal nociception in mice. Only a PKC-epsilon inhibitor abolished synergy between a delta-OR agonist and an alpha$_{2A}$-AR agonist. We tested a panel of combinations of opioid and adrenergic agonists in PKC-epsilon knockout mice and found that all four combinations of a delta-OR agonist and an alpha$_{2A}$-AR agonist required PKC-epsilon for antinociceptive synergy. None of the combinations of a mu-OR agonist with an alpha$_2$-AR agonist required PKC-epsilon. Immunohistochemistry confirmed that PKC-epsilon could be found in the population of peptidergic primary afferent nociceptors where delta-ORs and alpha$_{2A}$-ARs have been found to extensively co-localize. Immunoreactivity for PKC-epsilon was found in the majority of dorsal root ganglion neurons, and intensely labeled laminae I and II of the spinal cord dorsal horn. Protein kinase C-epsilon is widespread in the spinal nociceptive system, and in peptidergic primary afferents it appears to be specifically involved in mediating the synergistic interaction between delta-ORs and alpha$_{2A}$-ARs.

INTRODUCTION

Synergistic analgesic interactions between agonists of α_2-adrenergic receptors (α_2ARs) and opioid receptors (ORs) in rodents have been well documented (Hylden and Wilcox, 1983; Sullivan et al., 1987; Wilcox et al., 1987; Stone et al., 1997; Overland et al., 2009; Riedl et al., 2009), and poly-analgesic therapy using spinal co-administration of α_2AR and OR agonists can reduce opioid requirements for pain management in the clinic (Forster and Rosenberg, 2004; Paech et al., 2004; Gregoretti et al., 2009). The α_{2A}- and α_{2C}AR subtypes, and all three OR subtypes (μ, δ, κ) have been established as modulators of pain signaling at the spinal level (Stone et al., 1997; Fairbanks et al., 2002; Olave and Maxwell, 2002; Chakrabarti et al., 2010; Li et al., 2010). Certain α_2AR agonists, such as clonidine (CLON) and brimonidine (BRIM), require the α_{2A}AR-subtype for spinal analgesic efficacy, and analgesic synergy with OR agonists (Stone et al., 1997; Fairbanks and Wilcox, 1999).-Anatomical studies have shown that α_{2A}ARs are extensively co-localized with δORs in terminals of substance P-expressing primary afferent fibers in rodents (Overland et al., 2009; Riedl et al., 2009), making these receptors a good pair for investigation of intracellular mechanisms of spinal opioid-adrenergic analgesic synergy. Protein kinase C (PKC) has been established as an intracellular mediator of analgesic synergy between α_{2A}ARs and δORs, both *in vivo* and *in vitro*. Inhibition of PKC i) blocks *in vivo* synergy between spinally co-administered CLON and deltorphin II (DELT) in the mouse tail flick test, and ii) blocks *in vitro* CLON-DELT synergistic inhibition of depolarization-evoked calcitonin gene-related peptide (CGRP) release from rat spinal cord slices (Overland et al., 2009). In order to determine if a specific isoform of PKC

mediates the synergistic interaction between α_{2A}ARs and δORs, we evaluated the ability of isoform-specific PKC inhibitor peptides to prevent spinal BRIM-DELT synergy. Inhibitors of the α, β (Ma et al., 2006), δ (Chen et al., 2001), and ε (Johnson et al., 1996) isoforms of PKC were tested, but only the PKCε inhibitor prevented BRIM-DELT synergy. To confirm and extend this finding, a battery of combinations of OR and AR agonists was tested for spinal analgesic synergy in mice genetically lacking PKCε. Additionally, the PKCε activator peptide ΨεRACK (Dorn et al., 1999) was used to determine if activation of PKCε is sufficient to enhance potency of either BRIM or DELT delivered singly. Finally, expression of PKCε in spinal cord and dorsal root ganglia was evaluated using immunohistochemistry to determine if PKCε is expressed in spinal terminals of peptidergic nociceptors where analgesic synergy between α_{2A}ARs and δORs is thought to occur.

METHODS

Animals

Adult C57BL/6J PKCε wild-type (PKCε-WT), knockout (PKCε-KO) and heterozygous mice of both sexes (20±5g) used for all experiments were bred from pairs of hybrid (50% C57BL/6J, 50%129S4) mice heterozygous for the mutant PKCε gene (Khasar et al., 1999), and were maintained on a 12-hour light/dark cycle with food and water available *ad libitum* to all animals. Heterozygous mice were used only for the PKC isoform-specific peptide inhibitor experiments to conserve WT and KO mice as well as to make efficient use of all mice bred. Data from the thesis of Aaron C. Overland demonstrated

that PKCε-heterozygous mice show synergy between α_{2A}AR and δOR agonists that is comparable to that of PKCε-WT mice (ACO Thesis Chapter 4, Figures 5 and 6). All experiments were approved by the Institutional Animal Care and Use Committee of the University of Minnesota.

Drug Preparation and Administration

Agonists used were deltorphin II (Tocris Bioscience; Bristol, UK), SNC80, brimonidine (UK 14,304), clonidine, morphine sulfate, and endomorphin II (all from Sigma; St. Louis, MO). The peptide activator of PKCε (ΨεRACK; HDAPIGYD; Dorn et al., 1999) and isoform-specific peptide inhibitors of PKC including the PKCα/β inhibitor FARKGALRQ (Ma et al., 2006), PKCδ inhibitor SFNSYELGSL (Chen et al., 2001), and PKCε inhibitor EAVSLKPT (Johnson et al., 1996), were purchased from Biomatik (Wilmington, DE). The scrambled PKCε inhibitor (LSETKPAV) was from Anaspec (Fremont, CA). Peptide inhibitors or activator were administered 30min prior to agonist administration, and were preceded by an injection of 5 μL distilled water to produce hypo-osmotic shock and facilitate passage of peptides through cell membranes (Khasar et al., 1999; Aley et al., 2000). Brimonidine was dissolved in a solution of 80% acetone, 6% DMSO and normal saline to form a stock solution. SNC80 was dissolved with an equimolar amount of tartaric acid in saline. All other drug stocks were prepared in normal saline. All drugs were diluted from stock solution into sterile 0.9% saline and injected intrathecally in a volume of 5 μL in awake mice by the method of Hylden and Wilcox (1980).

Behavioral Measures

Thermal nociceptive responsiveness was assessed using the warm water (52.5°C) tail immersion assay as previously described (Janssen et al., 1963). Briefly, each animal was gently held wrapped in a cloth, and the tail dipped into a controlled temperature water bath. Withdrawal latency was recorded as the amount of time that passed before a rapid movement of the tail, and was not allowed to exceed 12 seconds. A baseline latency was recorded prior to drug administration, and subsequent latencies were recorded 7 min after each dose, immediately before the next dose. Each agonist or combination was administered sequentially approximately every 7 min in increasing doses to generate a cumulative dose-response curve, each mouse receiving no less than three, and no more than four doses (Shin and Eisenach, 2003). Each dose-response curve was generated with an N of 4 to 6 as indicated in each table or legend. For DELT, two dose-response curves were obtained on separate days to confirm the potency and efficacy of this drug in the PKCε mutant mice. These curves did not differ significantly in potency or efficacy and were combined for a total N of 12. This curve was then reused in the analysis for each combination tested. This allowed us to minimize the number of animals necessary to complete this study. Data are represented as percent maximum possible effect (%MPE) values, which are determined using the following equation:

100*(test-baseline)/(maximum-baseline)

Immunohistochemistry

All animal tissues were fixed by intracardial perfusion as previously described (Vulchanova et al., 1998). Tissue sections were cut at 14 μm thickness and thaw-mounted onto ProbeOn slides. Tissue sections were incubated for 1 hour at room temperature in

permeabilization buffer (TBS containing 0.2% Triton x-100, 0.2% Tween-20) and then incubated overnight at room temperature in primary antisera diluted in blocking buffer (TBS containing 0.2% Tween-20, 0.2% casein). Primary antibodies used were as follows: rabbit anti-PKCε (1:2000; Santa Cruz Biotechnology, Santa Cruz, CA); guinea pig anti-substance P (SP; 1:1000; Neuromics, Edina, MN); mouse anti-CGRP (1:2000; Research Biochemicals International, Natick, MA); mouse anti-PKCε (1:300; Santa Cruz Biotechnology, Santa Cruz, CA); rabbit anti-δOR (Dado et al., 1993; raised against amino acids 103-120 of δOR); and rabbit anti-α_{2A}AR (Stone et al., 1998). After rinsing with TBS, sections were incubated one hour at room temperature with Cy3- or Cy5-conjugated secondary antisera (1:500; Jackson ImmunoResearch, West Grove, CA). Sections were rinsed again in TBS, dehydrated through a series of increasing ethanol concentrations followed by xylenes, and coverslipped using DPX mounting medium. Tissues were visualized using an Olympus FluoView 1000 BX2 upright confocal microscope, and images processed for color, contrast and brightness using Adobe Photoshop.

Data Analysis

The ED_{50}, in nanomoles (nmol), and 95% confidence limits (CLs) of all agonists and combinations were calculated using the graded dose-response curve method of Tallarida and Murray (1987). Dose ratios for drug combinations were estimated based on comparison of ED_{50} values and dose-response curves, and were chosen to approximate equi-effective doses. Isobolographic analyses were performed using the numerical method (Tallarida et al., 1989; Ossipov et al., 1997). Theoretical additive and observed

combination ED_{50} values were compared statistically via the Student's t-test with the JFlashCalc Pharmacological Calculations Program software package generously provided by Dr. Michael Ossipov (Department of Pharmacology, University of Arizona College of Medicine, Tucson, AZ). For all isobolograms, error bars for theoretical additive and observed combination ED_{50} values represent the vector sum of vertical and horizontal confidence limits.

RESULTS

Selective inhibition of PKCε prevents analgesic synergy between brimonidine and deltorphin II

To determine if a specific isoform of PKC is necessary for spinal analgesic synergy between an α_{2A}AR agonist and a δOR agonist, we evaluated whether intrathecal pretreatment with various isoform-specific peptide inhibitors of PKC could prevent synergy between spinally delivered BRIM and DELT in the warm-water tail immersion assay. Isobolographic analysis revealed that pretreatment with 6nmol of either a PKCα/β dual isoform inhibitor (FARKGALRQ; Ma et al., 2006) or a PKCδ inhibitor (SFNSYELGSL; Chen et al., 2001) had no effect on analgesic potency or efficacy of BRIM and DELT co-administered in approximately equi-effective doses; however, pretreatment with a PKCε inhibitor (EAVSLKPT; Johnson et al., 1996) significantly reduced potency of the BRIM-DELT combination such that the interaction was no longer synergistic (Figure 1, Table 1). Additionally, a scrambled version of the PKCε inhibitor (LSETKPAV) had no effect on potency of co-delivered BRIM and DELT (Figure 1,

Table 1). These results indicate that of the four isoforms evaluated, only the epsilon isoform of PKC is involved in spinal analgesic synergy between agonist combinations acting at α_{2A}ARs and δORs. Numerical details for all statistical analyses are reported in Table 1.

Spinal analgesic synergy between δOR and α_{2A}AR agonists requires PKCε

To confirm that PKCε plays a role in spinal analgesic synergy between α_{2A}ARs and δORs, various α_{2A}AR and δOR agonists were administered intrathecally (i.t.) to PKCε-knockout (PKCε-KO) and wild type (PKCε-WT) littermates, and the effect of each single drug and each drug combination was evaluated using the warm-water tail immersion assay. Each of the δOR agonists, DELT or SNC80, was co-administered i.t. in approximately equi-effective doses with each of the α_{2A}AR agonists, CLON and BRIM. All agonists produced comparable antinociception in both PKCε-WT and PKCε-KO mice when administered alone (Table 2). All four combinations of an α_{2A}AR agonist and a δOR agonist produced analgesic synergy in PKCε-WT mice; however, none of these combinations synergized in PKCε-KO mice (Table 2). Dose-response curves and isobolograms for the BRIM + DELT (1:1) combination are shown in Figure 2 as representative examples of the synergistic interaction between the α_{2A}AR and δOR agonist combinations in WT but not in PKCε-KO mice. These data indicate that spinal analgesic synergy between α_{2A}ARs and δORs requires PKCε. Numerical details for all statistical analyses are reported in Table 2.

Analgesic synergy between μOR and α_2AR agonists does not require PKCε

To determine if PKCε is necessary for analgesic synergy between α_2ARs and μORs, each of the μOR agonists, morphine (MOR) and endomorphin II (ENDO), was co-administered i.t. in approximately equi-effective doses with CLON or BRIM, and tested using the warm-water tail immersion assay. Both MOR and ENDO produced antinociception that was comparable between PKCε-WT and PKCε-KO mice (Table 3). All four combinations of α_{2A}AR and μOR agonists produced analgesic synergy in both PKCε-WT and PKCε-KO mice (Table 3). Dose-response curves and isobolograms for the BRIM + MOR (1:1) combination shown in Figure 3 indicate that PKCε is not required for synergy between α_{2A}ARs and μORs. These data suggest that synergistic interactions between α_{2A}ARs and μORs occur through different mechanisms than those mediating synergy between α_{2A}ARs and δORs, and are independent of PKCε. Numerical details for all statistical analyses are included in Table 3.

Activation of PKCε does not alter potency or efficacy of brimonidine or deltorphin II delivered singly.

To determine if activation of PKCε is sufficient to enhance potency of α_{2A}AR or δOR agonists given singly, we preceded BRIM or DELT dosing with a pretreatment of the PKCε activator ΨεRACK (Dorn et al., 1999). Intrathecal delivery of ΨεRACK caused significant hyperalgesia as expected (Joseph and Levine, 2010). This hyperalgesia was dose-dependent (data not shown) and peaked at 30 min post delivery (Figure 4). Pretreatment with ΨεRACK had no effect on the potency or efficacy of BRIM or DELT

(Figure 4) indicating that activation of PKCε is not sufficient to enhance potency of these agonists when they are delivered alone.

Immunohistochemical evaluation of localization of PKCε in spinal cord and dorsal root ganglion.

To determine if PKCε is located in peptidergic primary afferent nociceptors, where spinal analgesic synergy between δORs and α_{2A}ARs is thought to occur, sections of spinal cord and lumbar dorsal root ganglion (DRG) were co-labeled with antibodies directed against PKCε and each of the following: substance P (SP), CGRP, α_{2A}AR and δOR. Similar to previous reports (Khasar et al., 1999; Hucho et al., 2005; Wu et al., 2012), PKCε-immunoreactivity (-ir) was observed in a large majority of DRG neurons (Figure 5), as well is in laminae I and II of the superficial dorsal horn of the spinal cord (Figure 6). As expected, PKCε-ir was not present in spinal cord or DRG of PKCε-KO mice (data not shown). In DRG, a sub-population of CGRP- and SP-expressing neurons also displayed PKCε-ir (Figure 5). In superficial dorsal horn, PKCε-ir was found in a portion of puncta displaying CGRP-ir or SP-ir (Figure 6). Additionally, we found that PKCε-ir partially co-localizes with both α_{2A}AR-ir and δOR-ir in the superficial dorsal horn (Figure 6). This pattern of labeling indicates that PKCε is found in the location consistent with its role in mediating synergistic interactions between α_{2A}ARs and δORs. While the pattern of labeling in superficial dorsal horn appears typical of that associated with incoming primary afferent terminals, closer examination at higher magnification revealed that PKCε-ir can also be found in neuronal cell bodies intrinsic to laminae I and

II of the spinal cord as evidenced by co-localization of PKCε-ir with ir for the neuronal label NeuN (data not shown). Together these results indicate that PKCε is expressed by multiple types of neurons involved in nociceptive processing at the spinal level.

DISCUSSION

The current study demonstrates that PKCε is necessary for synergistic analgesic interactions between α_{2A}AR and δOR agonists at the spinal level *in vivo*. In contrast, other combinations that produce spinal analgesic synergy, such as those involving α_2ARs and μORs, do not require PKCε. As previous reports have placed α_{2A}ARs and δORs on the spinal terminals of peptidergic primary afferent neurons (Riedl et al., 2009) and shown that α_{2A}AR and δOR agonists synergistically inhibit CGRP release from spinal cord slices (Overland et al., 2009) and spinal synaptosomes (Riedl et al., 2009), our behavioral data are consistent with the observations that PKCε co-localizes with α_{2A}ARs, δORs, SP and CGRP. Immunolabeling of δORs and subsequent identification of δOR localization within either peptidergic or non-peptidergic subpopulations of sensory neurons remains controversial. Considering this controversy, we believe that the functional evidence linking δOR agonists to inhibition of peptide release from primary afferents (Bao et al., 2003; Kondo et al., 2005; Wang et al., 2010; Beaudry et al., 2011) and the demonstrated involvement of PKC in the synergistic inhibition of CGRP release by co-administered α_{2A}AR and δOR agonists in spinal cord (Overland et al., 2009) strongly support co-localization of δORs and α_{2A}ARs in peptidergic primary afferents. Factoring in the observed co-localization of PKCε with SP and CGRP in dorsal horn

presented here strengthens our inference that PKCε is mediating the synergistic interaction between α_{2A}ARs and δORs within peptidergic terminals.

One caveat common to most *in vivo* pharmacological studies, including this one, is that agonists often have activity at receptors other than their primary target. The fact that four synergistic combinations thought to primarily involve α_{2A}ARs and δORs (CLON-DELT, BRIM-DELT, CLON-SNC80, BRIM-SNC80) all required PKCε strengthens the evidence that these two receptor subtypes are responsible for analgesic synergy between these compounds. Though opioid-adrenergic analgesic synergy is well documented at the spinal level, there has been little investigation into the mechanisms underlying these interactions. The current report indicates that different combinations of an OR and an AR agonist can produce analgesic synergy through different mechanisms. The combination of a) the co-localization of α_{2A}ARs and δORs on peptidergic primary afferent nociceptors (Stone et al., 1998; Overland et al., 2009; Riedl et al., 2009), b) the current result that PKCε can also be found in these neurons, and c) the observation that four different combinations of α_{2A}AR and δOR agonists all required PKCε for spinal analgesic synergy, suggests that synergy between these receptors occurs in primary afferent terminals.

Several studies indicate that signaling mechanisms initiated by agonist binding at α_{2A}ARs and/or δORs could lead to activation of PKCε. Agonist binding at either α_{2A}ARs or δORs induces release of intracellular calcium stores via $G\alpha_i$-associated Gβ/γ activation of phospholipase C (PLC) (Dorn et al., 1997; Yoon et al., 1999). Therefore, these receptors could produce activation of PKCε through increased production of

diacylglycerol via the same pathway. In fact, a link has been established between G_i signaling and activation of PKCε specifically in primary afferent neurons (Dina et al., 2009). It is also possible that α_{2A}ARs and/or δORs signal to PKCε through the more typical $G\alpha_q$ to PLC pathway. Delta ORs have been shown to couple to several G proteins including $G\alpha_q$ (Standifer et al., 1996; Sanchez-Blazquez and Garzon, 1998) and $G\alpha_{16}$, (Lee et al., 1998; Chan et al., 2003), both of which signal to PLC. While either α_{2A}ARs or δORs may activate PKCε, it is clear from our data showing similar efficacy of AR and OR agonists delivered individually in WT vs. PKCε-KO mice, that PKCε is not involved in the antinociceptive activity of these drugs when administered alone.

The effectors PKCε acts upon to produce the synergistic interaction between α_{2A}ARs and δORs remain unknown. On one hand, the failure of the PKCε activator ΨεRACK to increase the potency of either agonist given alone suggests that simple receptor phosphorylation by PKCε is not the only event necessary to increase agonist potency. Nonetheless, one mechanism by which PKCε may be exerting its effects is through phosphorylation of α_{2A}ARs or δORs themselves. Modification of these receptors may induce greater functional capability by increasing activity with inhibitory G proteins, making them more responsive to agonists, or altering the way they interact with each other. Indeed, there is evidence that PKC can directly induce functional competence of δORs trigeminal ganglion cultures (Patwardhan et al., 2005), as well as *in vivo* in the periphery (Rowan et al., 2009), though it is unknown which isoform of PKC is responsible for the observed effects. Additional evidence suggests that lack of the ε isoform of PKC decreases stimulus-induced release of CGRP (Sweitzer et al., 2004).

Because primary afferent plasma membrane δOR expression is thought to be limited at a basal state and augmented by trafficking of large dense-core vesicles under certain stimulus conditions (Zhao et al., 2011), including δOR agonist exposure (Bao et al., 2003; Overland et al., 2009), loss of PKCε may result in decreased surface and/or functional availability of δORs. Further studies are needed to determine what specific role, if any, PKCε plays in modulation of trafficking and function of δORs or α_{2A}ARs.

As PKCε is found in the majority of DRG neurons, it is not surprising that it is expressed in several subpopulations of sensory neurons (Hucho et al., 2005; Ferrari et al., 2010; Joseph and Levine, 2010). Studies by Ferrari et al. (2010) and Joseph and Levine (2010) have shown that PKCε mediates hyperalgesic priming in the peripheral terminals of isolectin-B4-binding neurons. The current report indicates a different role for PKCε in DRG by showing that in the central terminals of some peptidergic afferents it can be involved in enhanced antinociception upon activation of the appropriate receptor combination. We also report that PKCε can be found not only in primary afferent neurons but also intrinsic spinal neurons located in the superficial dorsal horn (laminae I and II). The complexity of the involvement of PKCε in nociceptive processing is becoming increasingly apparent as it clearly plays multiple roles across several neuronal subtypes at both the peripheral and spinal levels.

The data presented here show that synergistic analgesic interactions between adrenergic and opioid agonists at the spinal level occur through different mechanisms depending on the anatomical relationship between the targeted receptor subtypes. Specifically, synergistic interactions between agonist combinations acting at α_{2A}ARs and

δORs require PKCε, and likely occur in the spinal terminals of peptidergic nociceptors. Conversely, synergistic interactions between agonists acting at receptors thought to be located on different neurons, such as α_2ARs and μORs, do not require PKCε. Protein kinase C-ε is widespread in the spinal nociceptive system and has multiple known pro-nociceptive actions. In contrast, the current report shows that co-activation of α_{2A}ARs and δORs leads to involvement of PKCε in antinociceptive synergy. The present results have revealed a new role for PKCε in spinal nociceptive processing and furthered our understanding of synergistic analgesic interactions between α_2ARs and ORs at the spinal level. In chapter 5, the results on PKCε will be expanded to include pairs of agonists acting at μORs and δORs, α_{2C}ARs and δORs, and α_{2A}AR and α_{2C}ARs.

FIGURES

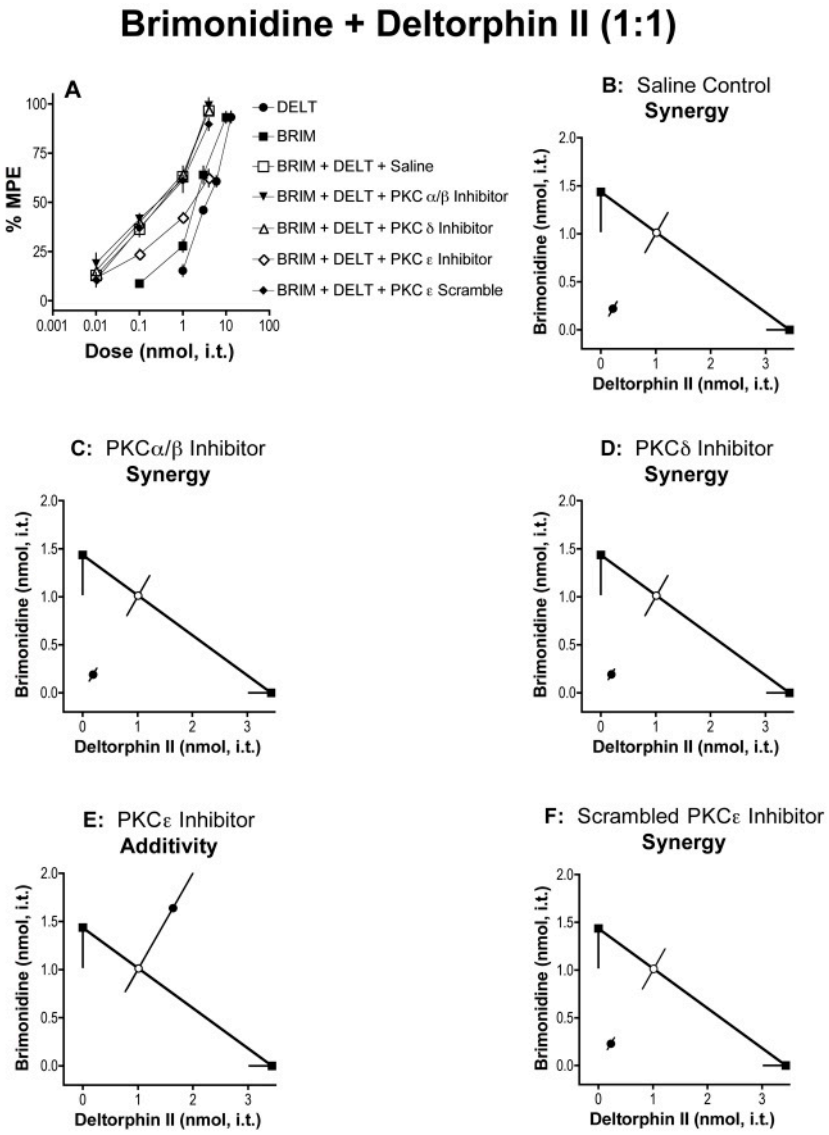

Figure 1. Selective inhibition of PKCε, but not PKCα, β, or δ, abolishes spinal analgesic synergy between brimonidine (BRIM) and deltorphin II (DELT). **A)** Dose-response curves for DELT (filled circles), BRIM (filled squares), and 1:1 combinations of both drugs with a pretreatment of one of the following: saline (open squares), PKCα/β inhibitor (FARKGALRQ; downward triangles), PKCδ inhibitor (SFNSYELGSL; upward

triangles), PKCε inhibitor (EAVSLKPT; open diamonds), or scrambled PKCε inhibitor (LSETKPAV; filled diamonds). All pretreatments were administered 30 min. prior to BRIM and DELT. Error bars for each data point represent SEM. **B-F)** Isobolograms showing DELT dose and ED_{50} (square) on the x-axis, BRIM dose and ED_{50} (square) on the y-axis, theoretical additive ED_{50} for a 1:1 combination (open circle on line of theoretical additivity), and observed combined ED_{50} (filled circle). Error bars represent 95% confidence limits. **B)** Isobologram for BRIM and DELT after saline pretreatment illustrating a synergistic interaction. **C)** Isobologram for BRIM and DELT after pretreatment with a PKCα/β inhibitor (6 nmol, i.t.) illustrating a synergistic interaction. **D)** Isobologram for DELT and BRIM after pretreatment with a PKCδ inhibitor (6 nmol, i.t.) illustrating a synergistic interaction. **E)** Isobologram for DELT and BRIM after pretreatment with a PKCε inhibitor (6 nmol, i.t.) illustrating an additive interaction. ED_{50} values for dose-response curves, and p-values for interactions can be found in Table 1.

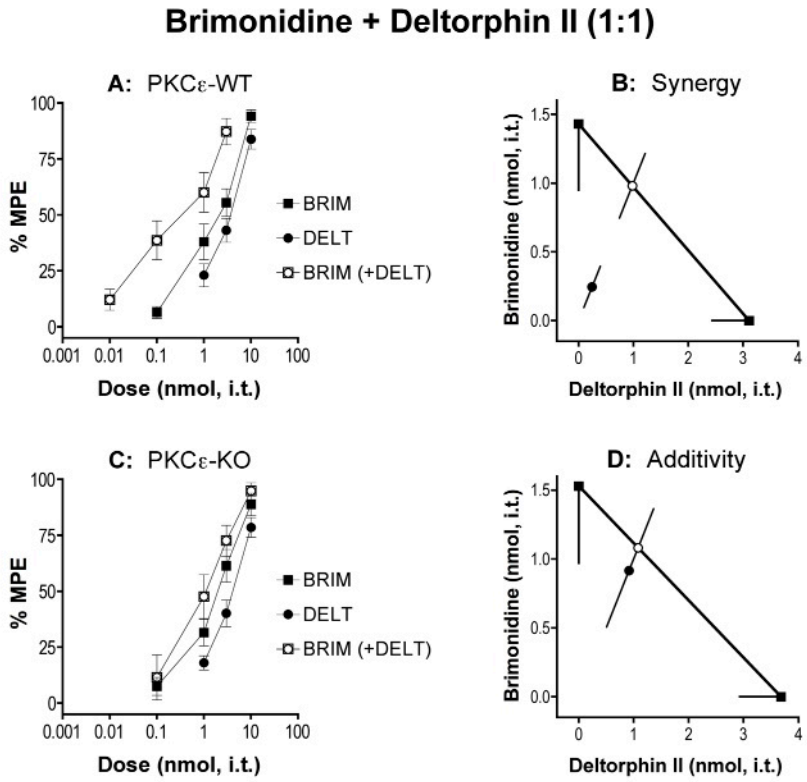

Figure 2. Brimonidine (BRIM) and deltorphin II (DELT) require PKCε for spinal analgesic synergy. **A and C**, Dose-response curves for BRIM (filled squares), DELT (filled circles) and a 1:1 combination of the two (open squares/circles) in PKCε-WT (**A**) and -KO (**C**) mice. Error bars for each data point represent SEM. **B and D**, Isobolograms showing DELT dose and ED_{50} (square) on the x-axis, BRIM dose and ED_{50} (square) on the y-axis, theoretical additive ED_{50} for a 1:1 combination (open circle on line of theoretical additivity), and observed combined ED_{50} (filled circle). Error bars represent 95% confidence limits. **B**, BRIM and DELT produce analgesic synergy at the spinal level in PKCε-WT mice. **D**, The combination of BRIM and DELT is additive in PKCε-KO mice. ED_{50} value for each dose-response curve, and p-value for each interaction can be found in Table 2.

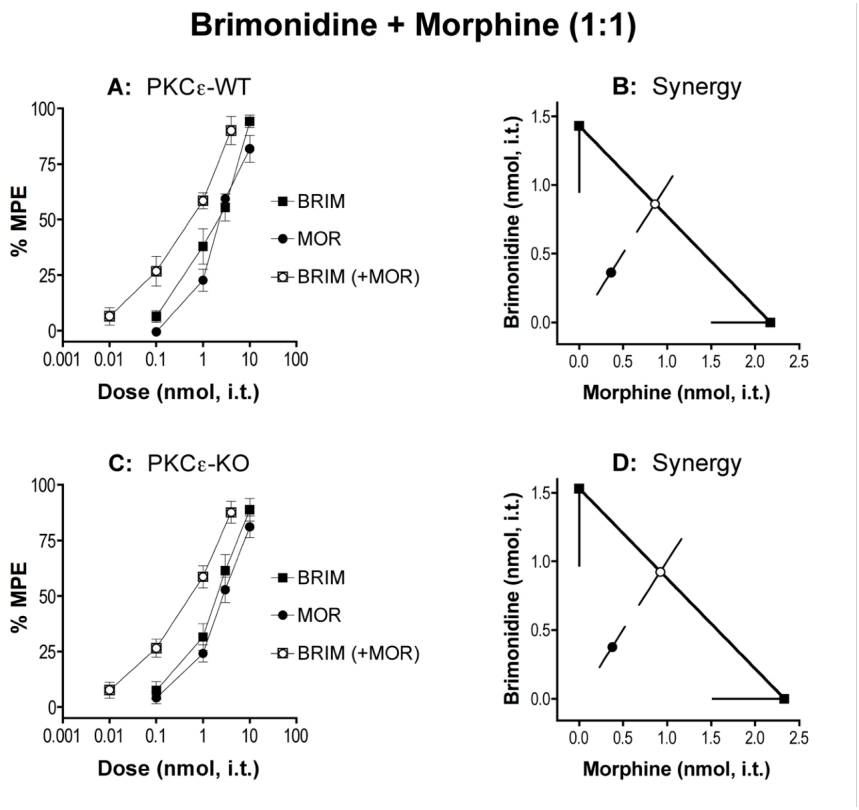

Figure 3. Brimonidine (BRIM) and morphine (MOR) do not require PKCε for spinal analgesic synergy. **A and C**, Dose-response curves for BRIM (filled squares), MOR (filled circles), and a 1:1 combination of the two (open squares/circles) in PKCε-WT (**A**) and -KO (**C**) mice. Error bars for each data point represent SEM. **B and D**, Isobolograms showing MOR dose and ED_{50} (square) on the x-axis, BRIM dose and ED_{50} (square) on the y-axis, theoretical additive ED_{50} for a 1:1 combination (open white circle on line of theoretical additivity), and observed combined ED_{50} (filled circle). Error bars represent 95% confidence limits. **B**, BRIM and MOR produce analgesic synergy at the spinal level in PKCε-WT mice. **D**, The combination of BRIM and MOR remains synergistic in PKCε-KO mice. ED_{50} value for each dose-response curve, and p-value for each interaction can be found in Table 3.

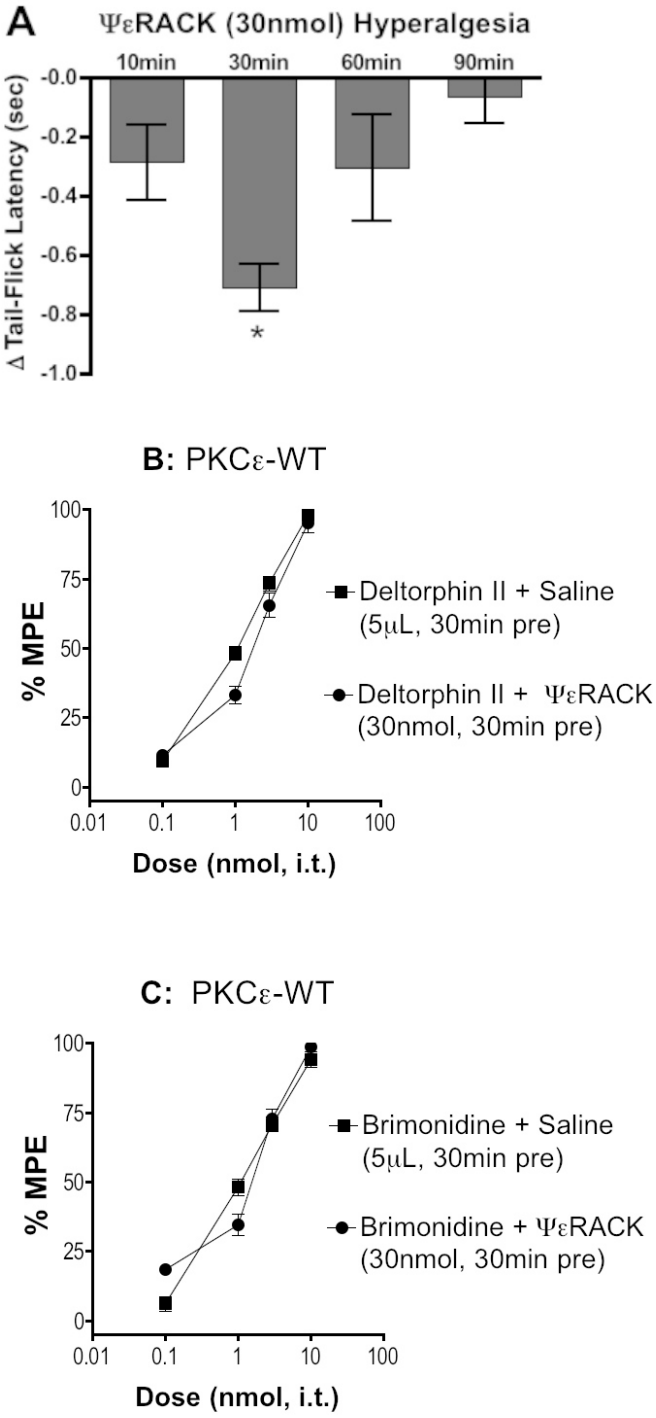

Figure 4. Activation of PKCε by intrathecal ΨεRACK does not significantly alter potency or efficacy of brimonidine (BRIM) or deltorphin II (DELT). **A,** Time course of

tail-flick latencies after intrathecal delivery of ΨεRACK (30nmol) revealed significant hyperalgesia 30 minutes after injection (* = significantly different from baseline, $p<0.01$, one way ANOVA with Bonferroni post hoc analysis). **B**, Pretreatment with ΨεRACK (30nmol, 30min) did not change potency or efficacy of DELT. **C**, Pretreatment with ΨεRACK (30nmol, 30min) did not change potency or efficacy of BRIM.

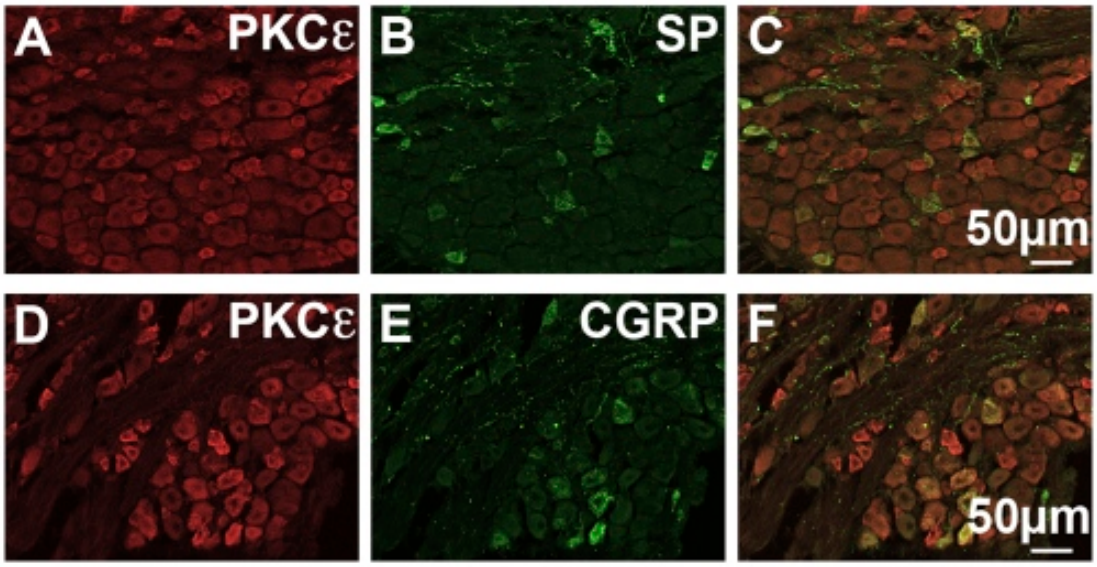

Figure 5. Co-localization of immunoreactivity (ir) for PKCε and the neuropeptides SP and CGRP in lumbar dorsal root ganglia. PKCε-ir is shown in red in the left panels (**A and D**), with either SP-ir (**B**) or CGRP-ir (**E**) in green in the middle panels, and overlaid images in the right panels illustrating that some neurons expressing PKCε also express SP or CGRP (**C and F**). **A-C,** Co-labeling for PKCε-ir and SP-ir. **D-F,** Co-labeling for PKCε-ir and CGRP-ir.

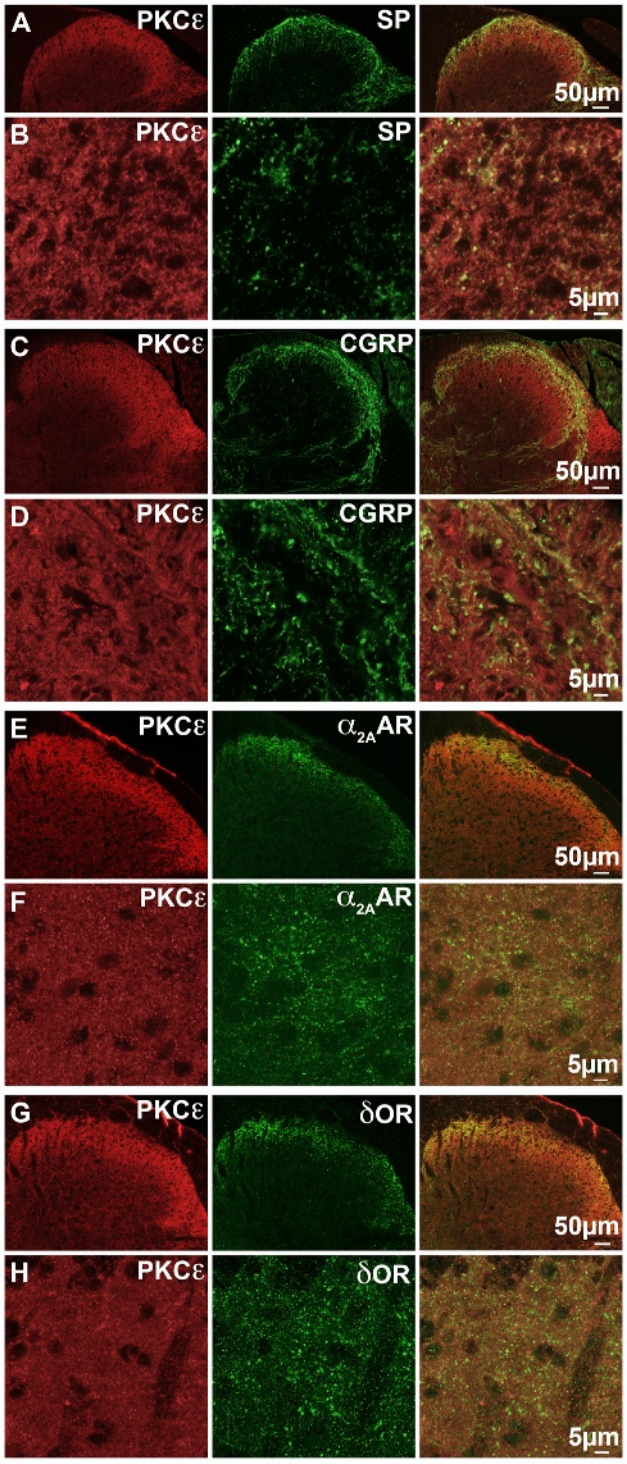

Figure 6. Immunoreactivity (ir) for PKCε in superficial dorsal horn of lumbar spinal cord relative to SP-ir, CGRP-ir, δOR-ir, or α_{2A}AR-ir. PKCε-ir is shown in red in the left

panels, with either SP-ir (**A and B**), CGRP-ir (**C and D**), α_{2A}AR-ir (**E and F**), or δOR-ir (**G and H**), in green in the middle panels, and overlaid images in the right panels. **A,** Low-magnification images of superficial dorsal horn illustrating the pattern of PKCε-ir and SP-ir in this tissue section. **B,** High-magnification images of lamina I/II showing in yellow that PKCε-ir and SP-ir partially co-localize in spinal terminals of primary afferent neurons. **C,** Low-magnification images of PKCε-ir and CGRP-ir in superficial dorsal horn. **D,** High-magnification images of lamina I/II showing in yellow that PKCε-ir and CGRP-ir partially co-localize in spinal terminals of primary afferent neurons. **E,** Low-magnification images of PKCε-ir and α_{2A}AR-ir in superficial dorsal horn. **F,** High-magnification images of lamina I/II showing in yellow that PKCε-ir and α_{2A}AR-ir partially co-localize in spinal terminals. **G**, Low-magnification images of PKCε-ir and δOR-ir in superficial dorsal horn. **H**, High-magnification images of lamina I/II showing in yellow that PKCε-ir and δOR-ir partially co-localize in spinal terminals.

TABLES

Table 1 - Interactions between brimonidine and deltorphin II in the presence or absence of PKC isoform-specific peptide inhibitors.

DRUG or PRETREATMENT	ED_{50}, nmol (95% CL)	OUTCOME	P-VALUE
BRIM	1.44 (±0.41)		
DELT	3.43 (±0.41)		
BRIM+DELT (1:1)			
Theoretical Additive	1.96 (±0.47)		
Saline	0.44 (±0.15)	Synergistic	$5.6*10^{-10}$
PKCα/β Inhibitor	0.38 (±0.14)	Synergistic	$1.8*10^{-9}$
PKCδ Inhibitor	0.38 (±0.11)	Synergistic	$1.3*10^{-9}$
PKCε Inhibitor	3.28 (±1.74)	Additive	0.15
PKCε Scramble	0.46 (±0.13)	Synergistic	$1.6*10^{-9}$

ED_{50} values listed are nmol (i.t.) with 95% confidence limits given in parenthesis. All pretreatments were administered 30 min. prior to BRIM and DELT, and inhibitors were given as a single 6nmol dose. A p-value less than 0.05 indicates a synergistic interaction. N for each group ranged from 4 to 6. Statistical analyses for all interactions were performed using JFlashCalc software (M. Ossipov, University of Arizona).

Table 2 - δOR and α_{2A}AR agonist combinations in PKCε-WT and PKCε-KO mice.

Geno-type	Agonists		Observed Combined	Theoretical Additive	Outcome (p-value)	Dose Ratio
	ED_{50}, nmol (95% Confidence Limits)					
	DELT	BRIM				
PKCε-WT	3.11 (±0.67)	1.43 (±0.48)	0.49 (±0.30)	1.96 (±0.47)	Synergistic ($1.9*10^{-6}$)	1:1
PKCε-KO	3.68 (±0.75)	1.53 (±0.56)	1.83 (±0.82)	2.16 (±0.57)	Additive (0.49)	
	DELT	CLON				
PKCε-WT	3.11 (±0.67)	3.46 (±1.09)	2.00 (±1.00)	3.28 (±0.63)	Synergistic (0.03)	1:1
PKCε-KO	3.68 (±0.75)	2.98 (±1.20)	2.61 (±1.49)	3.29 (±0.80)	Additive (0.40)	
	SNC80	BRIM				
PKCε-WT	49.30 (±6.31)	1.43 (±0.48)	4.16 (±1.75)	23.69 (±4.50)	Synergistic ($8.0*10^{-11}$)	1:30
PKCε-KO	49.50 (±5.42)	1.53 (±0.56)	41.73 (±16.54)	24.62 (±4.82)	SubAdditive (0.045)	
	SNC80	CLON				
PKCε-WT	49.30 (±6.31)	3.46 (±1.09)	14.69 (±4.69)	26.98 (±4.40)	Synergistic ($2.5*10^{-4}$)	1:15
PKCε-KO	49.50 (±5.42)	2.98 (±1.20)	18.76 (±6.08)	25.06 (±5.34)	Additive (0.11)	

Each δOR agonist (DELT, SNC80) was delivered in combination with an α_{2A}AR agonist (BRIM, CLON). ED_{50} values listed are given in nmol (i.t.) with 95% confidence limits

given in parenthesis. A p-value less than 0.05 indicates an interaction significantly different from the theoretical additive, either synergistic or sub-additive as indicated. Dose ratios are listed with adrenergic value first. N=6 for all groups except DELT, for which N=12. Statistical analyses for all interactions were performed using JFlashCalc software (M. Ossipov, University of Arizona).

Table 3 - μOR and α_{2A}AR agonist combinations in PKCε-WT and PKCε-KO mice.

Geno-type	Agonists		Observed Combined	Theoretical Additive	Outcome (p-value)	Dose Ratio
	ED_{50}, nmol (95% Confidence Limits)					
	MOR	BRIM				
PKCε -WT	2.17 (±0.66)	1.43 (±0.48)	0.72 (±0.32)	1.72 (±0.41)	Synergistic ($2.4*10^{-4}$)	1:1
PKCε -KO	2.33 (±0.81)	1.53 (±0.56)	0.75 (±0.30)	1.85 (±0.48)	Synergistic ($2.1*10^{-4}$)	
	MOR	CLON				
PKCε -WT	2.17 (±0.66)	3.46 (±1.09)	0.35 (±0.07)	2.67 (±0.59)	Synergistic ($2.1*10^{-10}$)	1:1
PKCε -KO	2.33 (±0.81)	2.98 (±1.20)	0.41 (±0.10)	2.61 (±0.68)	Synergistic ($3.3*10^{-8}$)	
	ENDO	BRIM				
PKCε -WT	1.24 (±0.58)	1.43 (±0.48)	0.14 (±0.04)	1.33 (±0.40)	Synergistic ($1.7*10^{-7}$)	1:1
PKCε -KO	1.16 (±0.55)	1.53 (±0.56)	0.24 (±0.05)	1.32 (0.41)	Synergistic ($2.1*10^{-6}$)	
	ENDO	CLON				
PKCε -WT	1.24 (±0.58)	3.46 (±1.09)	0.74 (±0.13)	2.39 (±0.66)	Synergistic ($7.7*10^{-6}$)	1:3
PKCε -KO	1.16 (±0.55)	2.98 (±1.20)	0.81 (±0.18)	2.33 (±0.72)	Synergistic ($1.7*10^{-4}$)	

Each μOR agonist (MOR, ENDO) was delivered in combination with an α_{2A}AR agonist (BRIM, CLON). ED_{50} values listed are given in nmol (i.t.) with 95% confidence limits

given in parenthesis. A p-value less than 0.05 indicates an interaction significantly different from the theoretical additive. Dose ratios are listed with adrenergic value first. N=6 for all groups. Statistical analyses for all interactions were performed using JFlashCalc software (M. Ossipov, University of Arizona).

Chapter 5

Biased agonism by select combinations of mu and delta opioid agonists for analgesic synergy requiring protein kinase C-epsilon

The results detailed in this chapter are a continuation of the work described in chapter 4, and as such, are the product of varied contributions from the same group of authors with the addition of Matthew D. Metcalf.

Author contributions:
DJS designed research, performed research, analyzed data and drafted the chapter
MDM designed research and edited the chapter
KFK performed research
ROM contributed published and unpublished reagents
CAF designed research and edited the chapter
GLW designed research and edited the chapter

Biased agonism has previously been described with regard to some individual opioid agonists. Here we report the novel finding of biased agonism at the level of co-delivered opioid agonists. We found that the mechanism underlying synergistic analgesic interactions between spinally co-delivered opioid agonists depends specifically on the two agonists used. Morphine was found to synergize with deltorphin II through a protein kinase C-epsilon (PKC-epsilon) dependent mechanism, whereas morphine synergy with deltorphin was independent of PKC-epsilon. Several additional delta opioid receptor agonists were co-delivered with morphine, and only deltorphin I and oxymorphindole yielded the same PKC-epsilon dependent synergy as deltorphin II. We also found that synergy between deltorphin II and all other mu opioid receptor agonists tested (other than morphine) did not require PKC-epsilon. Thus, the bias in agonism observed presently cannot be accounted for by a single drug, but rather is observed only when specific agonists are co-administered.

INTRODUCTION

The data detailed in chapter 4 showed that protein kinase C-ε (PKCε) is required for spinal analgesic synergy between agonist pairs acting at α_{2A}-adrenergic receptors (α_{2A}ARs) and δ opioid receptors (δORs), but not for interactions between α_{2A}ARs and μ opioid receptors (μORs). It is thought that the PKCε-dependent interaction between α_{2A}ARs and δORs occurs at the level of individual presynaptic terminals in the superficial dorsal horn of the spinal because all three proteins (α_{2A}ARs, δORs and PKCε) can be found to co-localize in spinal terminals of primary afferents (Riedl et al., 2009; Chapter 4, Figure 6), and the interaction has also been shown to occur in spinal cord slices (Overland et al., 2009) and spinal synaptosomes (Riedl et al., 2009). Thus, it is feasible that other pairs of G protein-coupled receptors located in the same cell with PKCε could also produce PKCε-dependent synergy. Furthermore, the requirement of PKCε for spinal analgesic synergy between a pair of G protein-coupled receptors can provide indirect functional evidence that the two receptors in question are expressed in a common cell.

Co-localization of μORs and δORs in peptidergic primary afferent neurons has been reported previously (Beaudry et al., 2011; He et al., 2011; Gupta et al., 2010; Wang et al., 2010). Considering that μORs and δORs are co-located in a population of DRG neurons where PKCε is also found and has previously been implicated to mediate synergistic analgesic interactions between a different pair of G protein-coupled receptors (chapter 4, Table 2), it is feasible that combinations of a μOR agonist and a δOR agonist may also synergize through a PKCε-dependent mechanism. In the current study, the goal was to determine if pairs of a μOR agonist and a δOR agonist require PKCε for spinal

analgesic synergy. Therefore, we tested a battery of agonist combinations in wild-type PKCε mice (PKCε-WT), and PKCε-knockout mice (PKCε-KO), for analgesic synergy in the hot-water tail-flick assay.

METHODS

Animals

Adult PKCε wild-type (PKCε-WT), and knockout (PKCε-KO) of both sexes (20±5g) used for all experiments were bred from pairs of hybrid (50% C57BL/6J, 50%129S4) mice heterozygous for the mutant PKCε gene (Khasar et al., 1999), and were maintained on a 12-hour light/dark cycle with food and water available *ad libitum* to all animals. All experiments were approved by the Institutional Animal Care and Use Committee of the University of Minnesota.

Drug Preparation and Administration

Agonists used were dermorphin, deltorphin (both from Bachem, Torrence, CA), deltorphin I (Biotrend, Destin, FL), deltorphin II (Tocris Bioscience; Bristol, UK), SNC80, morphine sulfate, endomorphin II, leu-enkephalin, beta-endorphin, codeine, oxycodone, oxymorphone, hydromorphone, DAMGO ([D-Ala^2, N-MePhe^4, Gly-ol]-enkephalin), fentanyl, DPDPE ([D-Pen^2, D-Pen^5]-enkephalin) (all from Sigma; St. Louis, MO), oxymorphamine, oxymorphindole and oxycodindole (gifts from the lab of Phillip Portoghese). SNC80 was dissolved with an equimolar amount of tartaric acid in saline. All other drug stocks were prepared in normal saline. All drugs were diluted from stock

solution into sterile 0.9% saline and injected intrathecally in a volume of 5 μL in awake mice by the method of Hylden and Wilcox (1980).

Behavioral Measures

Thermal nociceptive responsiveness was assessed using the warm water (52.5°C) tail immersion assay as previously described (Janssen et al., 1963). Briefly, each animal was gently held wrapped in a cloth, and the tail dipped into a controlled temperature water bath. Withdrawal latency was recorded as the amount of time that passed before a rapid movement of the tail, and was not allowed to exceed 12 seconds. A baseline latency was recorded prior to drug administration, and subsequent latencies were recorded 7 min after each dose, immediately before the next dose. Each agonist or combination was administered sequentially approximately every 7 min in increasing doses to generate a cumulative dose-response curve, each mouse receiving no less than three, and no more than four doses (Shin and Eisenach, 2003). Each dose-response curve was generated with an N of 4 to 6 as indicated in each table or legend. For deltorphin II, two dose-response curves were obtained on separate days to confirm the potency and efficacy of this drug in the PKCε mutant mice. These curves did not differ significantly in potency or efficacy and were combined for a total N of 12. This curve was then reused in the analysis for each combination tested. This allowed us to minimize the number of animals necessary to complete this study. Data are represented as percent maximum possible effect (%MPE) values, which are determined using the following equation:

100*(test-baseline)/(maximum-baseline)

Data Analysis

The ED_{50}, in nanomoles (nmol), and 95% confidence limits (CLs) of all agonists and combinations were calculated using the graded dose-response curve method of Tallarida and Murray (1987). Dose ratios for drug combinations were estimated based on comparison of ED_{50} values and dose-response curves, and were chosen to approximate equi-effective doses. Isobolographic analyses were performed using the numerical method (Tallarida et al., 1989; Ossipov et al., 1997). Theoretical additive and observed combination ED_{50} values were compared statistically via the Student's t-test with the JFlashCalc Pharmacological Calculations Program software package generously provided by Dr. Michael Ossipov (Department of Pharmacology, University of Arizona College of Medicine, Tucson, AZ). For all isobolograms, error bars for theoretical additive and observed combination ED_{50} values represent the vector sum of vertical and horizontal confidence limits.

RESULTS

To determine if PKCε is required for spinal analgesic synergy between mu and delta opioid agonists, we began testing combinations of agonists used in chapter 4 (μOR: morphine and endomorphin II, δOR: deltorphin II and SNC80) in the hot-water tail-flick assay. Morphine (MOR) or endomorphin II was delivered in approximately equi-effective combination with each δOR agonist, deltorphin II (DELT2) and SNC80. All four agonist pairs produced analgesic synergy, but only MOR with DELT2 resulted in PKCε-dependent synergy (Figure 1). Detailed numerical results are given for single agonists in Table 1, and for combinations in Table 2.

To determine if we could find other opioid agonist pairs that synergized through a PKCε-dependent mechanism, we tested a battery of agonist combinations. Additional combinations tested were delivered at an approximately equi-effective dose ratio, and were as follows: MOR + deltorphin I (DELT1), MOR + deltorphin (DELT; Figure 2), MOR + dermorphin, MOR + DPDPE, MOR + leu-enkephalin, MOR + beta-endorphin, MOR + oxymorphindole (OMI; Figure 3), MOR + oxycodindole (OCI; Figure 4), DELT2 + endomorphin II, DELT2 + codeine, DELT2 + oxycodone, DELT2 + oxymorphone, DELT2 + hydromorphone, DELT2 + DAMGO, DELT2 + fentanyl, DELT2 + oxymorphamine, and endomorphin II + SNC80. Detailed numerical results are given for single agonists in Table 1, and for combinations in Table 2. When delivered singly, all agonists had comparable potency and efficacy in PKCε-WT and PKCε-KO mice. All but one combination (DELT2 + codeine) produced analgesic synergy in PKCε-WT mice. Of all additional combinations tested that were synergistic in PKCε-WT mice, only MOR + DELT 1 and MOR + OMI (Figure 3) required PKCε for spinal analgesic synergy. Combinations of MOR + DELT (Figure 2) and MOR + OCI (Figure 4) were chosen for figures to represent combinations that produced synergy independent of PKCε, as well as for the similarity of the δOR agonists to those that did require PKCε for synergy with MOR (DELT2 and OMI).

DISCUSSION

The results reported in this chapter suggest that biased agonism can occur at the level of co-delivered agonists. For example, MOR co-delivered with DELT2, DELT1, or

OMI results in a synergistic interaction that differs in mechanism from the combination of MOR with any other agonist tested by requirement of PKCε. Furthermore, synergy resulting from co-delivery of DELT2 with any of the other tested agonists also differs in mechanism from the MOR + DELT2 combination. Thus, the bias in signaling does not lie with a single agonist, but requires a specific combination of two agonists.

The fact that MOR + DELT1 yielded the same result as MOR + DELT2 is not surprising when considering that these two deltorphin analogs share a nearly identical structure. The difference in result when MOR is combined with DELT rather than DELT1 or DELT2 suggests that the specific structure of the peptide agonist used helps determine the signaling bias of the combination. The peptide sequences for DELT, DELT1 and DELT2 are as follows: DELT (Tyr-D-Met-Phe-His-Leu-Met-Asp), DELT1 (Tyr-D-Ala-Phe-Asp-Val-Val-Gly), and DELT2 (Tyr-D-Ala-Phe-Glu-Val-Val-Gly) Two of the most striking structural differences between DELT and DELT1/DELT2 are the residues in position 4 (His in DELT vs. Asp and Glu in DELT1 and DELT2) and position 7 (Asp in DELT vs. Gly in DELT1 and DELT2). We synthesized four additional deltorphin analog peptides in an attempt to address the hypothesis that structural differences at the fourth and seventh residues in the peptide alter how it interacts with morphine. Two variations on DELT (Tyr-D-Met-Phe-Glu-Leu-Met-Asp and Tyr-D-Met-Phe-Glu-Leu-Met-Asn), and two variations on DELTII (Tyr-D-Ala-Phe-Ala-Val-Val-Gly and Tyr-D-Ala-Phe-Ala-Val-Val-Asp) were synthesized. Unfortunately, none of these peptides produced analgesic synergy when co-delivered with morphine, either in PKCε-WT or PKCε-KO mice. Though there is a clear difference in the functional result

observed when DELT is combined with MOR compared to when DELT2 is combined with MOR, further study is necessary to identify what about these peptides causes biased agonism when they are co-delivered with MOR.

The fact that we achieved comparable results with MOR + DELT2 and MOR + OMI suggests that this phenomenon of biased agonism which only occurs when certain δOR agonists are delivered in combination with morphine is not a special case for the deltorphin peptides. It is interesting that OCI delivered in combination with MOR yielded PKCε-independent synergy, unlike MOR-OMI synergy, which is PKCε-dependent. Oxymorphindole and oxycodindole are small molecule δOR agonists with very similar structures. They differ only in the change from a hydroxyl (OMI) to a methoxyl group (OCI) on carbon 3. It is not clear how this small difference can account for the difference in requirement of PKCε for spinal analgesic synergy with morphine, but it is apparent that OMI and DELT2 interact functionally with morphine at the spinal level in a very similar way. Future experiments testing co-delivery of OMI and each of the agonists with which DELT2 was tested with in the current study will reveal if they share further functional similarity.

Biased agonism has been documented previously with singly delivered agonists (Morse et al., 2013; Pradhan et al., 2012). The current report is the first to demonstrate this phenomenon at the level of interactions between two agonists that are co-delivered. These results expand the potential utility of opioid agonist co-delivery to include activation of specific signaling mechanisms that cannot be achieved with delivery of a single agonist.

FIGURES

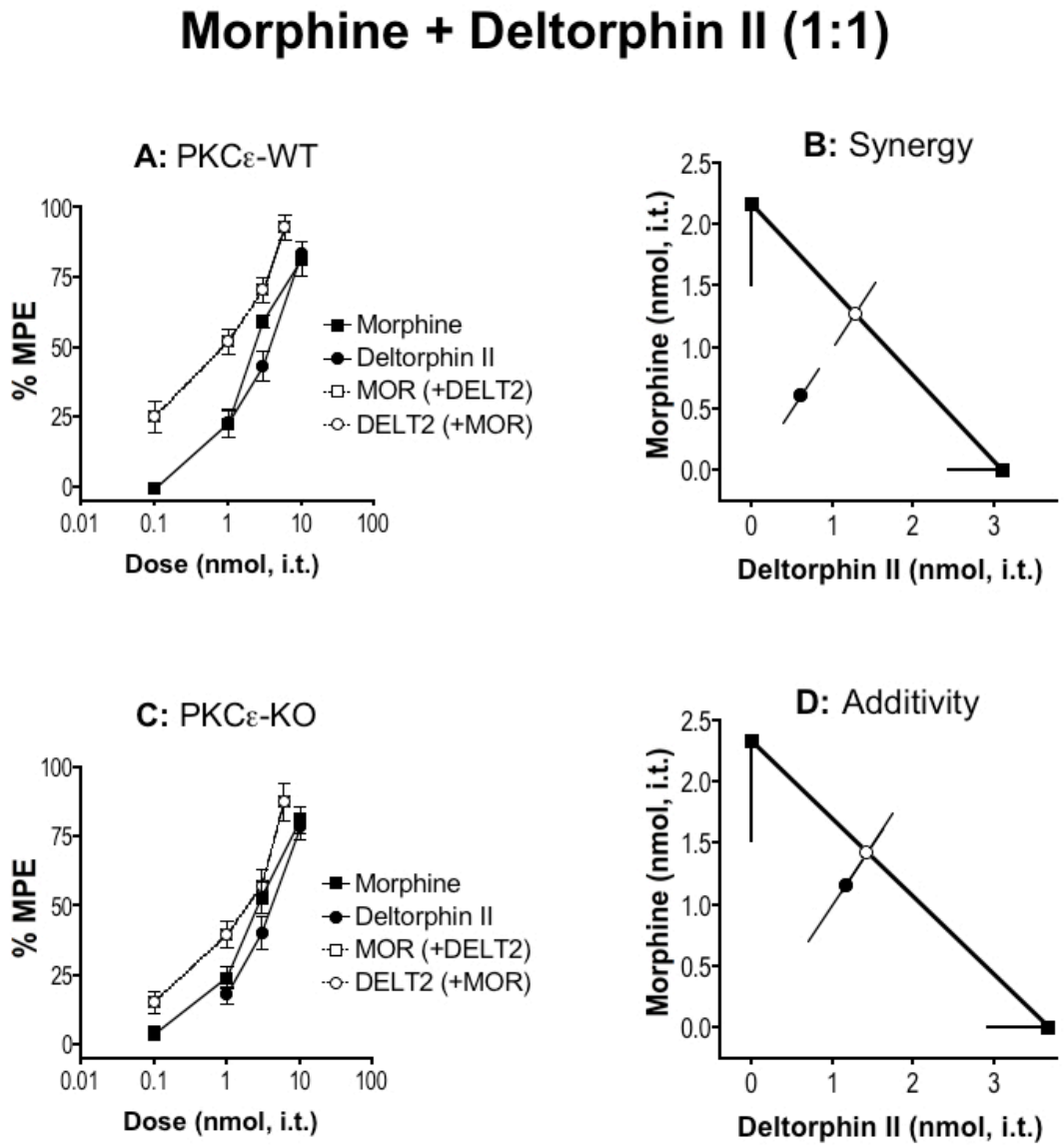

Figure 1. Morphine (MOR) and deltorphin II (DELT2) require PKCε for spinal analgesic synergy. **A and C**, Dose-response curves for MOR (filled squares), DELT2 (filled circles) and a 1:1 combination of the two (open squares/circles) in PKCε-WT (**A**) and -KO (**C**) mice. Error bars for each data point represent SEM. **B and D**, Isobolograms showing DELT2 dose and ED_{50} (square) on the x-axis, MOR dose and ED_{50} (square) on

the y-axis, theoretical additive ED_{50} for a 1:1 combination (open circle on line of theoretical additivity), and observed combined ED_{50} (filled circle). Error bars represent 95% confidence limits. **B**, MOR and DELT2 produce analgesic synergy at the spinal level in PKCε-WT mice. **D**, The combination of MOR and DELT2 is additive in PKCε-KO mice. ED_{50} value for each dose-response curve, and p-value for each interaction can be found in Table 1 and Table 2.

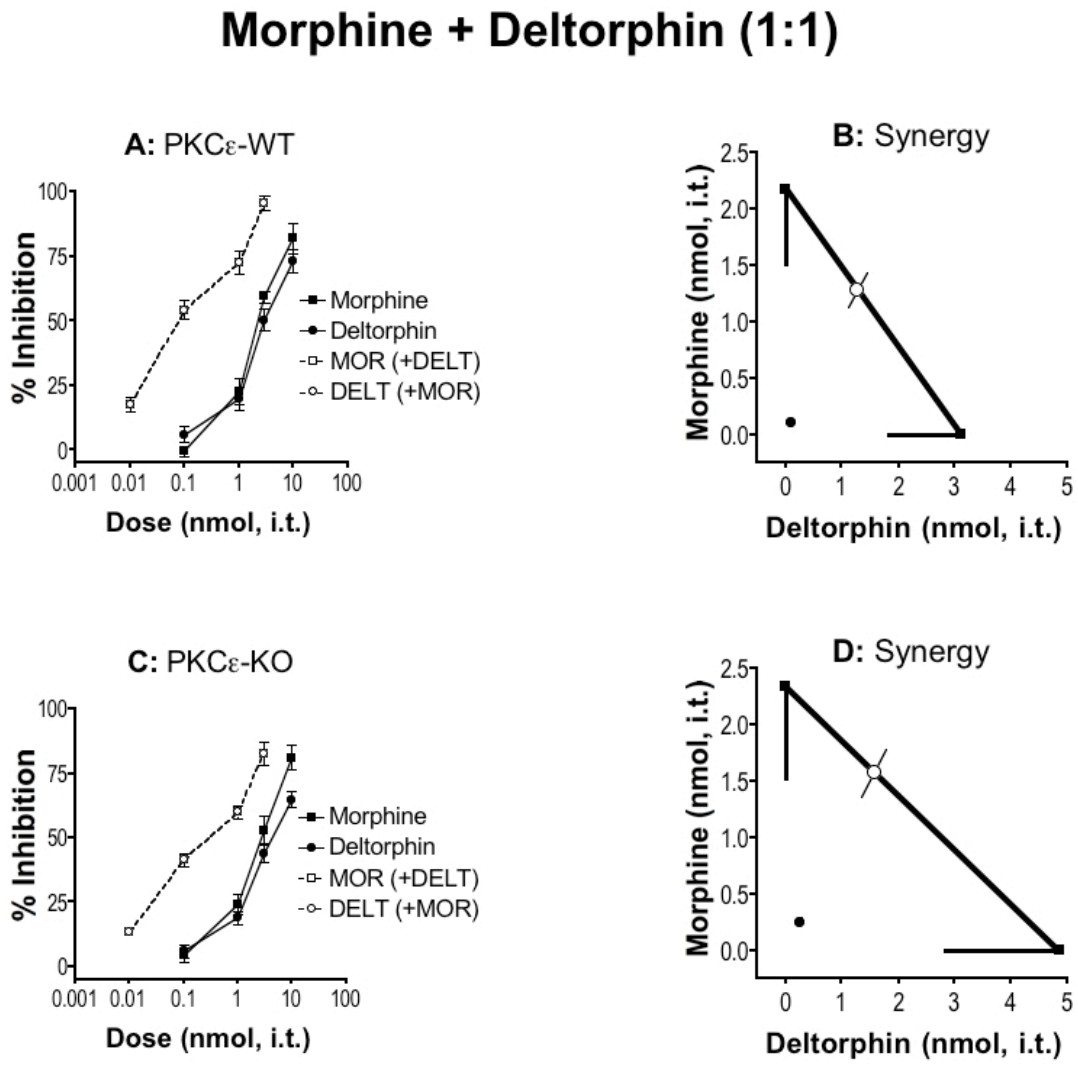

Figure 2. Morphine (MOR) and deltorphin (DELT) do not require PKCε for spinal analgesic synergy. **A and C**, Dose-response curves for MOR (filled squares), DELT (filled circles), and a 1:1 combination of the two (open squares/circles) in PKCε-WT (**A**) and -KO (**C**) mice. Error bars for each data point represent SEM. **B and D**, Isobolograms showing DELT dose and ED_{50} (square) on the x-axis, MOR dose and ED_{50} (square) on the y-axis, theoretical additive ED_{50} for a 1:1 combination (open white circle on line of theoretical additivity), and observed combined ED_{50} (filled circle). Error bars represent

95% confidence limits. **B**, MOR and DELT produce analgesic synergy at the spinal level in PKCε-WT mice. **D**, The combination of MOR and DELT remains synergistic in PKCε-KO mice. ED_{50} value for each dose-response curve, and p-value for each interaction can be found in Table 1 and Table 2.

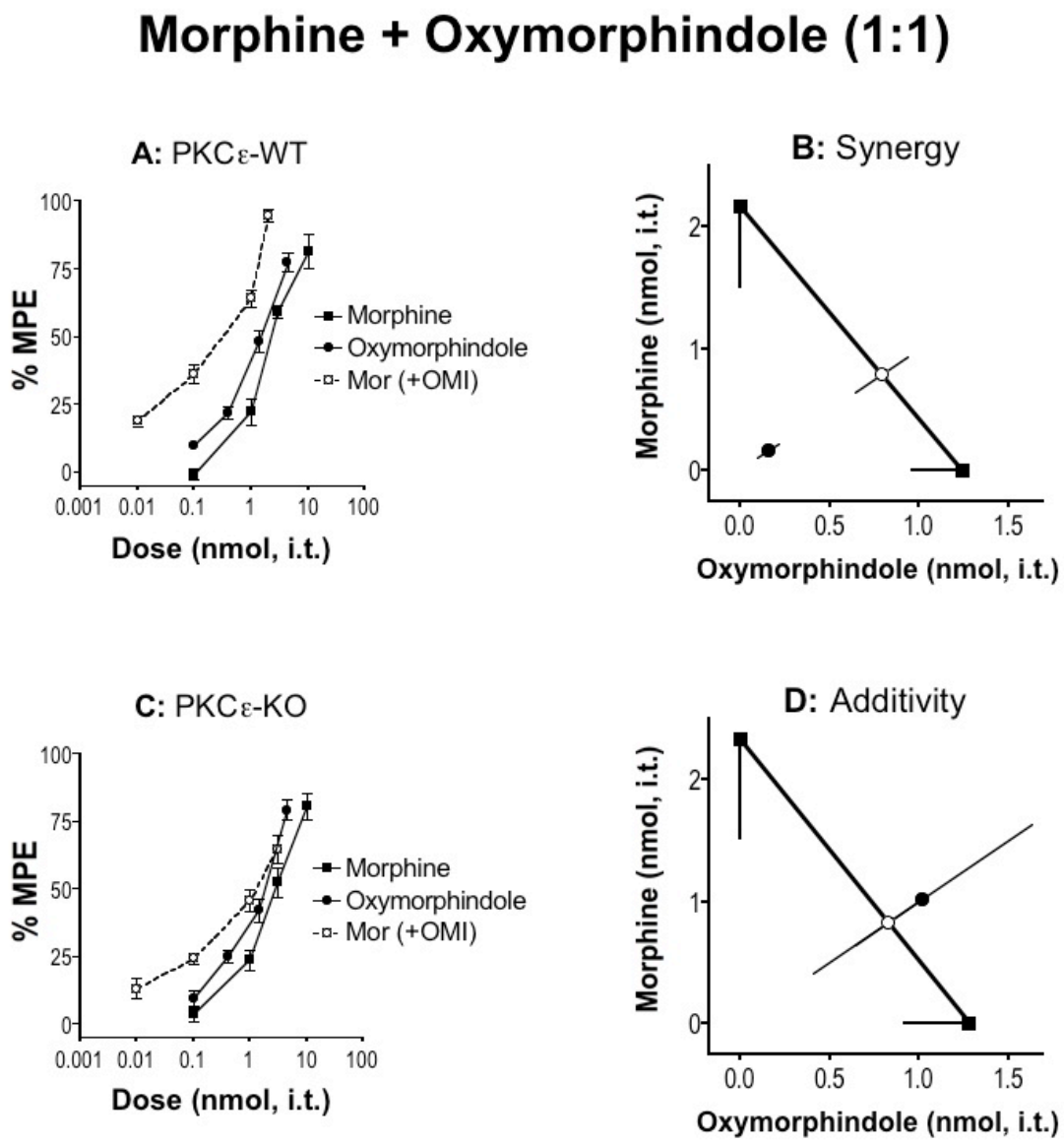

Figure 3. Morphine (MOR) and oxymorphindole (OMI) require PKCε for spinal analgesic synergy. **A and C**, Dose-response curves for MOR (filled squares), OMI (filled circles) and a 1:1 combination of the two (open squares/circles) in PKCε-WT (**A**) and -KO (**C**) mice. Error bars for each data point represent SEM. **B and D**, Isobolograms showing OMI dose and ED_{50} (square) on the x-axis, MOR dose and ED_{50} (square) on the y-axis, theoretical additive ED_{50} for a 1:1 combination (open circle on line of theoretical

additivity), and observed combined ED_{50} (filled circle). Error bars represent 95% confidence limits. **B**, MOR and OMI produce analgesic synergy at the spinal level in PKCε-WT mice. **D**, The combination of MOR and OMI is additive in PKCε-KO mice. ED_{50} value for each dose-response curve, and p-value for each interaction can be found in Table 1 and Table 2.

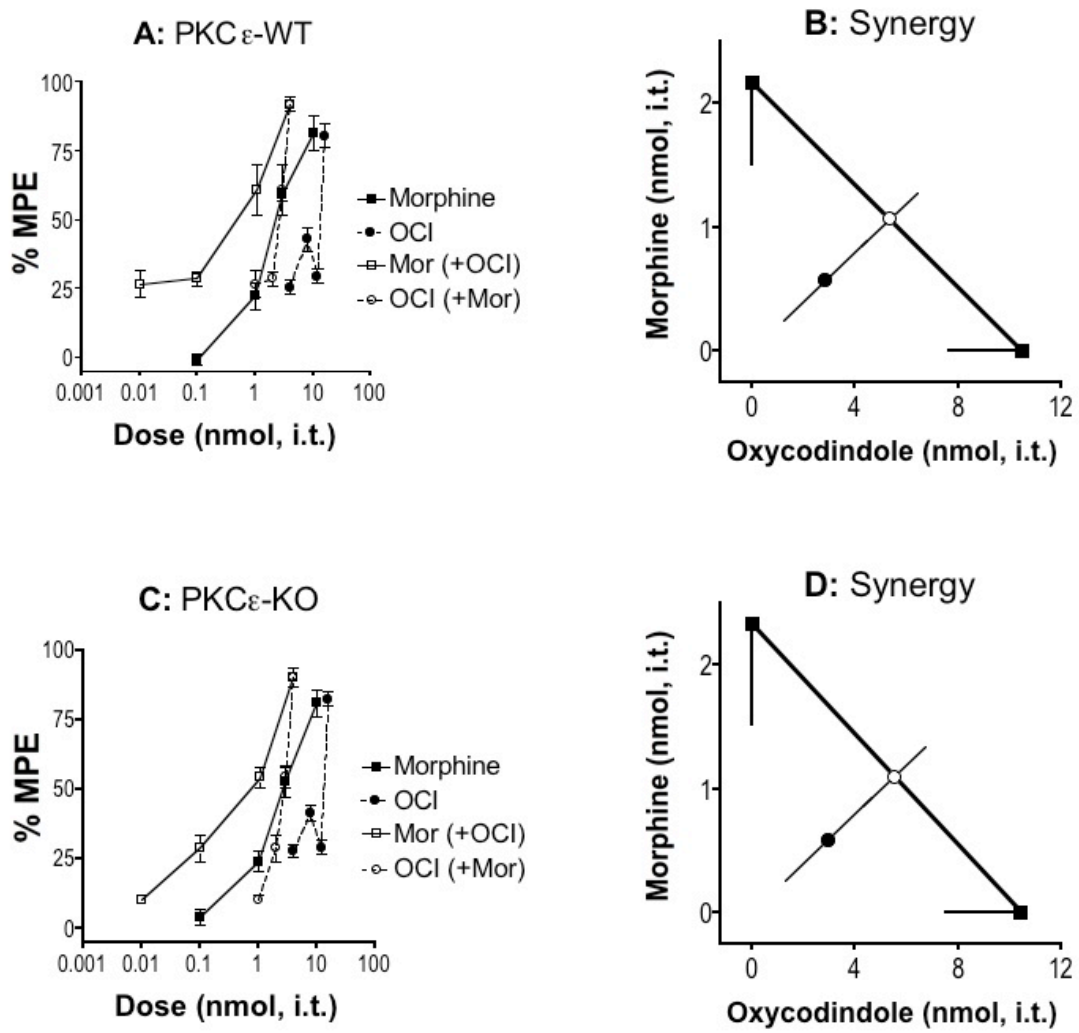

Figure 4. Morphine (MOR) and oxycodindole (OCI) do not require PKCε for spinal analgesic synergy. **A and C**, Dose-response curves for MOR (filled squares), OCI (filled circles), and a 1:1 combination of the two (open squares/circles) in PKCε-WT (**A**) and -KO (**C**) mice. Error bars for each data point represent SEM. **B and D**, Isobolograms showing OCI dose and ED_{50} (square) on the x-axis, MOR dose and ED_{50} (square) on the y-axis, theoretical additive ED_{50} for a 1:1 combination (open white circle on line of

theoretical additivity), and observed combined ED_{50} (filled circle). Error bars represent 95% confidence limits. **B**, MOR and OCI produce analgesic synergy at the spinal level in PKCε-WT mice. **D**, The combination of MOR and OCI remains synergistic in PKCε-KO mice. ED_{50} value for each dose-response curve, and p-value for each interaction can be found in Table 1 and Table 2.

TABLES

Table 1. Opioid agonist ED_{50} values in PKCε-WT and PKCε-KO mice.

	AGONIST	ED50, nmol (95% CL)
PKCε-WT	Morphine (MOR)	2.17 (±0.66)
PKCε-KO		2.33 (±0.81)
PKCε-WT	Deltorphin (DELT)	3.11 (±1.28)
PKCε-KO		4.84 (±2.00)
PKCε-WT	Deltorphin I (DELT1)	1.39 (±0.44)
PKCε-KO		1.24 (±0.46)
PKCε-WT	Deltorphin II (DELT2)	3.11 (±0.67)
PKCε-KO		3.68 (±0.75)
PKCε-WT	Oxymorphindole (OMI)	1.24 (±0.28)
PKCε-KO		1.28 (±0.36)
PKCε-WT	Oxycodindole (OCI)	10.47 (±2.84)
PKCε-KO		10.44 (±2.90)
PKCε-WT	Codeine	1.80 (±0.56)
PKCε-KO		1.90 (±0.46)
PKCε-WT	DAMGO	8.73E-4 (±1.96E-4)
PKCε-KO		7.80E-4 (±1.52E-4)
PKCε-WT	Dermorphin	0.60 (±0.24)
PKCε-KO		0.99 (±0.45)
PKCε-WT	DPDPE	1.86 (±0.62)
PKCε-KO		1.95 (±0.65)
PKCε-WT	Endomorphin II	1.24 (±0.58)
PKCε-KO		1.16 (±0.55)
PKCε-WT	beta-Endorphin	0.76 (±0.25)
PKCε-KO		0.74 (±0.29)
PKCε-WT	leu-Enkephalin	1.42 (±0.49)
PKCε-KO		1.49 (±0.47)
PKCε-WT	Fentanyl	0.98 (±0.28)
PKCε-KO		1.28 (±0.41)
PKCε-WT	Hydromorphone	0.05 (±0.01)
PKCε-KO		0.05 (±0.01)
PKCε-WT	Oxycodone	1.21 (±0.34)
PKCε-KO		1.30 (±0.34)
PKCε-WT	Oxymorphamine	1.12 (±0.30)
PKCε-KO		1.21 (±0.31)
PKCε-WT	Oxymorphone	0.06 (±0.02)
PKCε-KO		0.06 (±0.01)
PKCε-WT	SNC80	49.30 (±6.31)
PKCε-KO		49.50 (±5.42)

N=6 for all groups except DELT2, for which N=12. All ED_{50} values were calculated using JFlashCalc software (M. Ossipov, University of Arizona).

Table 2. Interactions between co-delivered opioid agonists.

	Agonists	Dose-Ratio	Combination ED_{50}, nmol (95% CL)	Theoretical Additive ED_{50}, nmol (95% CL)	Outcome
PKCε-WT	Morphine + Deltorphin II	1:1	1.21 (±0.45)	2.56 (±0.52)	SYN
PKCε-KO			2.32 (±0.92)	2.85 (±0.65)	ADD
PKCε-WT	Morphine + Deltorphin I	1:1	0.47 (±0.18)	1.70 (±0.39)	SYN
PKCε-KO			1.08 (±0.43)	1.62 (±0.44)	ADD
PKCε-WT	Morphine + Deltorphin	1:1	0.22 (±0.07)	2.56 (±0.63)	SYN
PKCε-KO			0.50 (±0.15)	3.14 (±0.85)	SYN
PKCε-WT	Morphine + Oxymorphindole	1:1	0.32 (±0.12)	1.58 (±0.29)	SYN
PKCε-KO			2.04 (±1.22)	1.65 (±0.36)	ADD
PKCε-WT	Morphine + Oxycodindole	1:5	3.43 (±1.96)	6.39 (±1.30)	SYN
PKCε-KO			3.55 (±2.04)	6.60 (±1.46)	SYN
PKCε-WT	Morphine + Dermorphin	2:1	0.57 (±0.23)	1.16 (±0.33)	SYN
PKCε-KO			0.94 (±0.46)	1.61 (±0.47)	SYN
PKCε-WT	Morphine + DPDPE	1:1	1.33 (±0.42)	2.00 (±0.45)	SYN
PKCε-KO			1.43 (±0.45)	2.12 (±0.51)	SYN
PKCε-WT	Morphine + beta-Endorphin	2:1	0.10 (±0.02)	1.34 (±0.31)	SYN
PKCε-KO			0.19 (±0.05)	1.36 (±0.37)	SYN
PKCε-WT	Morphine + leu-Enkephalin	1:1	0.09 (±0.02)	1.71 (±0.41)	SYN
PKCε-KO			0.14 (±0.04)	1.82 (±0.43)	SYN
PKCε-WT	Morphine + SNC80	1:25	1.11 (±0.52)	25.77 (±4.18)	SYN
PKCε-KO			1.72 (±0.74)	26.58 (±4.52)	SYN
PKCε-WT	Deltorphin II + endomorphin II	3:1	1.03 (±0.33)	2.41 (±0.74)	SYN
PKCε-			1.21 (±0.31)	2.70 (±0.83)	SYN

KO					
PKCε-WT	Deltorphin II + Codeine	1:1	2.19 (±0.55)	2.28 (±0.49)	ADD
PKCε-KO			2.52 (±0.65)	2.50 (±0.44)	ADD
PKCε-WT	Deltorphin II + DAMGO	1000:1	0.10 (±0.03)	0.68 (±0.12)	SYN
PKCε-KO			0.13 (±0.06)	0.64 (±0.11)	SYN
PKCε-WT	Deltorphin II + Fentanyl	1:1	0.20 (±0.05)	1.38 (±0.31)	SYN
PKCε-KO			0.25 (±0.07)	1.67 (±0.43)	SYN
PKCε-WT	Deltorphin II + Hydromorphone	10:1	0.14 (±0.03)	0.47 (±0.10)	SYN
PKCε-KO			0.14 (±0.03)	0.48 (±0.09)	SYN
PKCε-WT	Deltorphin II + Oxycodone	1:1	0.32 (±0.09)	1.74 (±0.37)	SYN
PKCε-KO			0.31 (±0.10)	1.92 (±0.38)	SYN
PKCε-WT	Deltorphin II + Oxymorphamine	2:1	0.75 (±0.12)	1.95 (±0.36)	SYN
PKCε-KO			0.65 (±0.09)	2.19 (±0.39)	SYN
PKCε-WT	Deltorphin II + Oxymorphone	10:1	0.14 (±0.02)	0.55 (±0.12)	SYN
PKCε-KO			0.14 (±0.02)	0.53 (±0.11)	SYN
PKCε-WT	Endomorphin II + SNC80	1:30	1.81 (±0.62)	21.15 (±5.67)	SYN
PKCε-KO			1.81 (±0.94)	20.40 (±5.57)	SYN

A synergistic (SYN) outcome indicates a p-value <0.05. An additive (ADD) outcome indicates a p-value >0.05. N=6 for all groups. Statistical analyses for all interactions were performed using JFlashCalc software (M. Ossipov, University of Arizona).

Chapter 6

Discussion and Conclusion

Pain signals from the periphery enter the central nervous system (CNS) via axons of primary afferent sensory neurons residing in dorsal root ganglia (DRG). The central terminals of these axons synapse onto neurons in the dorsal horn of the spinal cord, and pain signals are subsequently carried from these spinal neurons to the brain. Inhibition of pain signals directly at the spinal level provides an opportunity to reduce pain at the most basic level. Several G protein-coupled receptors, including opioid and adrenergic receptors, are known to be potent regulators of pain signaling at the spinal level. Furthermore, co-activation of different subtypes of these receptors can lead to synergistic inhibition of pain signaling. Understanding how these receptors interact at the cellular level may provide insight into how to exploit such mechanisms for improved pain management strategies. This thesis has taken two approaches to advance the study of interactions involving opioid and adrenergic receptors at the spinal level: develop the use of adeno-associated virus (AAV) vectors for gene-transfer to sensory neurons where the expression of involved proteins can be modulated, and to further characterize these interactions by understanding of the cellular processes underlying their outcomes.

Intrathecal delivery of AAV vectors

To evaluate transduction of sensory neurons by AAV vectors, intrathecal delivery was chosen as a minimally invasive route of delivery that concentrates virus particles at the spinal level. Subsequently, AAV serotypes 5, 8, and 9 carrying the gene for green fluorescent protein (GFP) were delivered by direct lumbar puncture, and the resulting pattern of gene expression in DRG, spinal cord, and brain was evaluated (Chapters 1 and

2). Several studies with AAV vectors have indicated that base penetration into CNS parenchyma after various routes of administration was limited, and could be enhanced by certain modifications to the delivery protocol, such as mannitol pretreatment (Carty et al., 2010; McCarty et al., 2009; Fu et al., 2003). In the studies reported here, the effect of pretreatment with mannitol on the transduction pattern of the chosen AAV serotypes was also evaluated. Overall, mannitol resulted in enhanced transduction in DRG and CNS by AAV5 (Ch. 2, Figure 1; Ch. 3, Figure 9) and AAV8, but had little effect on transduction of spinal cord and DRG by AAV9, which resulted in very robust gene expression. Thus, if AAV5 or AAV8 were the serotype of choice for a given experiment, mannitol pretreatment would be a useful tool. Though AAV5 and AAV8 resulted is less overall transduction than AAV9, the more limited expression pattern of these vectors may be useful in certain circumstances.

The general pattern of expression in CNS and DRG resulting from AAV5 and AAV8 was similar, but a few distinct differences between the two serotypes were observed. The most striking of these differences was the complete lack of expression in choroid plexus after AAV8 (not shown), whereas AAV5 resulted in substantial transduction of choroid plexus in the fourth ventricle and more limited transduction in the third and lateral ventricles (Ch. 3, Figures 3 and 9). Another difference between AAV5 and AAV8 was the expression of GFP in some endothelial cells of the CNS vasculature after AAV8 (not shown). Expression in endothelial cells is consistent with the observation of expression in livers of AAV treated animals (not shown), as it reiterates that some AAV particles enter the systemic circulation after intrathecal delivery. The

final difference observed in tropism of AAV5 compared to AAV8 was for the transduction of small diameter peptidergic primary afferent neurons. AAV5 transduced a significantly larger number of CGRP-positive neurons <22μm in diameter (Ch. 2, Figure 5). These specific differences in expression observed after AAV5 or AAV8 are likely due to variations in expression of the cell-surface molecules required for binding and entry of either serotype.

Intrathecal delivery of AAV9 resulted in very intense gene expression throughout DRG and CNS. The pattern of relative expression intensity in many brain regions (such as hippocampus and olfactory bulb) was consistent with that observed after AAV5 or AAV8 (Chapter 3), suggesting that the general distribution of virus through the cerebrospinal fluid and/or general access to these regions is common to many, if not all serotypes. In addition to the vastly increased overall level of transduction seen across the nervous system after AAV9, many areas that showed little or no expression after AAV5 and AAV8, including thoracic DRG and spinal neurons (Ch. 2 Figure 6), striatum, septal nuclei, and hypothalamus, displayed considerable expression after AAV9. It is possible that this difference could be due to the ability of AAV9 to penetrate the pia mater in locations where fenestrations are absent (Reina et al., 2004). As AAV9 has been shown to readily cross the blood-brain barrier (BBB) (Samaranch et al., 2012; Gray et al., 2011; Foust et al., 2009), it is feasible that it may also cross other cellular barriers. Alternatively, AAV9 may be capable of some form of peri-vascular transport that would allow it to enter thoracic levels through local vasculature. The fact that AAV9 is able to cross the BBB, and the observation that expression is often heavily concentrated around

CNS blood vessels in cerebral cortex after intrathecal delivery (Ch. 3, Figure 10), but less so after intravenous delivery (Samaranch et al., 2012), suggests that some local vascular distribution occurs after intrathecal administration.

Transduction of DRG neurons by AAV9 was very efficient, and there appeared to be less tropism for specific subpopulations than with AAV5 or AAV8, though this has yet to be quantitatively evaluated. AAV9 resulted in gene expression in primary afferent fibers terminating in lamina II of the spinal cord (Ch. 2, Figure 6), where many axons of small diameter DRG neurons, including those that bind isolectin-B4 (IB4), terminate. Neither AAV5 nor AAV8 resulted in substantial gene expression in lamina II of spinal cord, or in IB4-binding DRG neurons (Ch. 2, Figures 2, 4, and 5). AAV9 did not appear from gross observation to have specific tropism for any subpopulations of DRG neurons; rather it seemed to have a general tropism for all DRG neurons as it appeared to transduce the majority at all spinal levels. More detailed evaluation is necessary to determine if there are subtle differences in tropism of AAV9 for any subpopulations of primary afferent neurons.

The studies enumerated here on transduction of AAV vectors after intrathecal delivery have raised several considerations that should be taken into account with future experiments using these vectors for transfer of functional genes of interest to primary afferent neurons. Though AAV5 and AAV8 resulted in a very specific pattern of transduction in brain, transduction levels in brain were much lower than those observed in DRG. Based on the current studies, the estimated number of cells transduced in any single brain region, with the exception of choroid plexus after AAV5, is less than one

percent. This suggests that off-target transduction of brain areas may not be of particular concern for these vectors. The fact that AAV5 transduced a substantial number of choroid plexus cells also raises the possibility that this effect could be exploited for other therapeutic applications beyond the scope of this thesis.

The widespread transduction and high level of expression resulting from intrathecal delivery of AAV9 are potentially both pros and cons of this serotype. Substantial transduction throughout the brain could be useful for disease states where widespread expression would be appropriate, but for studies of pain transmission at the spinal level, such high expression in brain causes concern for off-target effects. Modification to the vector construct to include a promoter that is specific only to primary afferent neurons, or specific to dorsal horn neurons which were also transduced by AAV9, could be used to restrict expression to the area of interest. This approach would be highly desirable for expression specific to primary afferent neurons. As AAV9 appears to have minimal selective tropism for subpopulations of DRG neurons, results would have to be interpreted as such, and could not necessarily be attributed to a specific subpopulation.

Considering that AAV5 and AAV8 transduced more medium and large diameter neurons than those with diameter <22μm, these vectors may be most suited for study of larger DRG neurons which generally signal innocuous stimuli but may also carry pain signals in cases of nerve injury resulting in allodynia (Sun et al., 2001). AAV5 and AAV8 vectors could also be useful for studying peptidergic primary afferent neurons apart from non-peptidergic nociceptors, as both of these vectors failed to substantially

transduce IB4-binding neurons in mice. This could be of particular value for study of opioid and adrenergic receptor interactions that take place in peptidergic primary afferents. In any case, a mannitol pretreatment can also be used with these vectors to enhance transduction of DRG neurons. When the goal is transduction of small diameter neurons in general, without regard to subpopulations, AAV6 may be the preferred serotype (Towne et al., 2009).

The results from the aforementioned studies indicate that AAV vectors can be useful for transfer of genetic material to primary afferent neurons in dorsal root ganglia. The serotype of the AAV vector, and the promoter portion of the construct should be chosen relative to the goals of the experiment. The discussion will now shift focus to the experiments covered in chapters 4 and 5.

Involvement of PKCε in synergistic analgesic interactions between opioid and adrenergic agonists at the spinal level

The experiments covered in chapter 4 demonstrate that protein kinase C-ε (PKCε) is necessary for spinal analgesic synergy between delta opioid receptors (δORs) and alpha-2A adrenergic receptors (α_{2A}ARs). It was found that both acute inhibition as well as genetic knockout of PKCε was sufficient to abolish synergy between δOR and α_{2A}AR agonists. Furthermore, acute activation of PKCε did not significantly affect potency or efficacy of agonists delivered singly. Immunoreactivity for PKCε was found in the majority of DRG neurons and in several neurons of the superficial dorsal horn of the spinal cord. As such, it was not surprising that PKCε was found to co-localize with the

neuropeptides substance P (SP) and calcitonin gene-related peptide (CGRP), as well as with both δORs and α_{2A}ARs in primary afferent terminals of the dorsal horn.

The pathway from receptor interaction to involvement of PKCε is not well understood. It is clear from the studies shown in chapter 4 that neither lack of PKCε, nor activation of PKCε has an effect on agonists that are not delivered in combination. While it remains unknown if activity at both δORs and α_{2A}ARs is necessary for activation of PKCε, it has been shown that $G\alpha_i$-associated Gβ/γ and $G\alpha_q$ subunits can synergistically activate phospholipase C-β3 (PLCβ3) (Philip et al., 2010), and that PLCβ3 is directly upstream of PKCε (Joseph et al., 2007). Considering this, stimulation of either α_{2A}ARs or δORs alone might be insufficient to induce activation of PKCε. Instead, co-activation of different Gα subunits by α_{2A}ARs and δORs might be required for signaling to PKCε. Alternatively, receptor-mediated activation of PKCε may not occur at all. In this case, one would have to interpret the results as indicating that some baseline activity of PKCε makes the synergy observed between δORs and α_{2A}ARs possible. Further experiments are necessary to determine if receptor co-activation leads to activation of PKCε.

Delta opioid receptors and α_{2A}ARs have previously been found to heavily co-localize in SP-containing DRG neurons (Riedl et al., 2009). The co-localization of δORs, α_{2A}ARs, and PKCε in peptidergic primary afferent neurons, among other evidence (Overland et al., 2009; Riedl et al., 2009) suggests that the synergistic interaction between δORs and α_{2A}ARs occurs at the level of single cells. Additionally, because inhibition, or loss, of PKCε does not affect potency or efficacy of single agonists, dependence of a given synergistic interaction between two G protein-coupled receptors

on PKCε suggests that the interaction takes place at the level of single cells. There has in recent years been some disagreement among opioid researchers on the relative location of δORs and μORs in DRG. In contrast to the prevailing view, some have suggested that δORs and μORs do not co-localize within the same primary afferent neurons (Scherrer et al., 2009). More recent articles have since confirmed that δORs and μORs are in fact co-localized in peptidergic afferents (Beaudry et al., 2011; He et al., 2011; Gupta et al., 2010; Wang et al., 2010). The current finding that specific combinations of a δOR agonist and a μOR agonist require PKCε for spinal analgesic synergy (Chapter 5) further supports the view that these receptors are co-localized.

In addition to supporting co-localization of δORs and μORs, the data presented in chapter 5 indicate that biased agonism can occur at the level of co-delivered agonists. The requirement of PKCε for spinal analgesic synergy involving delta and mu opioid agonists was not determinable by the inclusion of a single agonist; rather specific combinations of two agonists were necessary to induce the bias in signaling toward requirement of PKCε. Several recent studies have indicated that opioid receptors may exist *in vivo* as hetero-dimers or hetero-oligomers containing more than one opioid receptor subtype, or even other types of G protein-coupled receptors (Berg et al., 2011; He et al., 2011; Chu et al., 2010; Gupta et a., 2010; Daniels et al., 2005). The fact that co-delivery of two agonists is necessary to induce PKCε-dependent signaling suggests that the agonists may be acting through receptor hetero-dimers. Overall, these findings suggest that in addition to producing greater-than-additive analgesia, co-delivery of two opioid agonists can also be

used to direct signaling through a specific pathway, possibly via G protein-coupled receptor hetero-dimers (or hetero-oligomers).

Conclusion

The data reported in this thesis has demonstrated efficient transduction of DRG neurons by intrathecally delivered AAV vectors, raised considerations for choices of serotype and composition of the genetic construct, and further characterized opioid-adrenergic and opioid-opioid interactions by the requirement of PKCε for spinal analgesic synergy. These results have indicated several applications for the use of AAV vectors to study analgesic interactions between G protein-coupled receptors at the spinal level. This document will close with the proposal of a few selected future directions that could be taken to build off of the groundwork that has been laid in the previous pages.

The experiments originally proposed when this thesis work was in the very beginning stages involved using AAV5 to overexpress δORs and/or α_{2A}ARs in DRG neurons, and subsequently evaluate effects on delta opioid and alpha-2A adrenergic agonists delivered singly or in combination. The necessary vectors were not available at the time of data collection for this thesis, but this experimental plan could provide insight into the potential of receptor overexpression for increased analgesic effects of single opioid or adrenergic agonists, or combinations of two agonists. AAV6, AAV8, or AAV9 vectors could also be used for the originally proposed experiments, and comparing results based on the chosen vector could provide insight relative to the tropism of that vector. For example, AAV5 and AAV8 would result in the most limited expression pattern

including medium and large DRG neurons as well as some of the small peptidergic subtype. AAV6 would be expected to result in expression mainly in small DRG neurons of both peptidergic and non-peptidergic subtypes, and AAV9 would result in robust expression across in both DRG and spinal neurons.

There are several reasons, as described above, to indicate that the involvement of PKCε in synergistic interactions between δORs and α_{2A}ARs, as well as between δORs and μORs, occurs in peptidergic primary afferent neurons; however, there is as of yet no directly definitive evidence for this. All methods used thus far to disrupt PKCε activity have not been selective for neurons in DRG. As PKCε is also heavily concentrated in spinal dorsal horn neurons, it is important to definitively demonstrate that PKCε in this location is not involved in the observed effects. The ability of AAV9 to transduce spinal neurons of the dorsal horn as well as DRG neurons could be used to make this determination if specific genetic promoters were available to selectively express in either DRG or dorsal horn neurons. The advillin gene is nearly exclusively expressed by primary afferent neurons in DRG and trigeminal ganglia (Minett et al., 2012; Hasegawa et al., 2007; Ravenall et al., 2002), and could be used in an AAV construct to restrict expression to primary afferent neurons. No gene has been found as of yet that is expressed solely in neurons of the superficial spinal dorsal horn. A short-hairpin-RNA (shRNA) construct directed at PKCε could be used with the advillin promoter to knock down PKCε in primary afferents separately from dorsal horn neurons, and effects on analgesic synergy between various opioid and adrenergic agonists could subsequently be evaluated.

An alternative approach to address the same question of PKCε activity in DRG versus spinal neurons would be to use the same shRNA construct directed at PKCε, but in an AAV5 or AAV8 vector with a strong generic promoter (such as CMV or Cags). This would allow expression in DRG, but not spinal neurons, and would provide the opportunity to knock down expression in peptidergic afferents without affecting the IB4-binding population. This experiment would have the potential to directly implicate activity of PKCε in peptidergic afferents as necessary for the previously defined synergistic interactions; however, it may have limited success due to the relatively low expression in small, presumably nociceptive, afferents. Recent experiments have suggested that positioning the animals vertically (head upward, under anesthesia) immediately after injection of AAV8 can enhance transduction of lower lumbar DRG neurons (Schuster et al., 2012). This approach may be especially useful for future rodent studies with AAV5 and AAV8, which appear to result in less transduction of DRG neurons compared to AAV6 and AAV9 (Chapter 2, Figures 1, 5 and 6; Samaranch et al., 2013; Towne et al., 2009).

The point has been raised that dependence of synergistic interactions by certain opioid and adrenergic agonist combinations on PKCε may not be due to receptor-mediated activation of PKCε, but could be alternatively explained by baseline activity of PKCε that somehow allows such interactions to take place. If PKCε-dependent synergy arises from receptor-mediated activation of PKCε, then there must be a signaling mediator between the receptor(s) and PKCε. It has been shown that PLCβ3 is directly upstream of PKCε in primary afferent neurons (Joseph et al., 2007), and that PLCβ3 can

be synergistically activated by co-agonism at two different G protein-coupled receptors (Phillip et al., 2010). If synergistic drug interactions that are PKCε-dependent also require PLCβ3, this would indicate that involvement of PKCε in such interactions is due to receptor mediated activation rather than baseline activity. AAV vectors could be used to determine if PLCβ3 is necessary for synergistic interactions between delta opioid and alpha-2A adrenergic, and predetermined combinations of two opioid agonists. An shRNA construct directed at PLCβ3 would be necessary, and could be placed in an AAV5 or AAV8 vector, or in an AAV9 vector with the primary afferent neuron-specific promoter for the advillin gene (Minett et al., 2012; Hasegawa et al., 2007; Ravenall et al., 2002), that would then be delivered intrathecally. If administration of such a vector resulted in significant knockdown of PLCβ3 and abolishment of synergy between indicated agonist combinations, this would suggest that PKCε is activated by those agonist combinations in a receptor-mediated fashion.

Clearly there is significant potential for the use of AAV-based experiments to study and better define interactions between opioid and adrenergic receptors, as well as their underlying mechanisms at the spinal level. The studies proposed here display a limited view of the vast overall potential for the development and use of AAV vectors to understand synergistic analgesic interactions and exploit them for enhanced therapeutic benefit.

Chapter 7

References

Aicher SA, Punnoose A, Goldberg A (2000) mu-Opioid receptors often colocalize with the substance P receptor (NK1) in the trigeminal dorsal horn. J Neurosci 20:4345-4354.

Aley KO, Messing RO, Mochly-Rosen D, Levine JD (2000) Chronic hypersensitivity for inflammatory nociceptor sensitization mediated by the epsilon isozyme of protein kinase C. J Neurosci 20:4680-4685.

Askou AL, Pournaras JA, Pihlmann M, Svalgaard JD, Arsenijevic Y, Kostic C, Bek T, Dagnaes-Hansen F, Mikkelsen JG, Jensen TG, Corydon TJ (2012) Reduction of choroidal neovascularization in mice by adeno-associated virus-delivered anti-vascular endothelial growth factor short hairpin RNA. J Gene Med 14:632-641.

Baiou D, Santha P, Avelino A, Charrua A, Bacskai T, Matesz K, Cruz F, Nagy I (2007) Neurochemical characterization of insulin receptor-expressing primary sensory neurons in wild-type and vanilloid type 1 transient receptor potential receptor knockout mice. J Comp Neurol 503:334-347.

Bao L, Jin SX, Zhang C, Wang LH, Xu ZZ, Zhang FX, Wang LC, Ning FS, Cai HJ, Guan JS, Xiao HS, Xu ZQ, He C, Hokfelt T, Zhou Z, Zhang X (2003) Activation of delta opioid receptors induces receptor insertion and neuropeptide secretion. Neuron 37:121-133.

Beaudry H, Dubois D, Gendron L (2011) Activation of spinal mu- and delta-opioid receptors potently inhibits substance P release induced by peripheral noxious stimuli. J Neurosci 31:13068-13077.

Berg KA, Rowan MP, Gupta A, Sanchez TA, Silva M, Gomes I, McGuire BA, Portoghese PS, Hargreaves KM, Devi LA, Clarke WP (2011) Allosteric interactions between delta and kappa opioid receptors in peripheral sensory neurons. Mol Pharmacol 81:264-272.

Beutler AS, Reinhardt M (2009) AAV for pain: steps towards clinical translation. Gene Ther 16:461-469.

Cahill CM, Morinville A, Lee MC, Vincent JP, Collier B, Beaudet A (2001) Prolonged morphine treatment targets delta opioid receptors to neuronal plasma membranes and enhances delta-mediated antinociception. J Neurosci 21:7598-7607.

Carty N, Lee D, Dickey C, Ceballos-Diaz C, Jansen-West K, Golde TE, Gordon MN, Morgan D, Nash K (2010) Convection-enhanced delivery and systemic mannitol increase gene product distribution of AAV vectors 5, 8, and 9 and increase gene product in the adult mouse brain. J Neurosci Methods 194:144-153.

Cesare P, Dekker LV, Sardini A, Parker PJ, McNaughton PA (1999) Specific involvement of PKC-epsilon in sensitization of the neuronal response to painful heat. Neuron 23:617-624.

Chakrabarti S, Liu NJ, Gintzler AR (2010) Formation of mu-/kappa-opioid receptor heterodimer is sex-dependent and mediates female-specific opioid analgesia. Proc Natl Acad Sci U S A 107:20115-20119.

Chan AS, Law PY, Loh HH, Ho PN, Wu WM, Chan JS, Wong YH (2003) The first and third intracellular loops together with the carboxy terminal tail of the delta-opioid receptor contribute toward functional interaction with Galpha16. J Neurochem 87:697-708.

Chen L, Hahn H, Wu G, Chen CH, Liron T, Schechtman D, Cavallaro G, Banci L, Guo Y, Bolli R, Dorn GW, 2nd, Mochly-Rosen D (2001) Opposing cardioprotective actions and parallel hypertrophic effects of delta PKC and epsilon PKC. Proc Natl Acad Sci U S A 98:11114-11119.

Cheng PY, Liu-Chen LY, Pickel VM (1997) Dual ultrastructural immunocytochemical labeling of mu and delta opioid receptors in the superficial layers of the rat cervical spinal cord. Brain Res 778:367-380.

Chu J, Zheng H, Zhang Y, Loh HH, Law PY (2010) Agonist-dependent mu-opioid receptor signaling can lead to heterologous desensitization. Cell Signal 22:684-696.

Ciesielska A, Mittermeyer G, Hadaczek P, Kells AP, Forsayeth J, Bankiewicz KS (2010) Anterograde Axonal Transport of AAV2-GDNF in Rat Basal Ganglia. Mol Ther.

Cloyd JC, Snyder BD, Cleeremans B, Bundlie SR, Blomquist CH, Lakatua DJ (1986) Mannitol pharmacokinetics and serum osmolality in dogs and humans. J Pharmacol Exp Ther 236:301-306.

Dado RJ, Law PY, Loh HH, Elde R (1993) Immunofluorescent identification of a delta (delta)-opioid receptor on primary afferent nerve terminals. Neuroreport 5:341-344.

Daniels DJ, Lenard NR, Etienne CL, Law PY, Roerig SC, Portoghese PS (2005) Opioid-induced tolerance and dependence in mice is modulated by the distance between pharmacophores in a bivalent ligand series. Proc Natl Acad Sci U S A 102:19208-19213.

Di Pasquale G, Davidson BL, Stein CS, Martins I, Scudiero D, Monks A, Chiorini JA (2003) Identification of PDGFR as a receptor for AAV-5 transduction. Nat Med 9:1306-1312.

Dina OA, Khasar SG, Gear RW, Levine JD (2009) Activation of Gi induces mechanical hyperalgesia poststress or inflammation. Neuroscience 160:501-507.

Dorn GW, 2nd, Mochly-Rosen D (2002) Intracellular transport mechanisms of signal transducers. Annu Rev Physiol 64:407-429.

Dorn GW, 2nd, Oswald KJ, McCluskey TS, Kuhel DG, Liggett SB (1997) Alpha 2A-adrenergic receptor stimulated calcium release is transduced by Gi-associated G(beta gamma)-mediated activation of phospholipase C. Biochemistry 36:6415-6423.

Dorn GW, 2nd, Souroujon MC, Liron T, Chen CH, Gray MO, Zhou HZ, Csukai M, Wu G, Lorenz JN, Mochly-Rosen D (1999) Sustained in vivo cardiac protection by a rationally designed peptide that causes epsilon protein kinase C translocation. Proc Natl Acad Sci U S A 96:12798-12803.

Erlich SS, McComb JG, Hyman S, Weiss MH (1986) Ultrastructural morphology of the olfactory pathway for cerebrospinal fluid drainage in the rabbit. J Neurosurg 64:466-473.

Fairbanks CA, Stone LS, Kitto KF, Nguyen HO, Posthumus IJ, Wilcox GL (2002) alpha(2C)-Adrenergic receptors mediate spinal analgesia and adrenergic-opioid synergy. J Pharmacol Exp Ther 300:282-290.

Fairbanks CA, Wilcox GL (1999) Spinal antinociceptive synergism between morphine and clonidine persists in mice made acutely or chronically tolerant to morphine. J Pharmacol Exp Ther 288:1107-1116.

Fang X, Djouhri L, McMullan S, Berry C, Waxman SG, Okuse K, Lawson SN (2006) Intense isolectin-B4 binding in rat dorsal root ganglion neurons distinguishes C-fiber nociceptors with broad action potentials and high Nav1.9 expression. J Neurosci 26:7281-7292.

Ferrari LF, Bogen O, Levine JD (2010) Nociceptor subpopulations involved in hyperalgesic priming. Neuroscience 165:896-901.

Forster JG, Rosenberg PH (2004) Small dose of clonidine mixed with low-dose ropivacaine and fentanyl for epidural analgesia after total knee arthroplasty. Br J Anaesth 93:670-677.

Foust KD, Nurre E, Montgomery CL, Hernandez A, Chan CM, Kaspar BK (2009) Intravascular AAV9 preferentially targets neonatal neurons and adult astrocytes. Nat Biotechnol 27:59-65.

Fruttiger M, Karlsson L, Hall AC, Abramsson A, Calver AR, Bostrom H, Willetts K, Bertold CH, Heath JK, Betsholtz C, Richardson WD (1999) Defective oligodendrocyte development and severe hypomyelination in PDGF-A knockout mice. Development 126:457-467.

Fu H, Muenzer J, Samulski RJ, Breese G, Sifford J, Zeng X, McCarty DM (2003) Self-complementary adeno-associated virus serotype 2 vector: global distribution and broad dispersion of AAV-mediated transgene expression in mouse brain. Mol Ther 8:911-917.

Fu H, Samulski RJ, McCown TJ, Picornell YJ, Fletcher D, Muenzer J (2002) Neurological correction of lysosomal storage in a mucopolysaccharidosis IIIB mouse model by adeno-associated virus-mediated gene delivery. Mol Ther 5:42-49.

Gray SJ, Matagne V, Bachaboina L, Yadav S, Ojeda SR, Samulski RJ (2011) Preclinical differences of intravascular AAV9 delivery to neurons and glia: a comparative study of adult mice and nonhuman primates. Mol Ther 19:1058-1069.

Gray SJ, Nagabhushan Kalburgi S, McCown TJ, Jude Samulski R (2013) Global CNS gene delivery and evasion of anti-AAV-neutralizing antibodies by intrathecal AAV administration in non-human primates. Gene Ther 20:450-459.

Gregoretti C, Moglia B, Pelosi P, Navalesi P (2009) Clonidine in perioperative medicine and intensive care unit: more than an anti-hypertensive drug. Curr Drug Targets 10:799-814.

Gu Y, Xu Y, Li GW, Huang LY (2005) Remote nerve injection of mu opioid receptor adeno-associated viral vector increases antinociception of intrathecal morphine. J Pain 6:447-454.

Gupta A, Mulder J, Gomes I, Rozenfeld R, Bushlin I, Ong E, Lim M, Maillet E, Junek M, Cahill CM, Harkany T, Devi LA (2010) Increased abundance of opioid receptor heteromers after chronic morphine administration. Sci Signal 3:ra54.

Hasegawa H, Abbott S, Han BX, Qi Y, Wang F (2007) Analyzing somatosensory axon projections with the sensory neuron-specific Advillin gene. J Neurosci 27:14404-14414.

He SQ, Zhang ZN, Guan JS, Liu HR, Zhao B, Wang HB, Li Q, Yang H, Luo J, Li ZY, Wang Q, Lu YJ, Bao L, Zhang X (2011) Facilitation of mu-opioid receptor activity by preventing delta-opioid receptor-mediated codegradation. Neuron 69:120-131.

Hirai T, Enomoto M, Machida A, Yamamoto M, Kuwahara H, Tajiri M, Hirai Y, Sotome S, Mizusawa H, Shinomiya K, Okawa A, Yokota T (2012) Intrathecal shRNA-AAV9 inhibits target protein expression in the spinal cord and dorsal root ganglia of adult mice. Hum Gene Ther Methods 23:119-127.

Howard DB, Powers K, Wang Y, Harvey BK (2008) Tropism and toxicity of adeno-associated viral vector serotypes 1, 2, 5, 6, 7, 8, and 9 in rat neurons and glia in vitro. Virology 372:24-34.

Hucho TB, Dina OA, Levine JD (2005) Epac mediates a cAMP-to-PKC signaling in inflammatory pain: an isolectin B4(+) neuron-specific mechanism. J Neurosci 25:6119-6126.

Hylden JL, Wilcox GL (1980) Intrathecal morphine in mice: a new technique. Eur J Pharmacol 67:313-316.

Hylden JL, Wilcox GL (1983) Pharmacological characterization of substance P-induced nociception in mice: modulation by opioid and noradrenergic agonists at the spinal level. J Pharmacol Exp Ther 226:398-404.

Ishii Y, Oya T, Zheng L, Gao Z, Kawaguchi M, Sabit H, Matsushima T, Tokunaga A, Ishizawa S, Hori E, Nabeshima Y, Sasaoka T, Fujimori T, Mori H, Sasahara M (2006) Mouse brains deficient in neuronal PDGF receptor-beta develop normally but are vulnerable to injury. J Neurochem 98:588-600.

Iwamoto N, Watanabe A, Yamamoto M, Miyake N, Kurai T, Teramoto A, Shimada T (2009) Global diffuse distribution in the brain and efficient gene delivery to the dorsal root ganglia by intrathecal injection of adeno-associated viral vector serotype 1. J Gene Med 11:498-505.

Jacques SJ, Ahmed Z, Forbes A, Douglas MR, Vigenswara V, Berry M, Logan A (2012) AAV8(gfp) preferentially targets large diameter dorsal root ganglion neurones after both intra-dorsal root ganglion and intrathecal injection. Mol Cell Neurosci 49:464-474.

Janssen PA, Niemegeers CJ, Dony JG (1963) The inhibitory effect of fentanyl and other morphine-like analgesics on the warm water induced tail withdrawl reflex in rats. Arzneimittelforschung 13:502-507.

Johnson JA, Gray MO, Chen CH, Mochly-Rosen D (1996) A protein kinase C translocation inhibitor as an isozyme-selective antagonist of cardiac function. J Biol Chem 271:24962-24966.

Joseph EK, Bogen O, Alessandri-Haber N, Levine JD (2007) PLC-beta 3 signals upstream of PKC epsilon in acute and chronic inflammatory hyperalgesia. Pain 132:67-73.

Joseph EK, Levine JD (2010) Hyperalgesic priming is restricted to isolectin B4-positive nociceptors. Neuroscience 169:431-435.

Kaemmerer WF, Reddy RG, Warlick CA, Hartung SD, McIvor RS, Low WC (2000) In vivo transduction of cerebellar Purkinje cells using adeno-associated virus vectors. Mol Ther 2:446-457.

Kaludov N, Brown KE, Walters RW, Zabner J, Chiorini JA (2001) Adeno-associated virus serotype 4 (AAV4) and AAV5 both require sialic acid binding for hemagglutination and efficient transduction but differ in sialic acid linkage specificity. J Virol 75:6884-6893.

Kaplitt MG, Leone P, Samulski RJ, Xiao X, Pfaff DW, O'Malley KL, During MJ (1994) Long-term gene expression and phenotypic correction using adeno-associated virus vectors in the mammalian brain. Nat Genet 8:148-154.

Khasar SG, Lin YH, Martin A, Dadgar J, McMahon T, Wang D, Hundle B, Aley KO, Isenberg W, McCarter G, Green PG, Hodge CW, Levine JD, Messing RO (1999) A novel nociceptor signaling pathway revealed in protein kinase C epsilon mutant mice. Neuron 24:253-260.

Kiwic G, Slusarczyk K, Slusarczyk R (1998) [The central nervous system and the lymphatic system. Lymphatic drainage of the cerebrospinal fluid]. Neurol Neurochir Pol 32:633-641.

Kondo I, Marvizon JC, Song B, Salgado F, Codeluppi S, Hua XY, Yaksh TL (2005) Inhibition by spinal mu- and delta-opioid agonists of afferent-evoked substance P release. J Neurosci 25:3651-3660.

Lee B, Kim J, Kim SJ, Lee H, Chang JW (2007) Constitutive GABA expression via a recombinant adeno-associated virus consistently attenuates neuropathic pain. Biochem Biophys Res Commun 357:971-976.

Lee JW, Joshi S, Chan JS, Wong YH (1998) Differential coupling of mu-, delta-, and kappa-opioid receptors to G alpha16-mediated stimulation of phospholipase C. J Neurochem 70:2203-2211.

Li XY, Sun L, He J, Chen ZL, Zhou F, Liu XY, Liu RS (2010) The kappa-opioid receptor is upregulated in the spinal cord and locus ceruleus but downregulated in the dorsal root ganglia of morphine tolerant rats. Brain Res 1326:30-39.

Luebke AE, Foster PK, Muller CD, Peel AL (2001) Cochlear function and transgene expression in the guinea pig cochlea, using adenovirus- and adeno-associated virus-directed gene transfer. Hum Gene Ther 12:773-781.

Ma HT, Lin WW, Zhao B, Wu WT, Huang W, Li Y, Jones NL, Kruth HS (2006) Protein kinase C beta and delta isoenzymes mediate cholesterol accumulation in PMA-activated macrophages. Biochem Biophys Res Commun 349:214-220.

Mason MR, Ehlert EM, Eggers R, Pool CW, Hermening S, Huseinovic A, Timmermans E, Blits B, Verhaagen J (2010) Comparison of AAV serotypes for gene delivery to dorsal root ganglion neurons. Mol Ther 18:715-724.

McCarty DM, DiRosario J, Gulaid K, Muenzer J, Fu H (2009) Mannitol-facilitated CNS entry of rAAV2 vector significantly delayed the neurological disease progression in MPS IIIB mice. Gene Ther 16:1340-1352.

Milligan ED, Sloane EM, Langer SJ, Cruz PE, Chacur M, Spataro L, Wieseler-Frank J, Hammack SE, Maier SF, Flotte TR, Forsayeth JR, Leinwand LA, Chavez R, Watkins LR (2005) Controlling neuropathic pain by adeno-associated virus driven production of the anti-inflammatory cytokine, interleukin-10. Mol Pain 1:9.

Minett MS, Nassar MA, Clark AK, Passmore G, Dickenson AH, Wang F, Malcangio M, Wood JN (2012) Distinct Nav1.7-dependent pain sensations require different sets of sensory and sympathetic neurons. Nat Commun 3:791.

Mollanji R, Bozanovic-Sosic R, Silver I, Li B, Kim C, Midha R, Johnston M (2001) Intracranial pressure accommodation is impaired by blocking pathways leading to extracranial lymphatics. Am J Physiol Regul Integr Comp Physiol 280:R1573-1581.

Morse M, Sun H, Tran E, Levenson R, Fang Y (2013) Label-free integrative pharmacology on-target of opioid ligands at the opioid receptor family. BMC Pharmacol Toxicol 14:17.

Newton PM, Messing RO (2010) The substrates and binding partners of protein kinase Cepsilon. Biochem J 427:189-196.

Olave MJ, Maxwell DJ (2002) An investigation of neurones that possess the alpha 2C-adrenergic receptor in the rat dorsal horn. Neuroscience 115:31-40.

Olave MJ, Maxwell DJ (2003) Axon terminals possessing the alpha 2c-adrenergic receptor in the rat dorsal horn are predominantly excitatory. Brain Res 965:269-273.

Olave MJ, Maxwell DJ (2003) Neurokinin-1 projection cells in the rat dorsal horn receive synaptic contacts from axons that possess alpha2C-adrenergic receptors. J Neurosci 23:6837-6846.

Olave MJ, Maxwell DJ (2004) Axon terminals possessing alpha2C-adrenergic receptors densely innervate neurons in the rat lateral spinal nucleus which respond to noxious stimulation. Neuroscience 126:391-403.

Ossipov MH, Lopez Y, Bian D, Nichols ML, Porreca F (1997) Synergistic antinociceptive interactions of morphine and clonidine in rats with nerve-ligation injury. Anesthesiology 86:196-204.

Overland AC, Kitto KF, Chabot-Dore AJ, Rothwell PE, Fairbanks CA, Stone LS, Wilcox GL (2009) Protein kinase C mediates the synergistic interaction between agonists acting at alpha2-adrenergic and delta-opioid receptors in spinal cord. J Neurosci 29:13264-13273.

Paech MJ, Pavy TJ, Orlikowski CE, Yeo ST, Banks SL, Evans SF, Henderson J (2004) Postcesarean analgesia with spinal morphine, clonidine, or their combination. Anesth Analg 98:1460-1466, table of contents.

Patwardhan AM, Berg KA, Akopain AN, Jeske NA, Gamper N, Clarke WP, Hargreaves KM (2005) Bradykinin-induced functional competence and trafficking of the delta-opioid receptor in trigeminal nociceptors. J Neurosci 25:8825-8832.

Paxinos G, Franklin KBj (2001) The Mouse Brain In Stereotaxic Coordinates, Second Edition: Academic Press.

Philip F, Kadamur G, Silos RG, Woodson J, Ross EM (2010) Synergistic activation of phospholipase C-beta3 by Galpha(q) and Gbetagamma describes a simple two-state coincidence detector. Curr Biol 20:1327-1335.

Pradhan AA, Smith ML, Kieffer BL, Evans CJ (2012) Ligand-directed signalling within the opioid receptor family. Br J Pharmacol 167:960-969.

Price TJ, Flores CM (2007) Critical evaluation of the colocalization between calcitonin gene-related peptide, substance P, transient receptor potential vanilloid subfamily type 1 immunoreactivities, and isolectin B4 binding in primary afferent neurons of the rat and mouse. J Pain 8:263-272.

Qing K, Mah C, Hansen J, Zhou S, Dwarki V, Srivastava A (1999) Human fibroblast growth factor receptor 1 is a co-receptor for infection by adeno-associated virus 2. Nat Med 5:71-77.

Ravenall SJ, Gavazzi I, Wood JN, Akopian AN (2002) A peripheral nervous system actin-binding protein regulates neurite outgrowth. Eur J Neurosci 15:281-290.

Reina MA, De Leon Casasola Ode L, Villanueva MC, Lopez A, Maches F, De Andres JA (2004) Ultrastructural findings in human spinal pia mater in relation to subarachnoid anesthesia. Anesth Analg 98:1479-1485, table of contents.

Riedl MS, Schnell SA, Overland AC, Chabot-Dore AJ, Taylor AM, Ribeiro-da-Silva A, Elde RP, Wilcox GL, Stone LS (2009) Coexpression of alpha 2A-adrenergic and delta-opioid receptors in substance P-containing terminals in rat dorsal horn. J Comp Neurol 513:385-398.

Rowan MP, Ruparel NB, Patwardhan AM, Berg KA, Clarke WP, Hargreaves KM (2009) Peripheral delta opioid receptors require priming for functional competence in vivo. Eur J Pharmacol 602:283-287.

Royo NC, Vandenberghe LH, Ma JY, Hauspurg A, Yu L, Maronski M, Johnston J, Dichter MA, Wilson JM, Watson DJ (2008) Specific AAV serotypes stably transduce primary hippocampal and cortical cultures with high efficiency and low toxicity. Brain Res 1190:15-22.

Samad OA, Tan AM, Cheng X, Foster E, Dib-Hajj SD, Waxman SG (2013) Virus-mediated shRNA knockdown of Na(v)1.3 in rat dorsal root ganglion attenuates nerve injury-induced neuropathic pain. Mol Ther 21:49-56.

Samaranch L, Salegio EA, San Sebastian W, Kells AP, Bringas JR, Forsayeth J, Bankiewicz KS (2013) Strong Cortical and Spinal Cord Transduction After AAV7 and AAV9 Delivery into the Cerebrospinal Fluid of Nonhuman Primates. Hum Gene Ther 24:526-532.

Samaranch L, Salegio EA, San Sebastian W, Kells AP, Foust KD, Bringas JR, Lamarre C, Forsayeth J, Kaspar BK, Bankiewicz KS (2012) Adeno-associated virus serotype 9 transduction in the central nervous system of nonhuman primates. Hum Gene Ther 23:382-389.

Sanchez-Blazquez P, Garzon J (1998) delta Opioid receptor subtypes activate inositol-signaling pathways in the production of antinociception. J Pharmacol Exp Ther 285:820-827.

Scherrer G, Imamachi N, Cao YQ, Contet C, Mennicken F, O'Donnell D, Kieffer BL, Basbaum AI (2009) Dissociation of the opioid receptor mechanisms that control mechanical and heat pain. Cell 137:1148-1159.

Schultz BR, Chamberlain JS (2008) Recombinant adeno-associated virus transduction and integration. Mol Ther 16:1189-1199.

Schuster DJ, Dykstra JA, Riedl MS, Kitto KF, Honda CN, McIvor RS, Fairbanks CA, Vulchanova L (2012) Visualization of spinal afferent innervation in the mouse colon by AAV8-mediated expression. Neurogastroenterol Motil 25:e89-100.

Schuster DJ, Kitto KF, Overland AC, Messing RO, Stone LS, Fairbanks CA, Wilcox GL (2013) Protein kinase C-epsilon is required for spinal analgesic synergy between delta opioid and alpha-2A adrenergic receptor agonist pairs. J Neurosci 33:13538-13546.

Seiler MP, Miller AD, Zabner J, Halbert CL (2006) Adeno-associated virus types 5 and 6 use distinct receptors for cell entry. Hum Gene Ther 17:10-19.

Shin SW, Eisenach JC (2003) Intrathecal morphine reduces the visceromotor response to acute uterine cervical distension in an estrogen-independent manner. Anesthesiology 98:1467-1471; discussion 1466A.

Standifer KM, Rossi GC, Pasternak GW (1996) Differential blockade of opioid analgesia by antisense oligodeoxynucleotides directed against various G protein alpha subunits. Mol Pharmacol 50:293-298.

Stone LS, Broberger C, Vulchanova L, Wilcox GL, Hokfelt T, Riedl MS, Elde R (1998) Differential distribution of alpha2A and alpha2C adrenergic receptor immunoreactivity in the rat spinal cord. J Neurosci 18:5928-5937.

Stone LS, MacMillan LB, Kitto KF, Limbird LE, Wilcox GL (1997) The alpha2a adrenergic receptor subtype mediates spinal analgesia evoked by alpha2 agonists and is necessary for spinal adrenergic-opioid synergy. J Neurosci 17:7157-7165.

Storek B, Harder NM, Banck MS, Wang C, McCarty DM, Janssen WG, Morrison JH, Walsh CE, Beutler AS (2006) Intrathecal long-term gene expression by self-complementary adeno-associated virus type 1 suitable for chronic pain studies in rats. Mol Pain 2:4.

Storek B, Reinhardt M, Wang C, Janssen WG, Harder NM, Banck MS, Morrison JH, Beutler AS (2008) Sensory neuron targeting by self-complementary AAV8 via lumbar puncture for chronic pain. Proc Natl Acad Sci U S A 105:1055-1060.

Sullivan AF, Dashwood MR, Dickenson AH (1987) Alpha 2-adrenoceptor modulation of nociception in rat spinal cord: location, effects and interactions with morphine. Eur J Pharmacol 138:169-177.

Summerford C, Samulski RJ (1998) Membrane-associated heparan sulfate proteoglycan is a receptor for adeno-associated virus type 2 virions. J Virol 72:1438-1445.

Sun H, Ren K, Zhong CM, Ossipov MH, Malan TP, Lai J, Porreca F (2001) Nerve injury-induced tactile allodynia is mediated via ascending spinal dorsal column projections. Pain 90:105-111.

Sweitzer SM, Wong SM, Peters MC, Mochly-Rosen D, Yeomans DC, Kendig JJ (2004) Protein kinase C epsilon and gamma: involvement in formalin-induced nociception in neonatal rats. J Pharmacol Exp Ther 309:616-625.

Sweitzer SM, Wong SM, Peters MC, Mochly-Rosen D, Yeomans DC, Kendig JJ (2004) Protein kinase C epsilon and gamma: involvement in formalin-induced nociception in neonatal rats. J Pharmacol Exp Ther 309:616-625.

Tallarida R, Murray R (1987) Manual of pharmacological calculations with computer programs. New York: Springer.

Tallarida RJ, Porreca F, Cowan A (1989) Statistical analysis of drug-drug and site-site interactions with isobolograms. Life Sci 45:947-961.

Towne C, Pertin M, Beggah AT, Aebischer P, Decosterd I (2009) Recombinant adeno-associated virus serotype 6 (rAAV2/6)-mediated gene transfer to nociceptive neurons through different routes of delivery. Mol Pain 5:52.

Vulchanova L, Riedl MS, Shuster SJ, Stone LS, Hargreaves KM, Buell G, Surprenant A, North RA, Elde R (1998) P2X3 is expressed by DRG neurons that terminate in inner lamina II. Eur J Neurosci 10:3470-3478.

Vulchanova L, Schuster DJ, Belur LR, Riedl MS, Podetz-Pedersen KM, Kitto KF, Wilcox GL, McIvor RS, Fairbanks CA (2010) Differential adeno-associated virus mediated gene transfer to sensory neurons following intrathecal delivery by direct lumbar puncture. Mol Pain 6:31.

Walters RW, Yi SM, Keshavjee S, Brown KE, Welsh MJ, Chiorini JA, Zabner J (2001) Binding of adeno-associated virus type 5 to 2,3-linked sialic acid is required for gene transfer. J Biol Chem 276:20610-20616.

Wang HB, Zhao B, Zhong YQ, Li KC, Li ZY, Wang Q, Lu YJ, Zhang ZN, He SQ, Zheng HC, Wu SX, Hokfelt TG, Bao L, Zhang X (2010) Coexpression of delta-

and mu-opioid receptors in nociceptive sensory neurons. Proc Natl Acad Sci U S A 107:13117-13122.

Wang X, Skelley L, Cade R, Sun Z (2006) AAV delivery of mineralocorticoid receptor shRNA prevents progression of cold-induced hypertension and attenuates renal damage. Gene Ther 13:1097-1103.

Watson G, Bastacky J, Belichenko P, Buddhikot M, Jungles S, Vellard M, Mobley WC, Kakkis E (2006) Intrathecal administration of AAV vectors for the treatment of lysosomal storage in the brains of MPS I mice. Gene Ther 13:917-925.

Weller ML, Amornphimoltham P, Schmidt M, Wilson PA, Gutkind JS, Chiorini JA (2010) Epidermal growth factor receptor is a co-receptor for adeno-associated virus serotype 6. Nat Med 16:662-664.

White EA, Bienemann AS, Sena-Esteves M, Taylor H, Bunnun C, Castrique ES, Gill SS (2010) Evaluation and Optimisation of the Administration of Recombinant Adeno-Associated Viral Vectors (Serotypes 2/1, 2/2, 2/rh8, 2/9 and 2/rh10) by Convection-Enhanced Delivery to the Striatum. Hum Gene Ther.

Wilcox GL, Carlsson KH, Jochim A, Jurna I (1987) Mutual potentiation of antinociceptive effects of morphine and clonidine on motor and sensory responses in rat spinal cord. Brain Res 405:84-93.

Williams AE, Blakemore WF (1990) Pathology of Streptococcal meningitis following intravenous intracisternal and natural routes of infection. Neuropathol Appl Neurobiol 16:345-356.

Wu DF, Chandra D, McMahon T, Wang D, Dadgar J, Kharazia VN, Liang YJ, Waxman SG, Dib-Hajj SD, Messing RO (2012) PKCepsilon phosphorylation of the sodium channel NaV1.8 increases channel function and produces mechanical hyperalgesia in mice. J Clin Invest 122:1306-1315.

Wu Z, Miller E, Agbandje-McKenna M, Samulski RJ (2006) Alpha2,3 and alpha2,6 N-linked sialic acids facilitate efficient binding and transduction by adeno-associated virus types 1 and 6. J Virol 80:9093-9103.

Xu Q, Chou B, Fitzsimmons B, Miyanohara A, Shubayev V, Santucci C, Hefferan M, Marsala M, Hua XY (2012) In vivo gene knockdown in rat dorsal root ganglia mediated by self-complementary adeno-associated virus serotype 5 following intrathecal delivery. PLoS One 7:e32581.

Xu Y, Gu Y, Xu GY, Wu P, Li GW, Huang LY (2003) Adeno-associated viral transfer of opioid receptor gene to primary sensory neurons: a strategy to increase opioid antinociception. Proc Natl Acad Sci U S A 100:6204-6209.

Yoon SH, Lo TM, Loh HH, Thayer SA (1999) Delta-opioid-induced liberation of Gbetagamma mobilizes Ca2+ stores in NG108-15 cells. Mol Pharmacol 56:902-908.

Zhang X, Bao L, Arvidsson U, Elde R, Hokfelt T (1998) Localization and regulation of the delta-opioid receptor in dorsal root ganglia and spinal cord of the rat and monkey: evidence for association with the membrane of large dense-core vesicles. Neuroscience 82:1225-1242.

Zhao B, Wang HB, Lu YJ, Hu JW, Bao L, Zhang X (2011) Transport of receptors, receptor signaling complexes and ion channels via neuropeptide-secretory vesicles. Cell Res 21:741-753.

Zhong L, Zhao W, Wu J, Li B, Zolotukhin S, Govindasamy L, Agbandje-McKenna M, Srivastava A (2007) A dual role of EGFR protein tyrosine kinase signaling in ubiquitination of AAV2 capsids and viral second-strand DNA synthesis. Mol Ther 15:1323-1330.

Zwick M, Davis BM, Woodbury CJ, Burkett JN, Koerber HR, Simpson JF, Albers KM (2002) Glial cell line-derived neurotrophic factor is a survival factor for isolectin B4-positive, but not vanilloid receptor 1-positive, neurons in the mouse. J Neurosci 22:4057-4065.